FAULT LOCATION IN ACTIVE DISTRIBUTION SYSTEMS

Ph.D. Thesis

RANJEET KUMAR

(Enroll. ID 2015REE9001)

DEPARTMENT OF ELECTRICAL ENGINEERING

MALAVIYA NATIONAL INSTITUTE OF TECHNOLOGY JAIPUR

January 2020

FAULT LOCATION IN ACTIVE DISTRIBUTION SYSTEMS

Submitted in

fulfillment of the requirements for the degree of

Doctor of Philosophy

by

Ranjeet Kumar

(Enroll. ID 2015REE9001)

Under the Supervision of

Dr. D. Saxena

DEPARTMENT OF ELECTRICAL ENGINEERING

MALAVIYA NATIONAL INSTITUTE OF TECHNOLOGY

JAIPUR

January 2020

DECLARATION

I, **Ranjeet Kumar** (Enroll. ID: 2015REE9001) declare that this thesis titled, **"FAULT LOCATION IN ACTIVE DISTRIBUTION SYSTEMS"** and the work presented in it, is my own, under the supervision of Dr. D. Saxena, Department of Electrical Engineering, Malaviya National Institute of Technology, Jaipur (Rajasthan), India. I confirm that:

- This work was done wholly or mainly while in candidature for Ph.D degree at MNIT Jaipur.
- No any part of this thesis has been submitted for a degree or any other qualification at MNIT Jaipur or any other institution.
- Where I have consulted the published work of others, this is clearly attributed.
- Where I have quoted from the work of others, the source is always given. With the exception of such quotations, this thesis is entirely my own work.
- I have acknowledged all main sources of help.
- The thesis is based on work done by myself.

Date: *January 2020*

Ranjeet Kumar
(2015REE9001)

CERTIFICATE

This is to certify that the thesis entitled **"FAULT LOCATION IN ACTIVE DISTRIBUTION SYSTEMS"** being submitted by Ranjeet Kumar(Enroll. ID 2015REE9001) is a bonafide research work carried out under my supervision and guidance in fulfillment of the requirement for the award of the degree of **Doctor of Philosophy** in the Department of Electrical Engineering, Malaviya National Institute of Technology, Jaipur, India. The matter embodied in this thesis is original and has not been submitted to any other University or Institute for the award of any other degree.

Dr. D. Saxena

January 2020

Supervisor & Associate Professor
Department of Electrical Engineering
Malaviya National Institute of Technology Jaipur

DEDICATIONS

This thesis is dedicated to my parents for their ever loving support over the years.

ACKNOWLEDGEMENTS

This doctoral thesis would not have been possible without the help and support of the kind people around me, to only some of whom it is possible to give particular mention here.

Foremost, I would like to express my deepest gratitude to my research supervisor, ***Dr. D. Saxena***, for her valuable guidance, scholarly inputs and consistent encouragement. This work is possible only because of the unconditional moral support provided by her. I had a great freedom to plan and execute my ideas in research without any pressure. This made me to identify my own strength and drawbacks, and particularly boosted my self-confidence. Thank you again for your care and kindness.

I feel profound privilege to thank ***Prof. Udaykumar R. Yaragatti***, Director M.N.I.T Jaipur for providing me an opportunity to work towards my Ph.D. degree and for excellent infrastructure facilities in the institute.

My heartily thanks goes to ***Prof. Rajesh Kumar***, Head, Electrical Engineering Department for extending all the necessary support and providing a healthy research atmosphere in the department. I thank all the faculty members of the department for their continuous encouragement and moral support, which motivated me to strive for better.

I wish to express fruitful thanks to ***Prof. Harpal Tiwari***, ***Dr. Prerna Jain***, ***Dr. Satyanarayana Neeli***, and ***Dr. Vijayakumar K***, members of Departmental Research Evaluation Committee, for the inspiring discussions and fruitful suggestions that enhanced the quality of my research work.

I would also like to thank the technical and support staff of the department for their support and help, whenever I needed.

Special thanks to my colleagues with whom I have enjoyed my past four years, especially ***Satyendra Singh*** and ***Vivek Prakash*** for their friendship and unconditional moral support. It was an immense pleasure to work alongside with them.

I would like to express profound gratitude to my family members for all they have undergone to bring me up to this stage. I wish to express gratitude to my

parents for their kind support, I would like to thank my wife for the continuous support and belief on me. You always motivated me like true friend and helped me to do best in every situation and finally, much love to my little daughter.

At end of my thesis, it is a pleasant task to express my thanks to all those who contributed directly or indirectly in many ways to the success of this study and made an unforgettable experience for me.

Ranjeet Kumar

ABSTRACT

The reliable electricity supply is now imperative for the utilities to retain/attract customers in deregulated electricity market. The addition of Distributed Generation (DG) sources into the distribution system have changed its nature from passive to active thus, making the fault location process even more difficult at distribution system level. The customers are mostly connected to the distribution system, therefore, in recent times there is a growing interest among power system engineers and researchers to develop fault location methods for distribution systems. The prime focus of this thesis is to explore, and further develop methods for fault location in distribution systems, with possible presence of DG units and PEV charging loads. Moreover, the developed methods should be simple, and the use of measurement units and communication channels from locations other than the substation should be kept at minimum. Finally, the developed fault location methods should be applicable for a general network.

Although the Plug-in Electric Vehicles (PEV) use is increasing day by day as it provides viable alternate to concern associated with the conventional vehicles, but integration of PEVs to the distribution system for charging purpose will pose operational difficulties to the distribution grid. Assessment of the impact of PEVs charging on a distribution system during fault conditions is important for proper selection of protective equipments such as relays and circuit breakers, so that fault is removed as soon as possible and equipment's in the power system are protected from heavy fault current. The work done to study the effect of PEVs charging on the distribution system during fault conditions is limited, and as faults in the electric distribution system are a common occurrence, the impacts of PEVs charging on distribution system at different fault conditions are investigated in this work.

Fault data have been generated using simulations in the MATLAB/SIMULINK, where IEEE 34 node distribution system is simulated. A distribution system may have various appearances, as the total length, number of laterals, loading and other parameters may vary greatly, considering all these factors, IEEE 34 node distribution system is chosen as test system for this work. The chosen system is an actual distribution feeder situated in Arizona. This is a long and lightly loaded feeder with the main feeder of rated voltage level 24.9 kV and also has laterals with rated

voltage level of 4.16 kV. The IEEE 34 node test feeder has unequal lateral spacing with uneven load distribution and is an unbalanced system. The actual system is modified for this work and DG unit and PEV charging load are added to the system.

Two methods for fault location based on travelling waves, which combines travelling wave theory and application of discrete wavelet transform (DWT) for fault location in active multi-lateral distribution system have been developed. One method locates fault using the time difference between the initial or subsequent wave peaks due to reflection from the fault point and another method uses arrival time of first peak of current travelling wave at the line terminals for fault location. The developed schemes are capable of fault detection, fault type identification, faulted line segment identification, and fault location respectively.

A hybrid method which combines high-frequency transient method and impedance based method is also developed for fault location in this thesis. The fault generated high-frequency transients are used for faulted line section identification and after identification of faulted line section the exact fault location is estimated using impedance based method. The proposed hybrid method uses high-frequency transients for faulted line segment identification only, therefore, it does not require very high sampling rate for obtaining the high time resolution for identification of travelling wave peaks.

Several scenarios were simulated on the test system for checking the performance of developed algorithm. Various DWT mother wavelets were considered for processing of fault signals but db4 mother wavelet is selected for analysis of signals due to its orthogonality, compact support and its good performance in transient analysis of power system. Rule-based decision taking algorithms were developed for the fault detection and fault type identification tasks respectively. The fault detection algorithm verifies if a fault occurs or not, while the fault type identification algorithm identify the fault type and faulted phase(s) involved in the fault.

The developed fault location methods are promising and would serve as a useful tool for system operators to aid them in fault detection, fault type identification, faulted line section identification and exact fault location in an active multi-lateral distribution system, thereby helping to reduce system power outage time and improve the reliability of electric power supply.

Contents

List of Figures

List of Tables

Abbreviations

AI	**A**rtificial **I**nteligence
ANN	**A**rtificial **N**eural **N**etwork
BEV	**B**attery **E**lectric **V**ehicles
CT	**C**urrent **T**ransformer
CV	**C**onventional **V**ehicle
CWT	**C**ontinuous **W**avelet **T**ransform
DG	**D**istributed **G**eneration
DWT	**D**iscrete **W**avelet **T**ransform
EV	**E**lectric **V**ehicle
GPS	**G**lobal **P**ositioning **S**ystem
HEV	**H**ybrid **E**lectric **V**ehicles
IED	**I**ntelligent **E**lectronic **D**evice
IGBT	**I**nsulated **G**ate **B**ipolar **T**ransistor
LG	**L**ine to **G**round
LL	**L**ine to **L**ine
LLG	**L**ine to **L**ine to **G**round
LLL	**L**ine to **L**ine to **L**ine
LLLG	**L**ine to **L**ine to **L**ine to **G**round
NHTS	**N**ational **H**ousehold **T**ravel **S**urvey
PI	**P**roportional **I**ntegral
PEV	**P**lug-in **E**lectric **V**ehicle
PHEV	**P**lug-in **H**ybrid **E**lectric **V**ehicle

PMU	**P**hasor **M**easurement **U**nit
PWM	**P**ulse **W**idth **M**odulation
SNR	**S**ignal to **N**oise **R**atio
SVM	**S**upport **V**ector **M**echanism
TW	**T**ravelling **W**ave
TWR	**T**ravelling **W**ave **R**ecoder
WMM	**W**avelet **M**odulus **M**axima
WT	**W**avelet **T**ransform
WTC	**W**avelet **T**ransform **C**oefficients

Symbols

V_1	Aerial mode component velocity
V_0	Ground mode component velocity
C_0	Zero sequence line capacitance[F]
L_0	Zero sequence line inductance[H]
C_1	Positive sequence line capacitance[F]
L_1	Positive sequence line inductance[H]
R_f	Fault resistance[Ω]
θ_f	Fault Inception angle
E_j	Total energy of signal at scale j
E_{jk}	Wavelet energy at scale j and instant k
$D_{calc.}$	Calculated fault distance
D_{actual}	Actual fault distance
t	time[s]
v	Propagation speed[km/s]
ζ_{dp}	Fault detection threshold
m	modal components
(e_{a2}, e_{b2}, e_{c2})	WEE of phase A, phase B and phase C at scale 2 respectively
T^{-1}	Clarke transformation matrix
$i_{0,1,2}$	Aerial mode components
T_v & T_i	Transformation matrix
B	Susceptances
Z	Impedance

Chapter 1

INTRODUCTION

1.1 Perspective

An electrical power system consists of generation, transmission and distribution of electrical energy. All components of power system are susceptible to disturbances, but the transmission and distribution systems witness majority of these faults, that causes the system to operate outside the normal operating conditions. The electrical power system has grown rapidly over the last few decades which have resulted in increase in overhead lines (and underground cables) in operation and their total length. These overhead lines expand over long distances and are subjected to harsh climatic conditions such as storms, snow, lightning and other uncontrollable factors such as insulation breakdown due to improper maintenance, short circuits caused by trees, birds, animals or other external objects, which make them prone to faults [1]. Some faults are transient in nature and return to the normal operating state. These faults are called temporary faults and they cause minor damage on distribution system as they are self-cleared by de-energizing and re-energizing the line. Other category of faults is permanent faults, which will persist until the short circuit is identified and cleared. In case of permanent fault, distribution line may experience some mechanical damage which has to be repaired before the supply is

restored. Temporary faults, if not cleared within time will eventually convert into permanent faults sooner or later.

The main objective of the distribution system of an electric power system is to deliver the generated electricity to the customers with least interruptions. If a fault occurs in a distribution system along the feeder at any location or any of the lateral feeders, the feeder will be disconnected from the source by a circuit breaker, and thus the electricity supply to the customers along the main feeder is interrupted. It is estimated that 80% of all interruptions occur due to the faults in distribution networks [2]. We are living in a technologically growing world, deeply dependent on electric power. The power outages degrade the quality of supply leading to expensive failures of equipment which may unavoidably cost customers in lost time and revenue. Huge financial and economic losses are associated with power outages. As reported in the study [3] the average cost for an outage duration of 1 h is reported to be USD 3 for household, USD 1200 for commercial and USD 82000 for big industries. Hence, to reduce the effects of interruption time and restoration time, quick identification and location of fault with reasonable accuracy is very important.

Nowadays, the technological innovation, environmental policies, and restructuring of electricity markets, are changing the way in which conventional power system operates. The electricity providers have to ensure a reliable and un-interruptible power supply service to remain competitive to meet the strict reliability indices enforced by the regulatory bodies and to retain/attract the customers. The most effective way of achieving this is to have an efficient fault location technique that can minimize the inspection time and expedite the service restoration process. Moreover, recurrence of permanent faults and consequently major damage of the equipment can be prevented by accurately locating the temporary faults.

The global impetus to "Go Green", the evolution in prices of oil and gas, the increasing pressure to reduce emission of CO_2 gas and the economic incentives provided by policy makers are important factors leading to the massive deployment of

renewable energy generation system and the growing interest in transportation electrification. The introduction of new type of loads such as Electric Vehicle (EV), whose behavior is difficult to predict is another change in the distribution system. The penetration of the new type of generation i.e. distributed generation DG technologies along with the new type of EV load in the distribution systems has transformed the traditionally passive distribution systems into active distribution systems. This change in characteristics of distribution system from passive to active makes the existing fault location techniques for radial networks to be inefficient and ineffective. The massive integration of both DG and EV create stress on the distribution system by disturbing the voltage level of network, overloading of the components and disturbing the functioning of relays [1]. Thus, the emerging power system calls for accurate and fast fault location technique to detect and isolate the faults in the power system to fulfilling the global objective of maintaining the continuous power supply and reliable service to the customers.

1.2 Fault Location in Active Distribution System with EV Charging Load

The limited reserve of fossil fuels and their unbalanced distribution across the globe has led to the global energy crisis. In response to this worldwide emergency, it is important to change the current method of energy generation and utilization, which depends on petroleum products, to a sustainable mode with clean unconventional energy sources and low carbon emissions [4]. This concept of "green and clean energy" has led to vary fast growth of DG installation, directly integrated to the distribution systems. An electricity generation unit ranging in capacity from a few kilowatts to a few megawatts (micro to large) are termed as a DG and are typically interconnected at substation, distribution feeder, or customer load level [5]. DG technologies include fuel cells, photo-voltaic, wind turbines, micro turbines, gas

turbines etc [5]. Traditional distribution system is single sourced and radial with power flow in only one direction, downstream from the generating station to the load centers. Integration of DG to the conventionally passive distribution system changes it into a multi-source unbalanced active network. Fault location in a distribution system is accomplished by the protection system comprising of protective devices such as fuses, reclosers and relays. The protection system in traditional distribution system is designed on the assumption of unidirectional power flow i.e. assuming the system to be single source and radial. Traditionally, the protective devices are coordinated in a way that, the sections farthest from the substation isolates first, until the fault is cleared [6]. The presumption of uni-directional power flow, however, is not valid when DG units are integrated into the distribution system. A distribution system with DG is no longer a single source system and power can flow upstream the feeder, which affects the co-ordination and working of protective devices. Since the underlying assumption for the fault location techniques in DG integrated system breakdowns, the existing fault location techniques need to be re-evaluated in the presence of DG and new fault location schemes for active distribution system need to be proposed. Protection underreach, sympathetic tripping, unsuccessful clearing of faults, and unintentional islanding are the main issues related with the successful operation of DG integrated systems [7–9]. Currently, many utilities alleviate these issues by strictly limiting the capacity, location and number of DG units [7].

Another major factor contributing to global warming and air pollution is conventional Gasoline Vehicles (CV) emission. Electrical vehicles provide a promising solution to mitigate the harmful consequences of CV. Different types of EV, such as Battery Electric Vehicles (BEV), Hybrid Electric Vehicles (HEV), Plug-in Electric Vehicles (PEV) are available in the market as an alternative to CV. Due to the ability of these EV to increase the energy efficiency and decrease the dependency on oil in transportation the electric vehicle market has emerged in both developed and developing countries [10, 11]. Due to the environmental friendly nature of these EV as compared to the CV, the use of EV is being promoted by offering lucrative

economic incentives by the policy makers. Policy makers in different countries are launching new policies to provide a major push for creation of a viable ecosystem for growth of EV in that country. The prime focus of these policies is to allow the EV to become the first choice for the customers so that the EVs can replace CVs and thus, reduce the consumption of fossil fuels. In the not so distant future it is expected that large fleets of electrical vehicles are to be integrated into the distribution system. Although EVs will alleviate some of the concerns associated with the CVs, the increased use of EVs will create new challenges for the electric utility companies. Since, the EVs are new type of loads faced by the distribution system and their characteristic are largely unknown, the utilities will have to devise methodologies to adapt their system to it [12]. Research on the impact that EV may have on unbalance distribution system during fault and on the performance of fault location algorithm is very limited. As occurrence of faults in the power distribution network is a common event, therefore, the impact of EVs charging on distribution system at fault conditions and on fault location estimation is needed to be studied in detail.

1.3 Challenges of Fault Location in Active Distribution Systems

Accurate fault location has always been an area of extensive research in transmission system because they are accountable for bulk electricity transfer from the generation sites to load centers. Recently, in a deregulated environment fault location in distribution system has gained attention as the utilities are competing with each other to improve continuity indexes and avoid penalties if they fail to accomplish these indexes. Faults in distribution system are inevitable and since the economic repercussions are associated with them, a fast and accurate fault location is inevitable, but is not an easy task due to its complex and varying structure. While

impedance based and travelling wave methods are most commonly used for fault location at transmission level, distribution feeders are usually protected by a non-directional overcurrent relay. The power distribution systems differ from the transmission systems by some important characteristics therefore, fault location methods developed for transmission systems are prone to errors when applied in distribution systems [13, 14]. A typical distribution network may consist of both overhead lines and underground cables. The conductors are non-homogeneous in nature because the cross-sectional area is not constant throughout the feeder length. As a result, the relationship between the measured impedance and the fault distance is not linear. The topology of the two networks is very different from each other, the distribution networks generally have a tree structure with the main feeder containing several laterals. Therefore, faults at different locations in the network can generate same impedance at the substation in such situations the estimated fault location may coincide with several possible fault locations, making it difficult to determine real fault location.

The integration of DGs to the distribution system affects the direction of power flow and the impact of EV charging load during the fault conditions on distribution system is largely unknown. The integration of new types of generation causes fundamental in the topological performance and the operational aspects of the traditional distribution systems. Additionally, the loads connected to distribution systems may be single phase or three phase and the load taps are typically found at irregular intervals all these cause the system to be unbalanced. Finally, the topology of a distribution system may be modified in different operating conditions. As a result it is important that updated information about the system topology is available at the substation for estimation of fault location. Thus the fault location in distribution system is a challenging task owing to the non-homogeneity of feeders, high number of laterals, many load taps and integration of new types of generation and load.

1.4 Motivation

Efficient fault location with minimum time and maximum accuracy is highly required to expedite service restoration and repair process thereby, helping utilities to reduce economic losses and to provide high quality customer service. It is also certain that distribution system of near future will depend on DG for continuous load support. The penetration of PEV in the distribution system will also increase significantly in the upcoming years.

The reliability and versatility of a fault location scheme are major factors which are considered before a scheme is selected for application in power distribution system. Literature survey of available work in the field of distribution system fault location has shown that most of the existing schemes have one limitation or another and thus, unable to detect faults under all possible conditions. Such as the impedance based method suffers from the problem of multiple fault position from the substation in a multi-lateral distribution system and its accuracy depends heavily on fault resistance and system loading whereas the travelling wave based methods faces difficulty in the configuration and location of fault transient detectors due to complexity in multi-lateral distribution system. The benefits of PEV come along with its adverse effects on power distribution systems. Very few works have been reported in the area of fault analysis of distribution systems in presence of PEV charging load and assessment of its impact on the performance of fault location algorithm.

Therefore, this work was motivated by the need to have in place, an all-round scheme capable of fault detection, classification and location in balanced/unbalanced multi-lateral power distribution system embedded with DG and PEV charging load.

1.5 Contributions

The major contribution of this thesis are following:

1. Analyzing the impacts of plug-in electric vehicle charging load on distribution system during unbalanced, balanced and open circuit faults.
2. The development of an efficient algorithm for fault detection and fault type identification in distribution system with DG and PEV charging load using Wavelet Energy Entropy of fault current and magnitude of ground mode component Wavelet Modulus Maxima.
3. The development of a single terminal travelling wave based fault location technique for multi-lateral distribution system with DG and PEV charging load.
4. The development of a two terminal travelling wave base method for fault location in multi-lateral distribution system with DG and PEV charging load.
5. The development of a hybrid method combining high-frequency transient based technique and impedance based technique for fault location in multi-lateral distribution system with DG and PEV charging load.

1.6 Thesis outline

The thesis is made up of eight chapters. Current chapter introduces major issues involved in fault location in active distribution networks. It analyses the involved problems in this area that motivated the work and based on that aim and objective of this thesis is given. The pictorial representation of the thesis structure is shown in Fig. 1.1. Colored boxes are used to show the flow of research objectives and theoretical background of the problem. White boxes indicate introductory

literature related to the proposed work. Light blue boxes indicate challenges, motivation and review of related works. Green boxes indicate the implementation of test system and modelling of PEV charging system in the proposed chapters. Blue boxes demonstrate the simulation results obtained for the fault analysis of PEV connected distribution system and for the proposed fault location methods. And the red boxes show conclusion, summary of significant findings and future scope of the work. Short descriptions of rest of the chapters of this thesis are given below.

Chapter 2 provides a comprehensive literature review on issues pertaining to fault location in active distribution system including the impact of PEV charging on distribution system. This chapter also provides a comparative analysis of different types of fault location technique for distribution system.

Chapter 3 presents modelling and simulation of IEEE 34 node test feeder and EV charging load including the bidirectional battery charger in SIMULINK. Details of the various components used in modelling the test feeder are presented and the load flow result comparison is done with the benchmark IEEE distribution sub-committee result in order to validate the simulation result obtained.

Chapter 4 describes fault analysis of IEEE 34 node distribution system in presence of plug-in electric vehicle charging load. The impact of PEV load at the time of fault in the system for both balanced and unbalanced fault condition is given in detail.

Chapter 5 introduces the fault detection and fault type identification method developed using Wavelet Energy Entropy (WEE) and magnitude of ground mode component Wavelet Modulus Maxima (WMM).

Chapter 6 deals with development of travelling wave based method for fault location in an unbalance multi-lateral distribution system in presence of DG and PEV load. Simulation results for both one terminal and two terminal method under verity of operating condition are presented.

Chapter 7 presents development of hybrid fault location method combining high-frequency transient method and impedance based method.

Chapter 8 contains conclusion and future scope of the work.

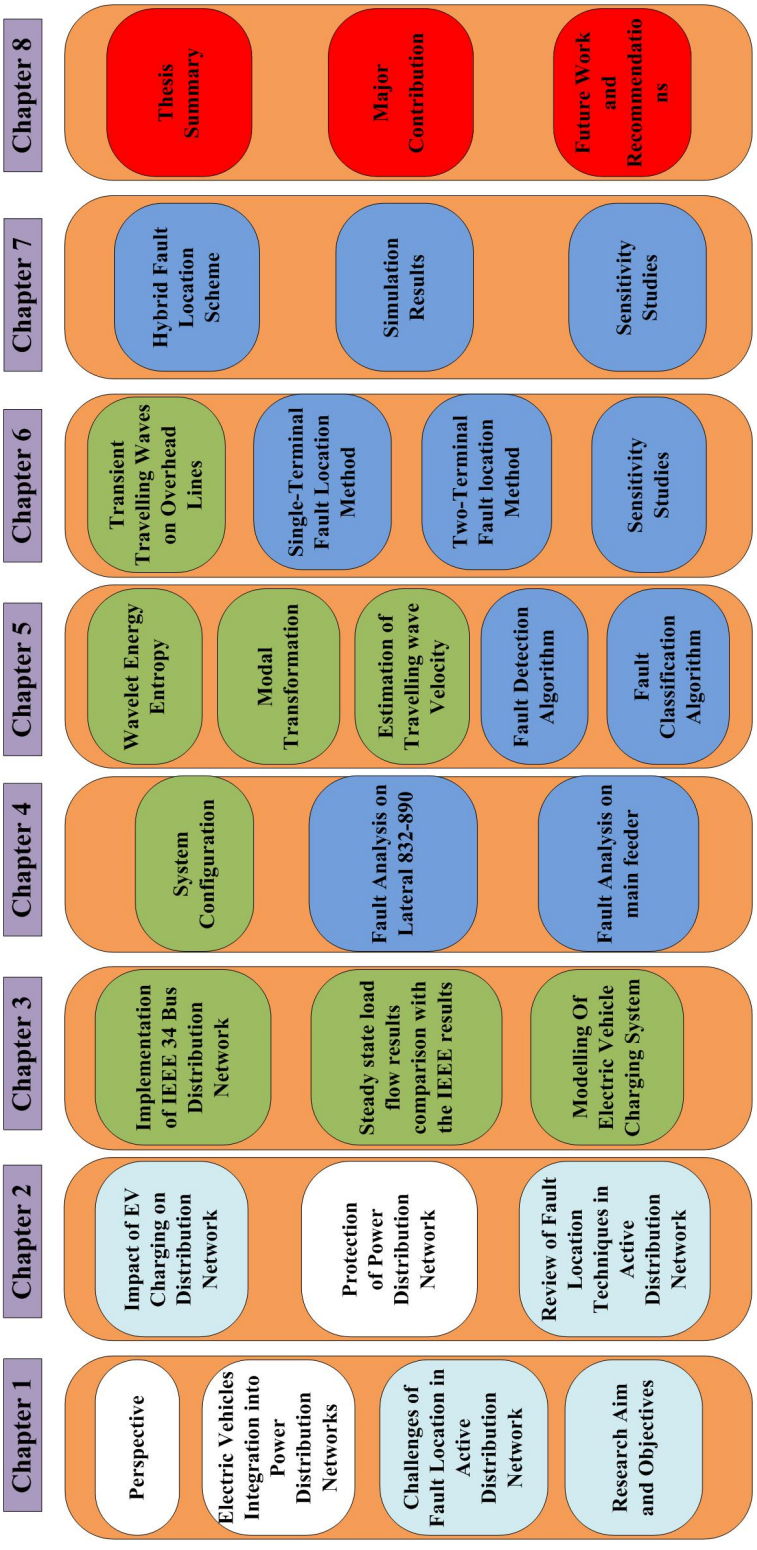

FIGURE 1.1: Thesis Structure

Chapter 2

LITERATURE REVIEW

2.1 Introduction

Electrical power distribution systems have expanded expeditiously and have become a complex network over the last few decades. The integration of Distributed Generation (DG) sources have turned the traditionally passive distribution system into an active system, which has resulted in several technical challenges for successful operation of protective devices in distribution system [1, 8]. Therefore, development of fast and accurate fault location algorithm for distribution system has become a challenging task for power system engineers and researchers.

Conventional protection systems prefer to disconnect DG sources from the distribution system in case there is a fault or any other disturbance in the system. This is done to retain the original coordination settings of protection devices by ensuring that there is no contribution to fault current by DG sources [15–18]. The practice of removing the DG from the network whenever a fault occurs makes DG supply and as a result the whole power system unreliable, this may also lead to possible blackout [19]. Furthermore, since the integration of DG to the distribution system is increasing, the unselective removal of healthy DG from the grid is not

recommended neither it is acceptable in a liberalized multi-player power supply market [20]. The connected DGs should have fault-ride-through capability to provide continuous power supply and improve system reliability [21].

2.2 Impact of PEV Charging on Distribution System

Assessment of the impact of PEV charging on a distribution system during fault conditions is important for proper selection of protective equipment's such as circuit breakers and relays, so that fault is removed as soon as possible and equipment's in the power system are protected from heavy fault current.

Much research has been done to explore the PEV charging effect on the distribution system and finding solutions to mitigate them. These works have been focused on understanding the effects of electrical vehicle charging system on distribution network voltage levels [22–25]. The integration of large fleet of PEVs to the power grid can have negative impact on the grid in the form of system losses, phase unbalances, harmonics, voltage drop, equipment overloading, the surge in power demand and stability issues [26, 27]. Large number of PEV load connected to the distribution system for charging purpose may overload the system components especially the distribution transformer. The impact of PEV charging on distribution transformer is studied in [28–30]. In reference [28] the ageing of a distribution transformer is studied with the help of National Household Travel Survey (NHTS) data. Work done in [29, 30] also conclude that large PEV charging load will have negative impact on distribution transformer life. Large penetration of PEVs to the distribution system and their uncoordinated charging may lead to the violation of safe voltage limits of the system [31, 32]. Phase unbalance can also occur in case of single phase AC charging of PEV loads [33]. Another problem associated with PEV charging is harmonics injection in the power grid. Charger required for PEV

charging operation contains power electronic switches which introduce power quality issues in the distribution system [34]. Research in the area of electric vehicle charging is also focused on development of fast charging methods to reduce losses and also to optimally utilize PEVs for supporting the grid [35, 36]. But the work done to study the effect of PEVs charging on the distribution system during fault conditions is very limited. In [37] a qualitative fault analysis in the presence of PEVs is done on a small model of 5 bus distribution system. In [38] the impact of PHEVs charging system on distribution system during fault conditions is studied on IEEE 13 bus system. In this work, a switching voltage of high-magnitude is detected during the time of fault recovery.

2.3 Protection of Power Distribution System

The prime objective of an electric power distribution system is to provide energy to the consumers in an economic, secure and reliable way. Primary and secondary distribution feeders are backbone of distribution network to deliver power from source to load centers. The distribution networks generally experience shunt faults [1]. The most common relays used for detecting and locating the faults in a distribution network are , (a) Phase-overcurrent relays and (b) Ground-overcurrent relays [39–41]. Distance relays are also sometimes used in a special condition such as for feeders which have a substantial generation or low fault current to load current ratios.

2.3.1 Shunt Faults

Among the different power system facilities, the distribution feeders are prone to faults more often than others. Primary reason for the line faults is insulation failure resulting in single line to ground faults and multiple line short circuits. For a three-phase overhead line, shunt faults are categorized as follows

1. Single phase-to-ground faults
2. Phase-to-phase faults
3. Two phase-to-ground faults
4. Three phase faults
5. Three phase-to-ground faults

2.3.1.1 Single Phase-to-Ground Faults

Single phase-to-ground faults are experienced in overhead lines when any one phase of the three-phase(s) comes into contact with the ground. Such types of faults has highest percentage of occurrence among all type of fault. Fig. 2.1 depicts the electrical circuit for a single phase to ground fault with phase A being the faulted phase. In this figure R_f is the fault resistance which includes the arc resistance and ground resistance of the contact between the conductor and the ground.

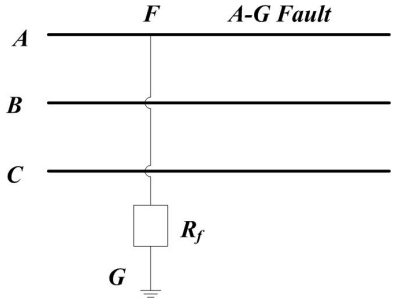

FIGURE 2.1: Single phase-to-ground fault on a three-phase line

2.3.1.2 Phase-to-Phase Faults

Phase-to-phase faults occur when there is a short circuit between any two phases, caused by the ionization of air, or when any two phase(s) comes into contact with each other. These faults can be divided into two categories, one is phase-to-phase faults where only any two phases are short-circuited to each other and another

is phase-to-phase to ground fault where the any two phases are short-circuited with ground as shown in Fig. 2.2.

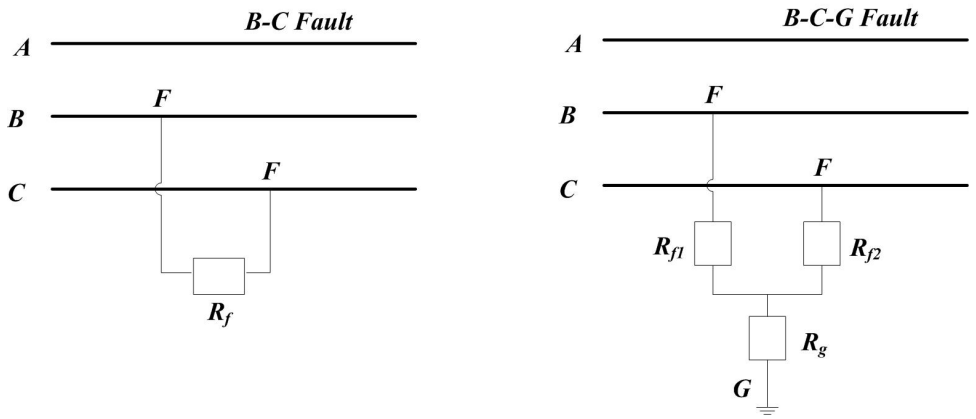

FIGURE 2.2: Phase-to-phase faults

2.3.1.3 Three Phase Faults

A three phase fault is described as a condition when all the three phases comes into contact with each other. These faults can also be divided into two categories, one involving ground and other not involving ground as shown in Fig. 2.3. Three phase faults are also called balanced fault because they generally have equal fault resistance in the three phases. Roughly 2-3% faults in the overhead lines are balanced faults.

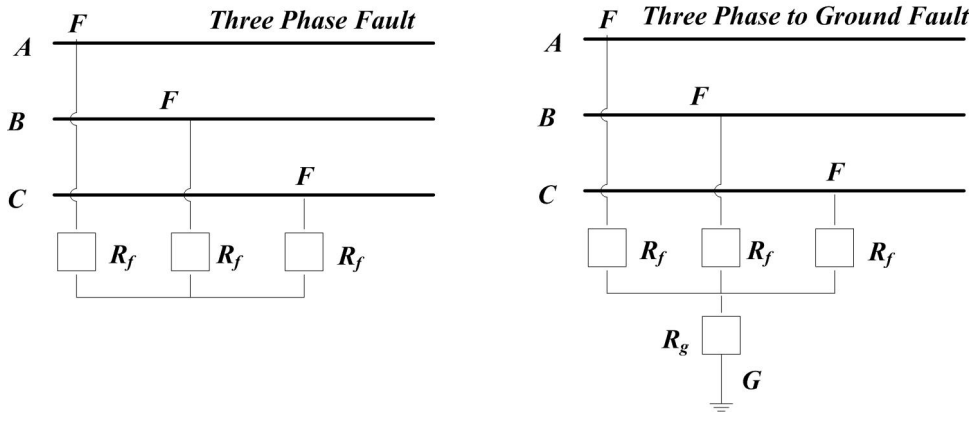

FIGURE 2.3: Three phase faults

2.4 Review of Fault Location Techniques in Active Distribution Systems

Faults on distribution feeders are caused by many events such as storms, lightning, insulation breakdown and short-circuit by a tree branch or any other external object. These faults could either be temporary or permanent faults. The temporary faults are self-cleared but in case of permanent faults the distribution lines experience some mechanical damage, which require to be repaired before the line could be restored. This restoration process can be accelerated if the fault location can be estimated with reasonable accuracy [1]. Therefore, an accurate fault location scheme plays an important role in reliable and fast restoration of power distribution network.

In recent times several techniques for fault detection and location in active distribution systems have been proposed. Fig. 2.4 depicts classification of fault location techniques. An appropriate fault location technique for DG integrated system should have the ability to locate fault under bi-directional power flow as is the case in presence of DG. The fault location techniques proposed are specifically classified in following subsections.

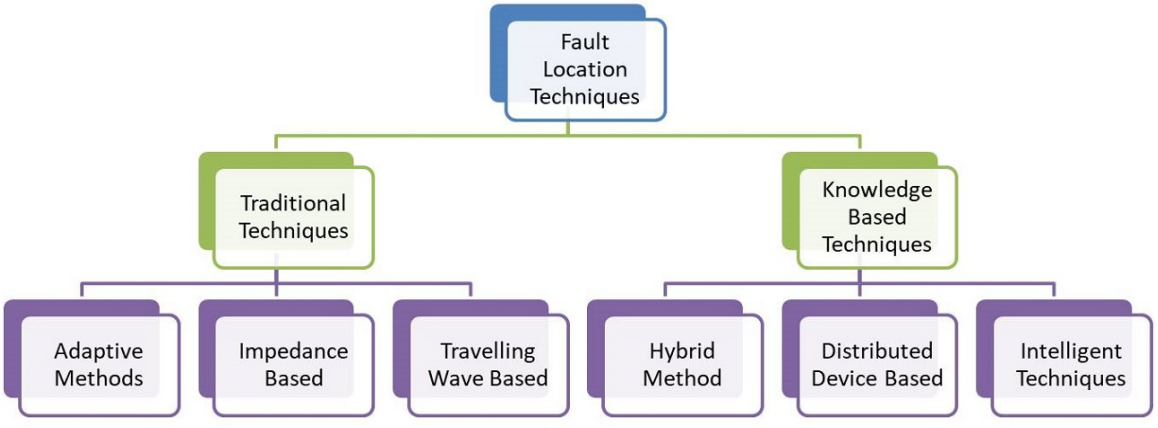

FIGURE 2.4: Classification of fault location techniques

2.4.1 Adaptive Methods: Proposed Schemes and their Challenges

In adaptive schemes the basic idea is to continuously adjust the setting of relay according to the present system state. This concept has been applied by many researchers for resolving protection coordination problems associated with DG integration [42–44]. Whenever there is a change in system state such as a generator is connected or disconnected or any switching action is made, the relay settings are re-calculated by the central computer and communicated to the individual protection relays. Such fault location schemes are economical as it retains the traditional protection structure and avoid new investment. These methods calculate optimum system setting, location and size of DGs and also the DG penetration level for minimizing the events of protection failure and improving system reliability. However, the choice of obtaining these optimal operating conditions are not always available in practice and such operating conditions can actually neutralize the very principle and benefits of distributed generation. An adaptive method based on optimized thevenin equivalent parameters estimation is presented in [45] where the sampled local measurements are utilized to obtain the thevenin equivalent circuit parameters and to mitigate the impact of DGs on the protection devices, an online method of fault current calculation under various system operation conditions is used. In [46] change in protection settings with load variations is suggested. A method which replaces all fuses by reclosers on a distribution feeder and utilizes conventional equipment for protection is presented in [47]. The limitation of this scheme is obviously the high installation cost of a recloser in each branch. In [48] the voltage and current are monitored at various points along the distribution feeder through a central protection device. Tripping signal is provided to reclosers and breakers after detecting and locating a fault by the central device. Reclosers and breakers operates before any of the fuses operate, this results in fuse saving. The main demerit of this scheme is that it heavily depends on the central unit and communication system to make a decision. In [49] a transfer trip scheme is presented which observes the status of all breakers

on the distribution line. When any detection about one of them being open is made, the generators downstream to that breaker receives tripping signal thus, unnecessary islanding of a section is prevented. Authors in [50] present an adaptive scheme utilizing the conventional relay-recloser-fuse structure. The relay operation is based on the algorithm that uses current measurement at all recloser and fuse positions to find all possible locations of DGs and then depending on the relative current magnitudes, operates the recloser to sustain recloser-fuse coordination. However, this method is effective in low level of DG input because at high level, the fault current falls beyond the recloser-fuse coordination setting. Methods proposed in [44, 51] adjust the settings of the protection devices whenever a DG goes offline or comes online or on information about the network configuration to maintain coordination among the protection devices. However, the system may lose protection during the time of calculation of the new settings and network reconfiguration.

The limitations of adaptive protection schemes are following

- The setting of the protective devices which are utilized in the distribution system needs to be continually adjusted according to the current system state.
- These techniques depends heavily on optimal location, capacity of DGs and penetration level, however in practice these choices might not be available.
- Most of the methods employ a central computer for adjusting the setting of protection devices as per the system condition to retain coordination, but coordination may not remain during the time of calculation of new settings.
- The requirement of communication and measurement infrastructure may be expensive.

2.4.2 Impedance Methods: Proposed Schemes and their Challenges

The impedance base method calculates the impedance of faulted line segment which is considered to be a measure of the distance to fault. The Impedance measurement based method utilizes the fundamental frequency component of voltage and current together with line parameters for determining the fault location. Depending upon the data input signals, these methods can be further classified into either single ended method or double ended method [52, 53]. The major advantage of single ended methods is that they do not require any communication means and can be implementation easily into digital relays. However, if communication means are available then more accurate estimation of fault location can be obtained with the help of double ended methods, where measurements are available from both ends of the line. The basic system model for fault location using impedance based method is depicted in Fig. 2.5 and the basic equations used in fault location is given below.

$$V_G = mZ_L I_G + R_F I_F \tag{2.1}$$

$$Z_{FG} = \frac{V_G}{I_G} = mZ_L + R_F \frac{I_F}{I_G} \tag{2.2}$$

Where, V_G is voltage at the terminal G, Z_L is the line impedance between the terminal G and H, m is distance to fault, I_G is the line current from terminal G, R_F is the fault resistance and I_F is the total fault current.

The fault location techniques using impedance measurement exhibits several advantages and are the most popular in real implementation in both overhead transmission and distribution lines. Work done in [54–57] presents fault localization method where measurement are taken from one end only. In [54] the impact of both the load and remote infeeds are considered on the fault location. F. M. Aboshady et al., [56] proposed sequence components method for fault location in a 11 kV feeder network, the method considers non-homogeneous feeder sections, fault resistance,

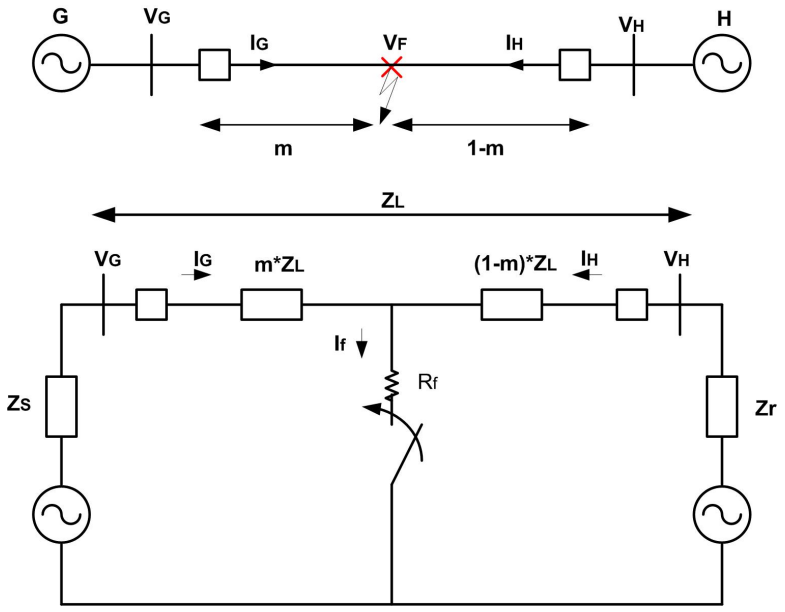

FIGURE 2.5: Basic model with system parameters

various types of faults, load distribution and high DG penetration level. Authors in [57] presents a fault location technique considering various uncertainties associated with the system such as variations in fault resistance, fault type and load magnitude. The DG power is accounted for by measuring the current which feeds the fault. A phase-to-phase fault location method is presented in [58]. In this method, measurement are taken at the main supply and at the DG supply, the network is divided into two sections one before DG connection and the other after DG connection, also special measure have been taken to reduce residual errors in the section before DG. Work done in [59] presents an impedance-based fault location method for unbalanced DG systems with low level of DG penetration, improving upon this work [60] proposes a fault location scheme for unbalanced distribution system based on positive sequence apparent impedance, the fault location algorithm is iterative in nature, the algorithm starts searching for possible fault location from the starting point of the feeder and runs till it converges, where it obtains an estimation of fault location. Method presented in [61] uses synchronized phasor data obtained by GPS and digital fault recorders during the fault for estimation of distance to fault. S.M.

Brahma [62] illustrate a method for fault location in a multi-source unbalanced system using thevenin equivalent of source. The scheme assumes that the waveforms obtained from all digital fault recorders are available as synchronized phasors. Table 2.1 presents comparative analysis of some of the key references.

TABLE 2.1: Comparative analysis of impedance based methods

Reference	**Network Model**	**Fault Type**	**Type of Diagnosis**
J.J. Mora Flórez et al., [57]	IEEE 34 node system, variation in load model, DG	All shunt fault type	Fault type, faulted section, fault location estimation
S.M. Brahma [62]	Actual 12.47 kV distribution system, constant power load, DG	LG, LLG, LLL	Faulted section, fault location
S.F. Alwash et al., [61]	IEEE 34 node system, constant impedance loads, DG	All shunt fault	Exact fault point estimation amid multiple candidates by voltage matching
M. T. Hagh et al., [58]	9 bus system with single phase and three phase laterals	Phase-to-Phase fault	Fault location
F. M. Abo-Shady et al., [56]	11 kV feeder	LG, LLL	Fault location
A. S. Bretas et al., [59]	13.8 kV distribution line, Synchronous generator DG	Grounded fault	Use of positive sequence apparent impedance for fault location
J.U.N. Nunes et al., [60]	12 buses distribution feeder, DG	Phase-to-phase fault	Fault location using pre fault analysis

Some challenges related with the implementation of these techniques are as follows:

- As the impedance based fault location techniques depend on fundamental frequency components of voltage and current, the harmonics and transient nature of current can create difficulty in accurately extracting the fundamentals.
- Fault resistance and system loading may create serious errors in the measured impedance which results in erroneous fault location estimation.

- In multilateral distribution network these schemes suffers from the problem of multiple fault position from the substation in the system.
- Fault events having small duration presents a challenge, due to short data window more analysis is required to get accurate results. For long duration fault, the fault location estimate gives better result.

2.4.3 Travelling-Wave Methods: Proposed Schemes and their Challenges

As the accuracy of impedance based methods for fault location depend heavily on system parameters, slight variation in system condition such as change in line loading, fault type, inception angle, fault resistance and source parameter of the network, results in inaccurate estimation of fault location [63]. For these reasons, the travelling wave based fault location techniques are increasingly used as an alternate to overcome the drawbacks of impedance-based methods, since their fault location estimation accuracy depends mainly on the sampling rates of data acquisition and time synchronization [64, 65]. The underlying concept of travelling wave-based fault location methods is to utilize the relationship between backward and forward travelling waves propagating along the line when fault occurs. The different power system events, such as line faults, switching maneuvers, and lightning strokes induces the transient travelling-waves in overhead lines [66]. The lattice diagram shown in Fig. 2.6 is generally used to depict the different propagation pattern of travelling waves. In Fig. 2.6 fault is assumed to occurred at a distance d from the node A, t_a is arrival time of first travelling wave peak at terminal A and t_b is the arrival time of first travelling wave peak at terminal B. In case of a fault, the originated travelling-wave travels in both directions at a speed very close to speed of light, until it arrives at the line terminals [67]. By detecting these impulses and determining the time difference between the arrival of an impulse and its reflection or by comparing the arrival times of the two impulses (wave fronts) at the respective terminals of a line, the location

of a fault can be determined if length of the line and the propagation velocity of travelling waves are known. Travelling waves based technique for fault location has been widely used in transmission systems and its application in distribution systems has also been explored in the past.

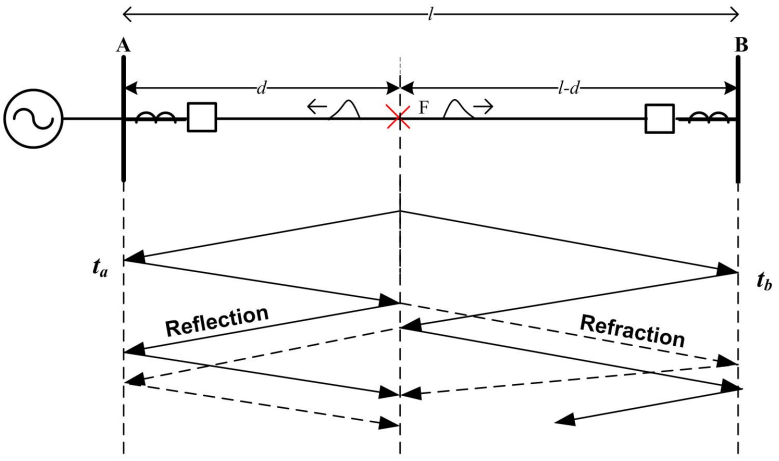

FIGURE 2.6: Lattice diagram showing propagation pattern of travelling waves

Travelling wave based fault location approaches for distribution system proposed in [68–73] uses single-terminal recording of fault generated travelling wave. These methods utilize either CWT or DWT analysis of voltage transients for extracting fault information. The method proposed in [70] uses travelling wave recording in radial distribution network for fault location. In this work, depth search method is applied to determine exact location of fault from multiple-candidate in the multi-lateral distribution system. K. Jia et al. [72] proposed a fault location method in distribution system using high-frequency transient method, here the influence of DG on fault location is avoided by using short window measurement. The technique proposed in [73] uses travelling wave information obtained from multi-measuring points in the distribution network for fault location. Two terminal methods using synchronized data for fault location are presented in [74–77]. In [74] the degradation of distribution feeders is identified by monitoring the generated travelling wave due to the sub-health condition of feeder in real time so that permanent fault conditions can be avoided. The method proposed in [75] consists three measurement points,

one at the mid-point of line and other two measurement point at the two terminals of the line. The measurement at mid-point records the time tags of the subsequent wavefronts to avoid time synchronization requirement. A directional protection using Rogowski coil is presented in [76] and the method proposed in [77] uses the first arrival time of travelling waves at each terminal is applicable in multi-terminal DC network. Comparative analysis of key references on travelling wave based method is presented in Table 2.2.

TABLE 2.2: Comparative analysis of travelling wave methods

Reference	**Network Model**	**Fault Type**	**Type of Diagnosis**
L. Rui et. al., [68]	Radial distribution network of 110kV	Grounded, ungrounded fault	BP neural network based velocity estimation, fault location using the difference in velocities of zero mode and aerial mode
A. Borghetti et al., [69]	Reduced-scale experimental setup	Phase to phase fault	Integrated time-frequency wavelet decomposition of the voltage transients
M. P. Nakhli et. al., [71]	6-bus distribution system loads, DG	Phase to ground fault	Path characteristic frequency-based fault location
K. Jia et al., [72]	IEEE 34 node distribution system	Phase to phase fault	Fault location using Impedance measurement at high frequency
M. Goudarzi et. al., [73]	IEEE 34 node distribution system	Shunt faults	DWT based fault section identification, fault location using difference between arriving times of voltage transients
J. Ding et al., [75]	220 kV power system model	Shunt faults	Distributed fault-location unit base fault location without time synchronization
D. Wang et al., [76]	500 kV power transmission system model	Phase to ground fault	Travelling wave directional protection using electronic transformers
Q. Lin et al., [77]	DC Network	Not specified	Graph theory and travelling wave method

For a travelling wave based technique, the key factors influencing the accuracy of fault location are as follows:

- Small fault inception angles and faults close to the place of fault locator installation affect the accuracy of travelling wave fault location estimation.

- There is a need of accurate synchronization of devices in case of double ended travelling wave fault location schemes.
- In case of multiple discontinuities (reflection points) in distribution system, errors associated with detecting travelling wave.
- Difficulties in the configuration and location of the fault transient detectors due to complexity in distribution system.

2.4.4 Distributed Device based: Proposed Schemes and their Challenges

In smart grid environment, wide area protection is often employed for fault location. Wide area protection can share the field devices and communication system with the distribution network automation system [78–80]. Traditional protection system is usually centralized control, where breakdown of central computing unit or a communication channel will disable the protection of whole network. Hence a distributed protection scheme has its advantage as problem at one node causes failure of local protection only. Protection scheme utilizing distributed architecture using devices such as Phasor Measurement Unit (PMU), Intelligent Electronic Devices (IEDs) and Relay Agents are introduced in distribution systems to improve fault detection and location.

PMU based fault location schemes are proposed in [81–84], the schemes proposed in these works uses PMUs to improve the observability of distribution system under both normal condition and faulty condition. Knowledge of voltage signals at both end of the lines and the current at either end of the lines during faulty condition are used for fault location purpose. The proposed methods give good accuracy but none of them have considered DG in the distribution system. IEDs based fault location scheme is presented in [85, 86]. In [85] advanced metering infrastructure (AMI) based centralized fault management system is introduced, from this

system fault currents of the sources and fault voltage profile of buses are gathered for state estimation of the system these estimation are processed in order to have real-time monitoring and fault location estimation. This technique requires advance infrastructure with measurement at number of location in the distribution system. Authors in [86] proposed a wide area protection scheme using advance feeder terminal units (AFTUs) for fault zone location and faulted section identification, the scheme is dependent on DG capacity. Multi-agent based methods for fault location is proposed in [87–89]. An agent can be called as an intelligent device which is capable of taking independent action (protection in this case) within an environment to achieve the desired objective. In [87] entropy value calculated from the wavelet coefficients of the measured current signal is used to identify and isolate the faulty segment of distribution system with DGs, the relay agents are installed at the boundary of network sections. J. Ghorbani et. al., [88] proposes a multi-agent system in which an agent communicates with its neighboring agents and uses the local differential current information to detect and isolate the faulted section in distribution system with 50% DG penetration level. Work done in [89] also proposes agent-based protection method utilizing wavelet technique in which the relay agents acting as protection devices are used to determine the faulty section. Table 2.3 shows comparative analysis of key references.

The key issues related with the deployment of such devices in the distribution system are as follows

- Advanced communication infrastructure is required for sharing network information between the devices, which is costly.
- For optimally placing PMU or other intelligent devices it is often required to run some optimization algorithm.
- Such schemes often use a central computer to process the data obtained from distributed devices in the network, failure of which may result in loss of protection.

TABLE 2.3: Comparative analysis of distributed device based methods

Reference	Network Model	Fault Type	Type of Diagnosis
A.M. El-Zonkoly [87]	66 kV distribution network	Shunt faults	Fault classification, faulted line, fault location
J. Ghorbani et al., [88]	Feeders of West Virginia super circuit	Shunt faults	Identification of faulted zone, fault type and fault location using MAS system with 50% DG penetration
J. Cordova et al., [85]	IEEE 37 node test feeder	Shunt faults	Advanced Metering Infrastructure (AMI) and other IEDs based fault location identification
M. Xu et al., [86]	10 kV distribution network	Not specified	Fault location using AFTUs and IEDs
N. Parera et al., [89]	CIGRE MV benchmark network, constant impedances load	All shunt fault	Faulted section identification
K. Mazlumi et al., [83]	41-bus 230kV network	Grounded faults	Less number of (PMUs)are used for fault location

2.4.5 Intelligent Techniques: Proposed Schemes and their Challenges

An intelligent fault location technique relies on artificial intelligence and mathematical techniques for fault detection and location. These techniques comprise of wavelet based methods, artificial neural network (ANN) based methods, fuzzy based methods and statistical learning theory based methods. The wavelet based schemes generally locate fault by analyzing high frequency transients in the fault current or voltage signals with the help of suitable mother wavelet. Method proposed in [90] estimates the fault point and faulted section by using the transient fault current wavelet coefficients recorded at the interconnecting points of the network. In [91] separate schemes are proposed for fault classification and fault direction identification. The scheme has a wider application and gives high speed protection. A scheme based on modern communication arrangement is proposed in [7]. The scheme has a master-slave structure which is substation oriented, it has the capability of providing

protection to entire distribution system with high DG penetration level. The application of ANN based methods in distribution system is done by H. Zayandehroodi et al., in [92] they proposed a two stage radial basis function neural network (RBFNN) based method to locate fault distance and to identify the faulted line segment, the first stage RBFNN is used to estimate the fault distance from each source and the second stage RBFNN is used to determine the exact faulted segment. In a later work the author's uses same methodology only the RBFNN function is replaced by Radial Basis Neural Network function learning algorithm with Optimum Steepest Descent for faulted segment identification [93]. In [94] a Multilayer Perceptron (MLP) neural network scheme for fault localization and classification is presented, the algorithm uses proportion of injected supply current as input for training of neural network. A multi class Support Vector Mechanism (SVMs) based approach is presented in [95]. SVM is a statistical learning theory based method, the proposed approach uses offline data generated from load flow for training the SVM and online calculation are done for fault location and diagnosis. The approach shows good accuracy but requires retraining of SVM whenever there is a change in system topology. Table 2.4 presents comparative analysis on intelligent methods.

Implementation of intelligent techniques for fault location suffers from the main challenges listed below

- Choice of mother wavelet, support size and noise in the signal affects the performance of wavelet based methods.
- The ANN based methods highly depend on the amount and the quality of training data provided to ANN algorithm. A limited or inaccurate training data can affect the accuracy of fault location algorithm.
- Other problems with AI based method are slow convergence in the training process, also the algorithm requires to be retrained every time there are changes in the system state.

- The performance of SVM suffers when dimension of input vector is large because in such condition it is difficult to find the optimum solution due to large sizes of the data set.

TABLE 2.4: Comparative analysis on intelligent methods

Reference	Network Model	Fault Type	Type of Diagnosis
G. Celli et al., [90]	Typical rural distribution network	Grounded faults	To find direction and location of fault, wavelet coefficients of transients faults are utilized
Hadi Zayandehroodi et al., [92, 93]	20 kV 32-bus distribution system	Shunt faults	Fault classification, faulted line, fault location
S. A. M. Javadian et al., [94]	22-bus, 20 kV distribution network	Shunt faults	To determine type and location MLP neural network is used
M. A. Figueroa et al., [91]	33-kV distribution feeder	Shunt faults	Discrete wavelet transform for identification and classification
R. Agrawal et al., [95]	Practical distribution feeder emanating from 132/11kV-grid substation	Shunt faults	Fault location and diagnosis in distribution network in presence of DGs, using multi-class SVMs

2.4.6 Hybrid Methods: Proposed Schemes and their challenges

The hybrid methods for fault identification and location are adopted to develop a novel method which exploits the benefits provided by the incorporation of more than one fault location methods. The idea is to utilize the strengths of individual methods while restraining the shortcomings. Some techniques using hybrid methods for fault location in distribution network have been proposed till now [96–105]. These methods generally use artificial intelligence techniques along with advanced signal processing techniques to extract fault information from the recorded signals and locate fault. Work done in [96] proposes a method combining wavelet theory and

fuzzy logic for islanding detection and fault location in distribution systems with distributed generations, the method claims to be very fast and detects fault within 10 ms from its inception. A. Rafinia et. al., [97] presents a method combining artificial neural network (ANN) and fuzzy logic for fault location in three phase underground distribution system, wavelet is used for feature extraction from the simulated data. The method is tested under various conditions like load shedding, load increase and load unbalance, also the method is tested against the effect of DG addition to the network. Hybrid methods combining ANN and support vector mechanism (SVM) are proposed in [98, 99]. Authors in [98] use ANN and SVM for faulted section identification and fault location respectively. Feature extraction is done using measurements obtained at substation, relay status and at circuit breaker. The data is analyzed using principal component analysis technique. This method robustness is tested under verity of conditions but the distribution system used does not contain any DG source. Whereas, the method proposed in [99] use ANN and SVM application for fault location in power transmission lines in presence of non-linear loads. In [100] a method based on wavelet transform and SVM is presented for locating fault in micro grid. In this the search space for faulted section identification is reduced by detecting the DG with the lowest harmonics and finally the faulted segment is determined using the wavelet and optimized multi-class support vector mechanism (OMSVM). Another method combining WT and SVM proposed in [101] is used for fault location in distribution network in case of high impedance faults. In [102] a hybrid method combining SVM and smart meters are proposed. Smart meters are used for providing data for training of SVM which are used for fault location purpose. A faulted section identification followed by fault location for distribution network with multiple branches based on WT and ANN is proposed in [103] in this paper, WT is used for faulted section identification and ANN is used for fault location. Fault location method using impedance based method and voltage sag matching algorithm in [104] is applicable for single phase faults only and the method proposed in [105] locates fault in an active distribution network using polarities of current transients. Table 2.5 presents comparative analysis on hybrid

methods.

Table 2.5: Comparative analysis of hybrid methods

Reference	Network Model	Fault Type	Type of Diagnosis
M. Dehghani et al., [96]	20 kV 5 km pi section distribution line	Shunt faults	Fault location in distribution systems with DG based on combination of wavelet singular entropy and fuzzy logic
A. Rafinia et al., [97]	20 kV underground power distribution system	Shunt faults	Combination of ANN and FLS to classify and locate fault
D. Thukaram et al., [98]	52 bus distribution system	Shunt faults	Combination of ANN and SVM forfault location and classification
E. Koley et al., [99]	400 kV three phase double circuit transmission line	Shunt faults	(SVM), ANN and Kalman filter based algorithm
S. Hamid Mortazavi et al., [101]	20-kV radial distribution feeder	High impedance fault	Stationary wavelet transform and SVM based fault location
M. Daisy et al., [104]	IEEE 34 node system	Single phase faults	Impedance based method combinedwith voltage sag matching
Amila Pathirana et al., [105]	230 kV transmission system and IEEE 34 node system	Not specified	Rogowski coil sensors based transient protection scheme

Some limitations associated with application of hybrid method in distribution system are as follows

- These methods generally use some AI technique therefore reliable modeling of the system is required to generate data for AI training.
- Application to distribution system is difficult because of network complexity, different conductor size and multiple branches.
- When two methods are combined decision regarding which relay output to be used for fault location requires careful decision making process.

TABLE 2.6: Comparative analysis of different methods

Techniques	Merits	Demerits
Adaptive methods	Provides correct settings for different operating conditions Retains the original protection setup hence economical	Communication system requirements which increases system cost Complex relay setting calculation in case of high DG penetration Requirement of modification in FL algorithm following an alteration in the system
Impedance based	Communication channels not required in one ended technique and simple utilization into digital protection relay More accurate results can be obtained with two ended method with communication channel	Multiple fault positions in multilateral distribution network Assumes homogenous network, error due to system loading and fault impedance
Travelling wave based	Very fast and accurate Independent of many system parameters	Needs high frequency data acquisition Requires very precise common time reference
Distributed device based	Provides continuous monitoring of system Distributed architecture of protection	Requires large investment Requirement of communication between the devices
Intelligent techniques	Possess characteristics such as fast learning rate, fault tolerant Able to deliver accurate output with partial input	Slow convergence, amount and quality of data provided for training Retraining of algorithm in case of system change
Hybrid methods	Exploits benefit of two or more methods	Requires careful decision making for relay output to be used Reliable models to create training data

2.5 Conclusion

From the reviewed references it can be observed that since each of the fault location method are developed considering specific topology and assumptions, none of them have the capability to solve all problems related to the fault location. Each method may solve problem of particular system depending on the availability of the

monitoring technology and complexity of the system. Such as, fault location based on intelligent techniques can be suitable for use in a distribution system which is equipped with monitoring equipment's. Whereas, impedance measurement techniques are more suited for single end measurement. Therefore, it can be concluded that the working principle of a fault location technique must be understood before its application to a specific system to use it effectively. Table 2.6 shown above presents the comparative analysis of all type of fault location method presented above.

Chapter 3

NETWORK MODELLING AND SIMULATION

3.1 Introduction

This chapter is focused on developing an accurate model of the distribution network test system and the electric vehicle charging load. The IEEE 34 node distribution system [106] is selected as the test system to evaluate the performance of the developed fault location schemes. A distribution system may have various appearances, as the total length, number of laterals, loading and other parameters may vary greatly, considering all these factors, among the available benchmark distribution feeder from the IEEE power engineering society distribution subcommittee, the 34 node distribution system is selected for this work, also it is the most versatile and widely used network for fault location studies. This distribution system is an actual feeder located in Arizona, USA. The IEEE 34 node distribution system is characterized by a nominal voltage level of 24.9 kV and it is an unbalanced system with uneven load distribution and unequal lateral spacing.

3.2 Implementation of IEEE 34 Bus Distribution System

The IEEE 34 node distribution system shown in Fig. 3.1 is implemented in MATLAB/SIMULINK. This is a radial distribution network having only one path for power flow from the source to the load centers. The distribution network is made up of one main feeder having total length of 57.7 km at a voltage level of 24.9 kV and eight side laterals. Of these side laterals four are single phase lines, three are three phase line and one lateral contains both three phase and single phase lines. All lateral operates at main feeder voltage level except lateral 832-890, which operates at 4.16 kV voltage level. It also contains two transformers, two voltage regulators, two shunt capacitor banks, six spot loads and nineteen distributed loads. The network was validated by performing a load flow calculation on the system and by comparing the results with the IEEE results shown in Table 3.1. The network elements consist of the following:

(a) Main feeder

(b) Side laterals

(c) Distribution transformers

(d) Loads

(e) Capacitor banks

(f) Voltage regulators

Detail parameter of each element of the network is provided in Appendix A

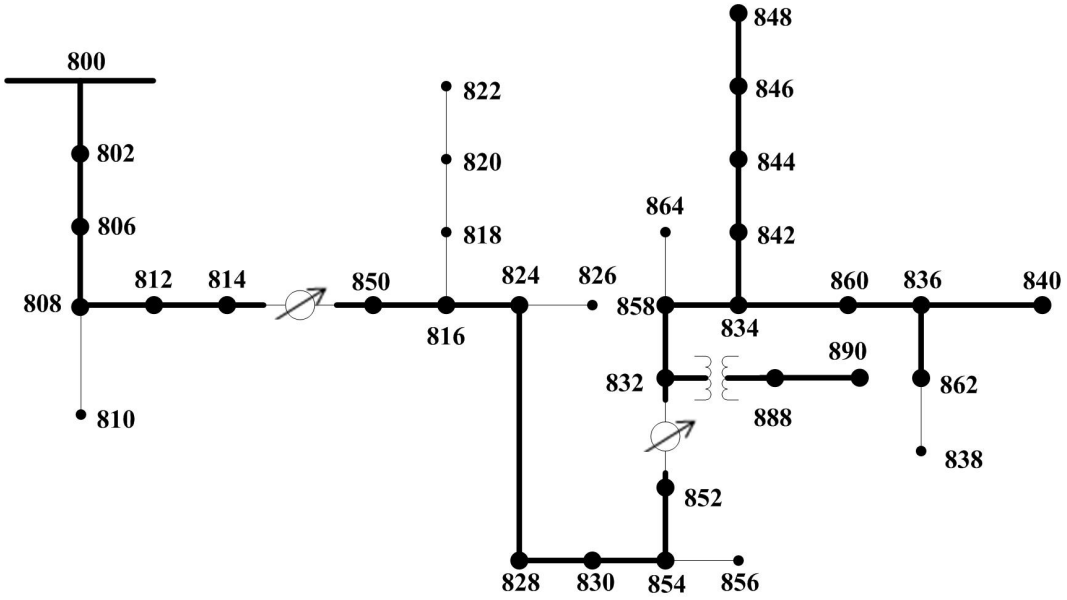

FIGURE 3.1: IEEE 34 node distribution system

3.2.1 Feeder Modelling

The distribution feeders are made up of five different overhead line configurations (300-304) and contain thirty line segments. The main feeder is modelled with configuration type 300 and 301 and the different single phase laterals are modelled using 302, 303 and 304 line configuration types. The distributed parameter line model has been used to model all the line segments. The input parameter of the line sections are positive and zero sequence impedances and shunt susceptances, which are obtained from impedance (Z) and susceptances (B) matrices using Carson's equation and Kron's reduction technique [107]. The test feeder modelled in SIMULINK showing various line segments is depicted in Fig. 3.2.

3.2.2 Load Modelling

The loads in IEEE 34 node distribution network is specified either as star or delta loads and modeled as constant power load, constant current load and constant impedance load. The sum of entire load on the network is 1769 kW, of which six

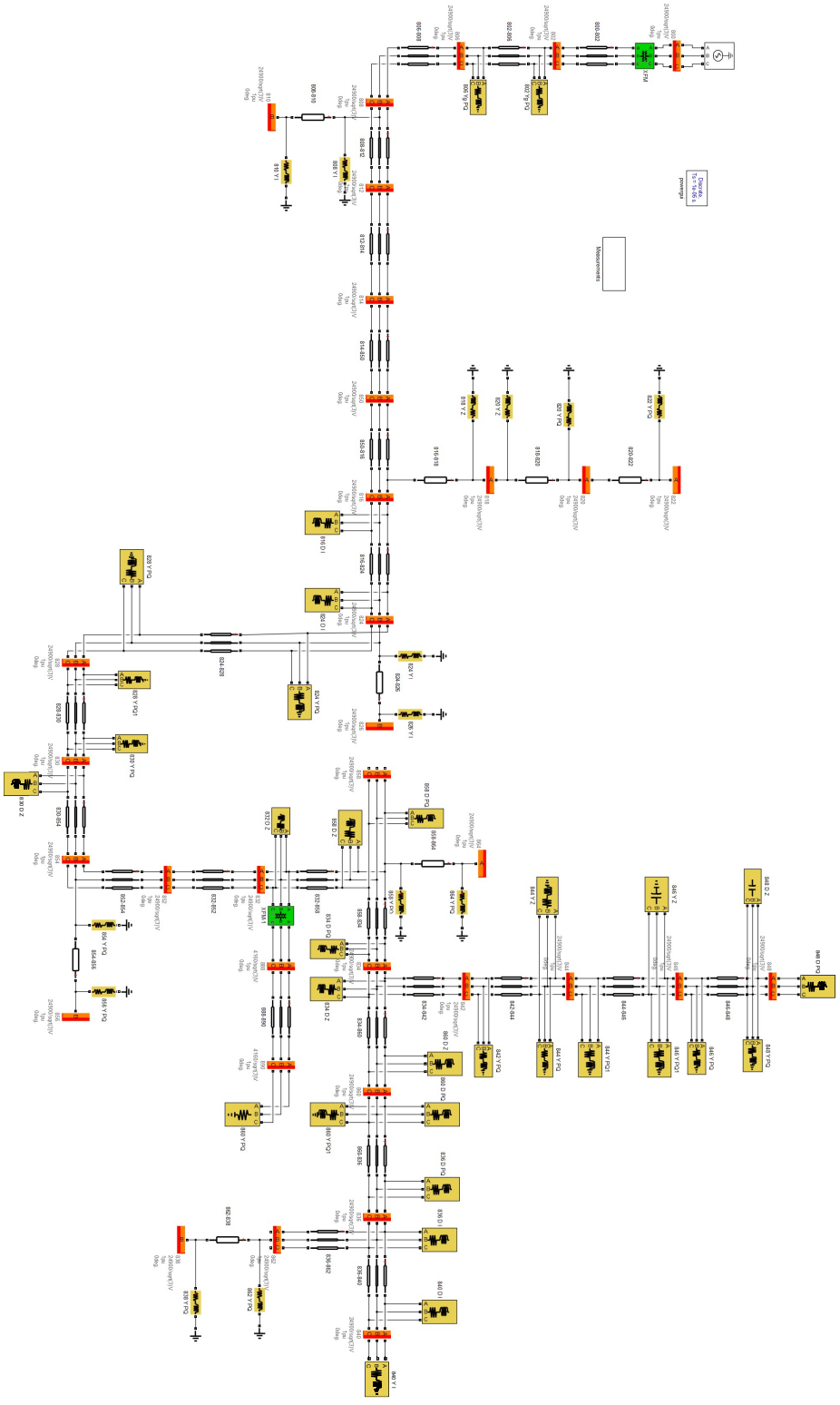

FIGURE 3.2: Modelling of IEEE 34 node distribution system in simulink

loads are spot load and nineteen loads are distributed loads as given in Appendix A. The spot loads were connected to their respective nodes and the distributed loads are divided into two half and each half is placed at the two ends of the respective line section. Three phase series RLC load block in SIMULINK is used to model all the three phase loads of the network and series RLC load block is used to model all single phase loads.

3.2.3 Transformer Modelling

Two transformers are used in this network. One transformer is located at substation node (800) and another one is located at node 832. The substation transformer is a 2.5 MVA 69/24.9 kV transformer and the in-line transformer has a rating of 0.5 MVA, 24.9/4.16 kV. Detail parameters of the transformer are shown in Appendix A. Both transformers are modelled using three-phase two windings transformer block available in SIMULINK.

3.2.4 Voltage Regulator Modelling

The IEEE 34 node network has two voltage regulators, one regulator is located between node 814 and node 850 and another one is located between node 852 and node 832. No voltage regulator block is available in Simulink component library. Hence, the voltage regulators are implemented as ideal instrument transformer using three phase autotransformer. The primary side of the autotransformer is set equal to the input voltage of regulator and the secondary side voltage is set equal to the regulator output voltage.

3.2.5 Shunt Capacitor Modelling

The shunt capacitor banks are used for voltage regulation and reactive power support. Two shunt capacitor banks are located on line section 834-848 at node 844 and node 848 respectively. The capacitors are modelled as three phase banks. The parameters used for modelling is given in Appendix A.

3.3 Modelling of Distributed Generation

A synchronous generator DG and a PV source type of DG are used in this work to test the performance of developed fault location algorithm in the DG integrated distribution network. The parameters for 350 kW synchronous generator DG are based on work carried out in [108] as given in Appendix B. A 500 kVA step up transformer is used to connect the synchronous generator to the distribution network. In addition to this a 100 kW PV source [109] is also connected to the network. The specification of PV source is given in Appendix B. The size and location of installed DGs are based on recommendations given in [110].

3.4 Steady State Load Flow Results Comparison with the IEEE Results

In order to verify the modeled distribution network for further studies, the published IEEE results are compared with the steady state load flow results of the modeled network. Table 3.1 presents the comparison of the node voltage obtained from MATLAB/SIMULINK simulation with the published IEEE results. The slight error in results can be due to the modelling difference in SIMULINK and that used by the IEEE subcommittee.

TABLE 3.1: Comparison of IEEE 34 Node Test Feeder Results

	MATLAB/SIMULINK results/voltage p.u			**IEEE published results/voltage p.u**			**Relative error %**		
Node	**Phase A**	**Phase B**	**Phase C**	**Phase A**	**Phase B**	**Phase C**	**Phase A**	**Phase B**	**Phase C**
800	1.0500	1.0500	1.0500	1.0500	1.0500	1.0500	0	0	0
802	1.0479	1.0488	1.0487	1.0475	1.0484	1.0484	-0.0381	-0.0364	-0.0364
806	1.0464	1.0480	1.0479	1.0475	1.0474	1.0474	0.1150	-0.0573	-0.0477
808	1.0194	1.0344	1.0331	1.0136	1.0296	1.0289	-0.5722	-0.4662	-0.4082
810		1.0343			1.0294			-0.4760	
812	0.9879	1.0197	1.0156	0.9763	1.0100	1.0069	-1.1881	-0.960	-0.8640
814	0.9628	1.0081	1.0016	0.9467	0.9945	0.9893	-1.7006	-1.3675	-1.2433
850	0.9828	1.0081	1.0016	1.0176	1.0255	1.0203	3.4198	1.6967	1.8327
816	0.9855	1.0079	1.0014	1.0172	1.0253	1.0200	3.1163	1.6551	1.8235
818	0.9816			1.0163			3.4143		
820	0.9690			0.9926			2.3775		
822	0.9561			0.9895			3.3754		
824	0.9687	1.0005	0.9940	1.0082	1.0158	1.0116	3.9178	1.0632	1.739
826		1.0003			1.0156			1.5064	
828	0.9741	0.9999	0.9934	1.0074	1.0151	1.0109	3.3055	1.4973	1.7311
830	0.9934	0.9588	0.9785	0.9894	0.9982	0.9938	-0.4042	3.9471	1.5395
854	0.9595	0.9868	0.9782	0.9890	0.9978	0.9934	2.9828	1.1024	1.5300
852	0.9287	0.9656	0.9549	0.9581	0.9680	0.9637	3.0685	0.2479	0.9131
832	0.9947	0.9956	0.9949	1.0359	1.0345	1.0360	3.9772	3.7602	3.9671
858	0.9997	0.9985	0.9996	1.0359	1.0322	1.0338	3.4945	3.2598	3.3081
834	0.9991	0.9925	0.9912	1.0309	1.0295	1.0313	3.0846	3.4849	3.6882
842	0.9910	0.9926	0.9912	1.0309	1.0294	1.0313	3.8704	3.5748	3.8882
844	0.9912	0.9926	0.9914	1.0307	1.0291	1.0311	3.8323	3.5467	3.8502
846	0.9918	0.9929	0.9920	1.0309	1.0291	1.0313	3.7928	3.5176	3.8107
848	0.9988	0.9989	0.9971	1.0310	1.0291	1.0314	3.0261	2.9346	3.3255
860	0.9903	0.9920	0.9906	1.0305	1.0291	1.0310	3.9010	3.6050	3.9185
836	0.9902	0.9917	0.9906	1.0303	1.0287	1.0308	3.8920	3.5967	3.8998
840	0.9901	0.9916	0.9905	1.0303	1.0287	1.0308	3.9017	3.6064	3.9095
862	0.9902	0.9917	0.9906	1.0303	1.0287	1.0308	3.8920	3.5967	3.8998
838		1.0015			1.0285			2.6251	
864	0.9983			1.0336			3.4152		
888	0.9659	0.9654	0.9764	0.9996	0.9983	1.000	3.3713	3.2956	2.36
890	0.8830	0.8918	0.8836	0.9167	0.9235	0.9177	3.6762	3.4325	3.6158
856		0.9868			0.9977			1.0925	

3.5 Modelling Of Electric Vehicle Charging System

The Electric Vehicle (EV) or Plug-in Electric Vehicle (PEV) can be categorized into two types as Battery Electric Vehicle (BEV) and Hybrid Electric Vehicle (HEV). The BEVs depends solely on their battery pack to meet all the power requirements. The HEVs use combination of both conventional power and battery power, the HEVs are of two type, Plug-in Hybrid Electric Vehicle (PHEV) and Extended Range Electric Vehicle (EREV). The PHEV and EREV contains both conventional engine and a battery pack to meet the power requirement, the basic difference between the two is that the PHEV depends mainly on conventional combustion engine whereas the the EREVs first exhaust its battery pack then switches to the conventional fuel. Of all these types, the BEVs has the highest electrical range for an electrical vehicle. In this work, the electrical vehicle load is designed as per the specification of PEV.

Appropriate modelling of electric vehicle charger is necessary for accurate assessment of the effects of EV charging infrastructure on distribution system. According to the Society of Automotive Engineers (SAE) Standard J1772 [111], there are three charging levels that provide the ability to charge the EVs faster by increasing the charging voltage, as shown in Table 3.2. Most of the electric vehicles can be plugged into an outlet at home for Level 1 charging (slow charging). Level 2 charging which requires 240 V outlets is typically described as the primary method for both private and public facilities. Future developments focus on fast Level 3 charging (AC or DC). Hence, considering these factors AC level 2 EV charging system is selected for work in this thesis.

The charger considered in this work is an AC single phase level 2, bidirectional charger. The charging system modeled contains an AC-DC converter and a DC-DC converter; both are capable of bi-directional operation. Fig. 3.3 shows the configuration of the charging system. The topology consists of six IGBT switches,

TABLE 3.2: Rating of EVs charger based on SAEJ1772 standard

Charging Level	**Nominal Supply Voltage**	**Max. Current**	**Input Power**
1-phase AC Level 1	120 V	12 A	1.4 kW
		16A	1.92 kW
1-phase AC Level 2	208 to 240 V	17 A	4 kW
		32A	8 kW
		80A	19.2 kW
3-phase AC Level 3	208 to 600 V	400 A	$>$ 7.68 kW
DC Charging	600 V maximum	400 A	$<$ 240 kW

four switches used in AC-DC converter stage and two in the DC-DC stage [112]. The charger is designed to deliver 6.6 kW power at 240 V to the battery for charging purpose. The following section gives detail about the battery charger.

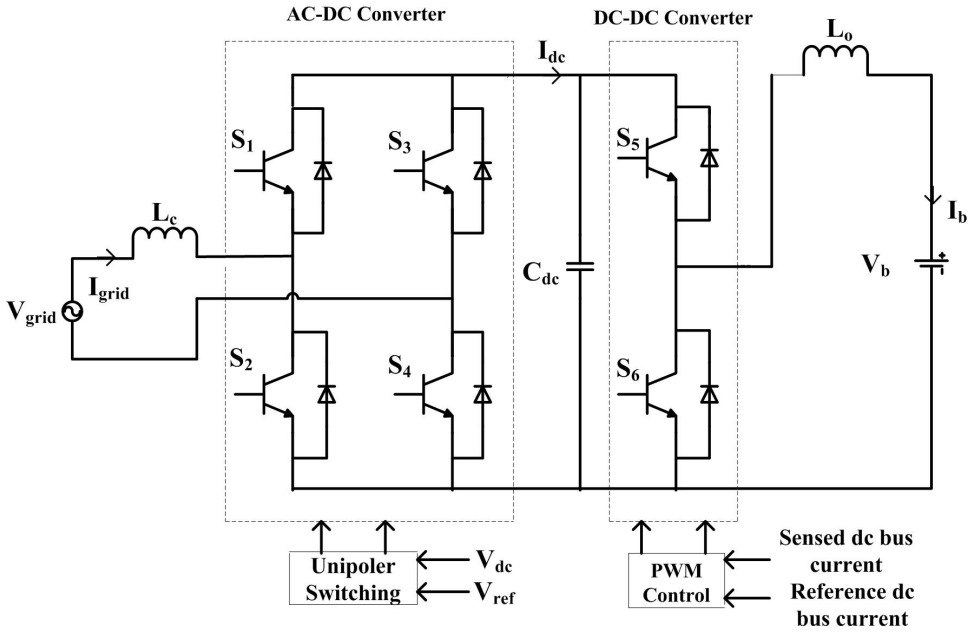

FIGURE 3.3: Configuration of PEV battery charger

3.5.1 Bidirectional AC-DC Converter

During the charging of battery power is transferred from grid to vehicle as shown in Fig. 3.4, the direction of current from grid to converter is taken as positive.

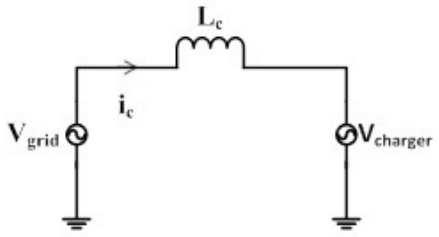

FIGURE 3.4: Representations of Grid and Charger

The sinusoidal grid voltage is taken as,

$$v_{grid}(t) = \sqrt{2}V_{grid}\sin(wt) \tag{3.1}$$

Where, $v_{grid}(t)$ is instantaneous grid voltage and V_{grid} is RMS (root mean square) value of grid voltage. The fundamental component of converter voltage is

$$v_{conv}(t) = \sqrt{2}V_{conv}\sin(wt - \delta) \tag{3.2}$$

Where, $v_{conv}(t)$ is instantaneous voltage of converter and V_{conv} is the RMS value, δ denotes angle between grid voltage and the converter voltage. The grid current is given as

$$i_{grid}(t) = \sqrt{2}I_{grid}\sin(wt - \theta) \tag{3.3}$$

Where, θ is the angle between $i_{grid}(t)$ and $v_{conv}(t)$

Active power flows from the grid when $v_{conv}(t)$ lags $v_{grid}(t)$, and it flows to the grid when $v_{grid}(t)$ lags $v_{conv}(t)$. Phase angle of determines the direction of flow of reactive power. For a positive value of θ the reactive power flows from converter to grid and for negative θ the reactive power flow from grid to converter. The converter is capable of meeting the requirement of bidirectional power flow. The fundamental value of the converter voltage is related to dc link voltage as

$$V_{conv} = \frac{mV_{dc}}{\sqrt{2}} \tag{3.4}$$

Here, m is the modulation index taken as 0.9 and V_{dc} is the voltage of dc link which is set at 380 V. The fundamental component of converter voltage is related to grid voltage by the relation given as

$$V_{conv} = \sqrt{V_{grid}^2 + (I_{grid}^2 \times X_l^2)} \tag{3.5}$$

Here, X_l is the inductive reactance. The rating of capacitor in dc bus is given as,

$$C_{dc} = \frac{I_{dc}}{2 \times w \times V_{dcripple}} \tag{3.6}$$

Where, I_{dc} is the DC link current, w is the angular frequency and $V_{dcripple}$ is 5% of V_{dc}. The output of AC-DC converter is the dc link voltage V_{dc} and it is the input to the DC-DC converter. For control of bidirectional AC-DC converter a unipolar switching scheme is used, in which a fixed frequency triangular carrier wave is compared with the positive reference signal and the negative reference signal. The output dc link voltage varies between $\pm V_{dc}$. For controlling the dc link voltage a PI controller is used. This PI voltage controller compares the reference voltage to the sensed dc link voltage to calculate the error as the difference between the two. The PI voltage controller then generates the control signal to minimize the error so that the dc link voltage closely tracks the reference voltage. The output of this voltage PI controller is the reference current to the PI current controller, which closely tracks the reference current by minimizing the error between the sensed current the reference current. The switching signals for triggering the switches of the AC–DC converter at different instants are generated by comparing the amplified control signal to a fixed frequency sinusoidal wave.

3.5.2 Bidirectional DC-DC Converter

The working of bidirectional DC-DC converter is divided into two modes. One is charging and other is discharging mode. Switch S_5 in Fig. 3.3 will be turned

on during charging mode and converter will work as a buck converter to charge the battery. During the discharging mode switch S_6 will be turned on and the converter will function as a boost converter. While boosting the DC-DC converter will boost up the initial voltage to 380 V. For designing the DC-DC converter the inductor value is calculated from the relationship between switching frequency f, inductance L_c given as:

$$f = \frac{1}{2 \times P \times L_c}\left(\frac{1}{\frac{1}{V_{dc}} + \frac{1}{V_b}}\right) \tag{3.7}$$

Where, P is the power delivered from grid to battery, V_{dc} is DC link voltage and V_b is the battery voltage and f is the switching frequency and its value is 50 kHz. PWM technique is applied for controlling the battery charging and discharging using bi-directional converter. A PI controller controls the input current (I_b) of battery. The PI controller compares the dc link current to the reference current and error is minimized with the help of control signal generated by the controller. The switching signals for the IGBTs of the DC-DC converter is generated by comparing the controller's output to a fixed frequency saw-tooth carrier waveform [113]. The above control strategy is applicable for both buck and boost mode of operation.

The battery used in the PEV load is modeled as lead-acid battery, implemented in SIMULINK using the model parameters given in [114]. The performance of charger is tested by simulation for 2 sec; charging is done for 1 sec and for another 1 sec discharging is done. Simulation results obtained are shown in Fig. 3.5. Fig. 3.5(a) shows, that the voltage across the DC link bus is maintained at 380 V during both buck (charging) and boost (discharging) mode by the converter. The current delivered to the battery for charging and current provided by battery while discharging maintains a magnitude of 30 A as shown in Fig. 3.5(b), the change in polarity of current while giving energy back to grid shows that the supplied current is in phase opposition of the grid voltage. The battery voltage profile while operating in both buck and boost mode are shown in Fig. 3.5(c). During the one second of buck mode of operation battery voltage level increases from 202.6 V to 207.9 V

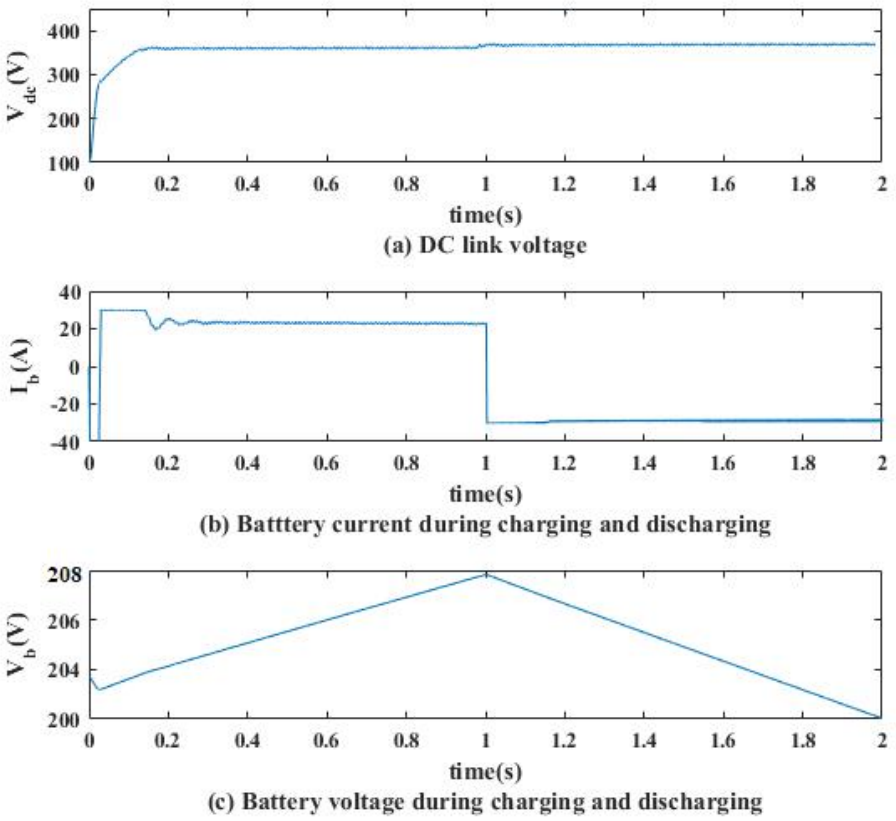

FIGURE 3.5: Charging system performance under normal operating conditions

and during boost mode it discharges back to 200.1 V. In all these profiles there is change in operating mode at 1 sec i.e. from charging of battery to discharging of battery. The simulated results validate the performance of charger which is used for the integration of PEVs to the grid.

3.6 Conclusion

The selected distribution network is modeled in SIMULINK for further work related to fault analysis and fault location estimation. Steady state load flow simulation studies are performed to validate the network and obtained results are compared with published IEEE results. Furthermore, detail modelling of PEV charger and its

control strategy is provided in this chapter. Simulation results for charging system performance under normal operating conditions is also given in this chapter.

Chapter 4

IMPACT OF PLUG-IN ELECTRIC VEHICLES ON FAULTED DISTRIBUTION SYSTEM

4.1 Introduction

Plug-in Electric Vehicle (PEV) provides one of the most promising solutions to reduce NO_X and SO_X emissions from the conventional vehicles. However, integration of large-scale PEVs to the existing grid may introduce new challenges especially at distribution system level as the existing distribution grid was not designed to accommodate such electrical vehicle loads. Therefore, fault analysis of distribution system in the presence of electric vehicle charging load is required to access the impact of this new type of load during fault conditions. This chapter evaluates the impact of PEV charging on distribution system under different fault conditions. IEEE 34 node distribution system with AC level 2 single phase PEV

charging station coupled to one of its nodes is used to investigate the effect of PEV charging on the system under balanced and unbalanced fault conditions. The impact of PEV charging load is compared to the impact of equivalent constant power load at main feeder and lateral respectively under balanced and unbalanced faults.

4.2 System Configuration

To evaluate the impact of PEV charging load on an unbalanced distribution system during fault conditions, the IEEE 34 node test feeder shown in Fig. 3.1 is used as test system. A charging station consisting of fifteen PEV, each with a maximum capacity of drawing 6.6 kW of power from the grid to charge the battery is connected to the distribution system node, contributing to a load of 33 kW per phase above the base system load. Connection of PEVs to the system is shown in Fig. 4.1. The impact is investigated for the for two locations of PEV charging load, one with PEV charging load connected at the node 890 of the low voltage lateral 832-890 and other with PEV charging load connected at the node 840 of the main feeder of the distribution system under both unbalanced and balanced fault conditions respectively. In order to compare the impacts of PEV charging load to the impact of constant power loads on the distribution system during fault conditions, two cases were simulated on this test system as follows:

Case 1: Faults are applied with PEV load connected to the distribution system.
Case 2: Faults are applied with PEV load replaced by an equivalent constant power load at the same node of distribution system.

The impact of PEV charging on distribution system during fault condition is determined by observing the voltage, active power, reactive power and the fault current at all major nodes of the system.

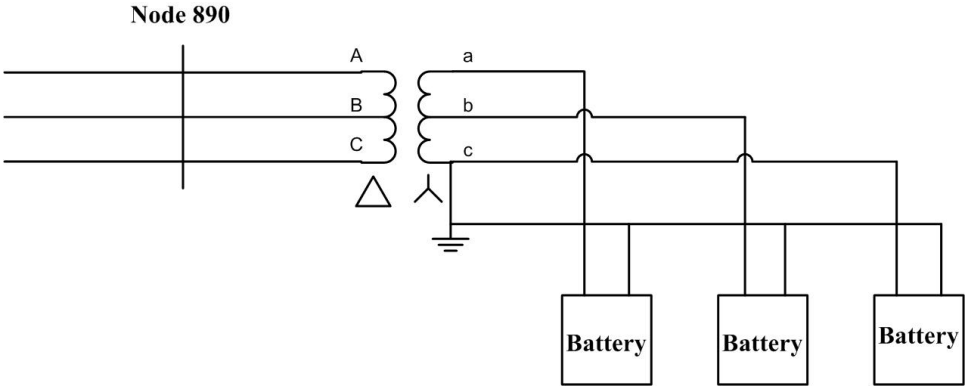

FIGURE 4.1: Connection of PEVs in distribution system

4.3 Simulation Results

Case1 and Case 2 were simulated at two different locations in the distribution system. One with charging load connected to node 890 of the lateral and other with the charging load connected to the main feeder at node 840. Faults in power system are categorized as short circuit faults and open circuit faults. The short circuits faults are of two types, unbalanced (asymmetrical) faults and balanced (symmetrical) faults. All types of unbalanced faults, balanced faults and open circuit faults have been investigated in this work. The result are compared to the equivalent constant power load case as observed during the fault period, and after the fault is cleared from the system but the faulted phase is yet to be reconnected to the system by the circuit breaker. Considerable variations are observed in fault voltage, fault current and reactive power demand at the faulted node of the system.

4.4 PEV Charging load Connected to Lateral 832-890 at Node 890

The PEV charging load is connected at first, to node 890 of lateral 832-890 for analyzing the impact of PEV charging on distribution system.

4.4.1 Unbalanced Fault

Unbalanced or unsymmetrical faults are very common in distribution systems, this type of fault leads to unequal current and unequal phase shift in a three phase system. There are three types of unbalanced faults namely single line to ground fault (LG), line to line faults (LL) and double line to ground fault (LLG). Impact of EV charging on each of these faults are discussed below.

(a) Single line to ground faults (LG)

Single line to ground faults are the most common fault in power system. As per the fault statistics of overhead lines [115], 80 % of the faults that occur in power system are single line to ground faults. In this work, a line to ground fault in phase A is applied at 0.33 s between node 888 and node 890 of the distribution feeder and the fault is cleared from the system at 0.42 s. Both case 1 i.e. with charging load connected at node 890 and case 2 with charging load replaced by equivalent constant power load are simulated.

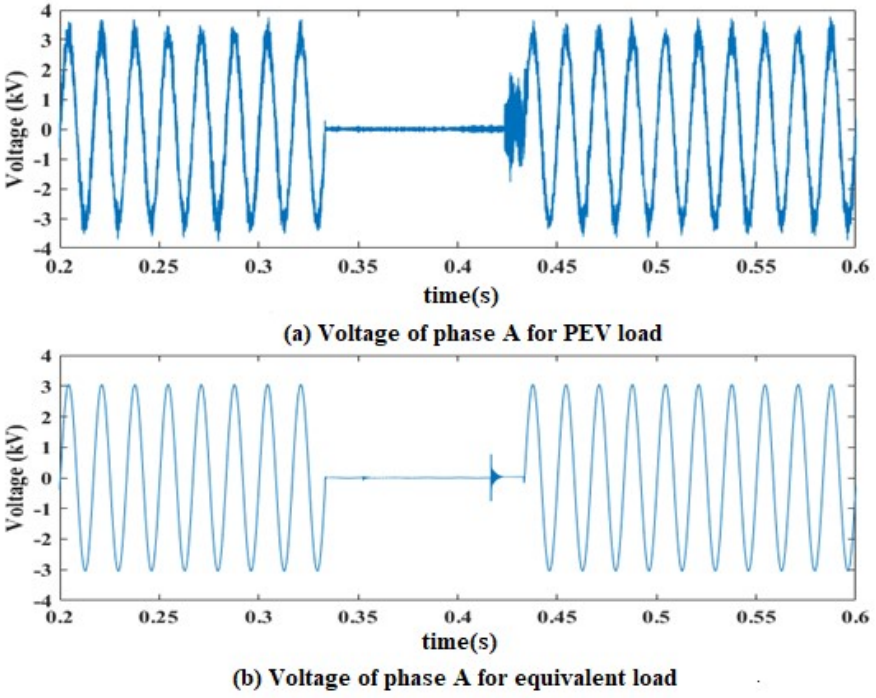

FIGURE 4.2: Voltage of faulted phase A for LG fault

Fig. 4.2(a) gives the voltage of faulted phase A at node 890 for the period of fault and fault recovery for PEV load case and Fig. 4.2(b) shows the voltage of faulted phase A at node 890 during the period of fault and fault recovery for equivalent load case. As can be seen in Fig. 4.2(a) for the case 1 with PEV load connected at node 890, a transient voltage of high frequency having peak magnitude of approximately half of the steady-state peak voltage is observed at the time of reconnection of phase A to the system as compared to the equivalent constant power load case 2. Once the phase A is reconnected back to the distribution system the voltage regains its steady-state value. This transient voltage appears due to continuous switching of charging system of PEV load connected to the distribution node.

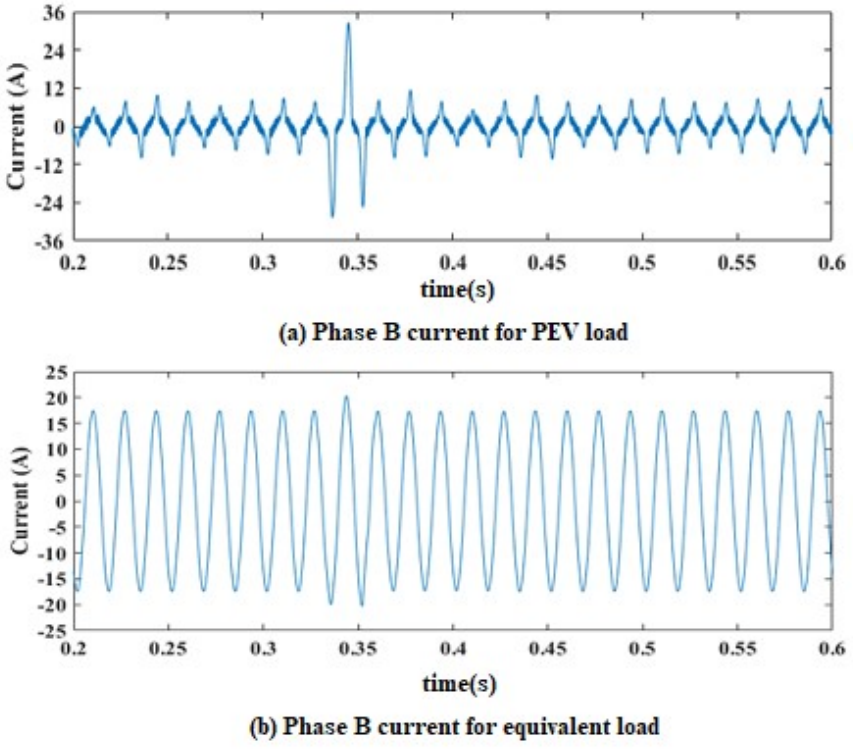

FIGURE 4.3: Phase B current for LG fault

Fig. 4.3 gives phase B current at node 890 during fault condition and recovery period. Fault current is an important fault parameter which determines the severity of fault and affects the function of protective device in the system. As can be seen from Fig. 4.3(a) for case 1, with charging vehicle load connected to the node 890,

the phase B current at the time of fault shows the peak magnitude of 3 times the magnitude of steady state current. An increase in magnitude is also observed in both phase C current but major increase is observed in the phase B current due to mutual coupling of the distribution lines which is shown in Fig. 4.3(a). For case 2 with charging vehicles load replaced by equivalent constant power load the effect is not significant and the transient in the current during the fault is much less pronounced as compared to case 1.

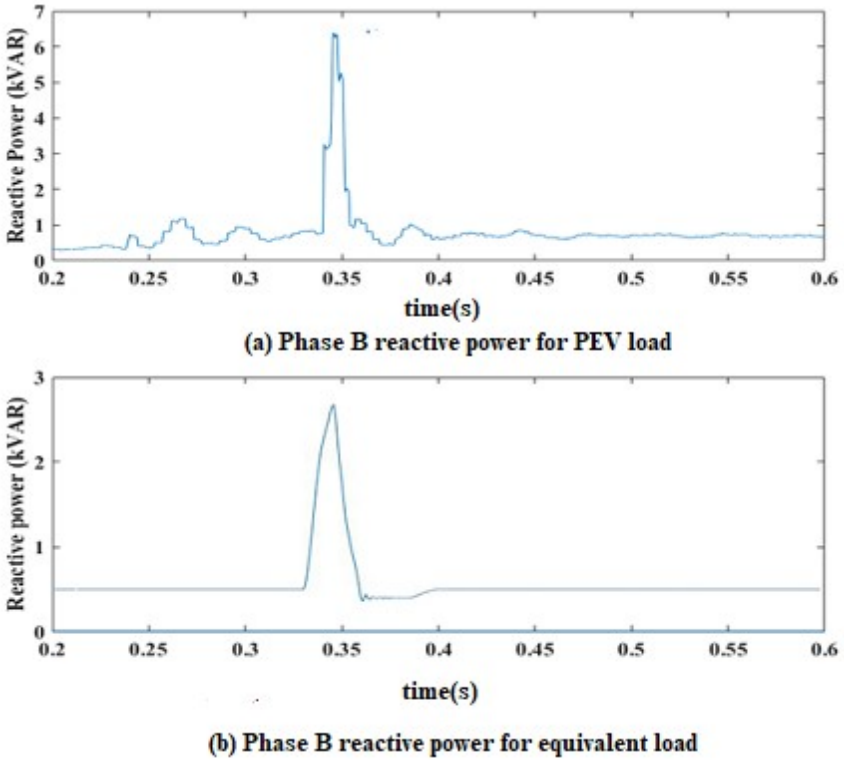

FIGURE 4.4: Phase B reactive power for LG fault

Another significant change is observed in reactive power requirement in phase B during fault condition at node 890. For PEV load connected case the reactive power of phase B shows a sudden jump of approximately 21 times from 0.31 kVAR before fault to 6.6 kVAR at the time of fault and then settles to a value of 0.45 kVAR shown in Fig. 4.4(a). The sudden rise in reactive power observed in phase B is nearly 2.5 times the reactive power rise during fault with equivalent constant power load connected to node 890 as can be seen in Fig. 4.4(a) and Fig. 4.4(b). This

increase in reactive power requirement can have undesired effects like low voltages, increased system losses and equipment heating.

(b) Double line to ground faults (LLG)

Double line to ground faults are considered less severe as compared to the three phase fault and single line to ground faults on the overhead lines. In this work a double line to ground fault is simulated with phase A and phase B as the faulted phases in the line section connecting node 888 and node 890. The fault is applied at 0.33 s into the simulation and removed at 0.42 s. The simulation results are displayed in Fig. 4.5, in this fig (a), fig.(c) and fig.(e) shows results for PEV load case and fig (b), fig.(d) and fig.(f) display results for equivalent load case respectively. The voltage, current and the reactive power demand at node 890 are observed for each of the two cases. Fig. 4.5(a) and Fig. 4.5(b) show the voltage waveform at node 890 for the double line to ground fault for PEV load case and for equivalent load case respectively. As can be seen from the Fig. 4.5(a) with PEV load connected, a high frequency transient voltage appears during the breaker reclosing period whereas in equivalent load case shown in Fig. 4.5(b) no such transient voltage appears during breaker reclosing.

The effect on phase currents due to PEV charging load at node 890 is shown in Fig. 4.5(c). The fault current show sharp rise in magnitude from 15 A to 25 A in the first cycle of the fault and a switching transient current can be observed in the faulted phases during the fault and reclosing period. The fault current in equivalent load case is depicted in Fig. 4.5(d), here; the faulted phase current waveform does not show any sharp rise or transient during the fault time and the reclosing period.

With PEV charging load connected at node 890 the reactive power requirement show a sharp rise in healthy phase C from 386 VAR to 890 VAR as the fault strikes, which settles down to normal value after two cycles as shown in Fig. 4.5(e). The reactive power requirement for faulted phase A and phase B reduces to zero for the fault duration. Not much variation in reactive power requirement is observed in

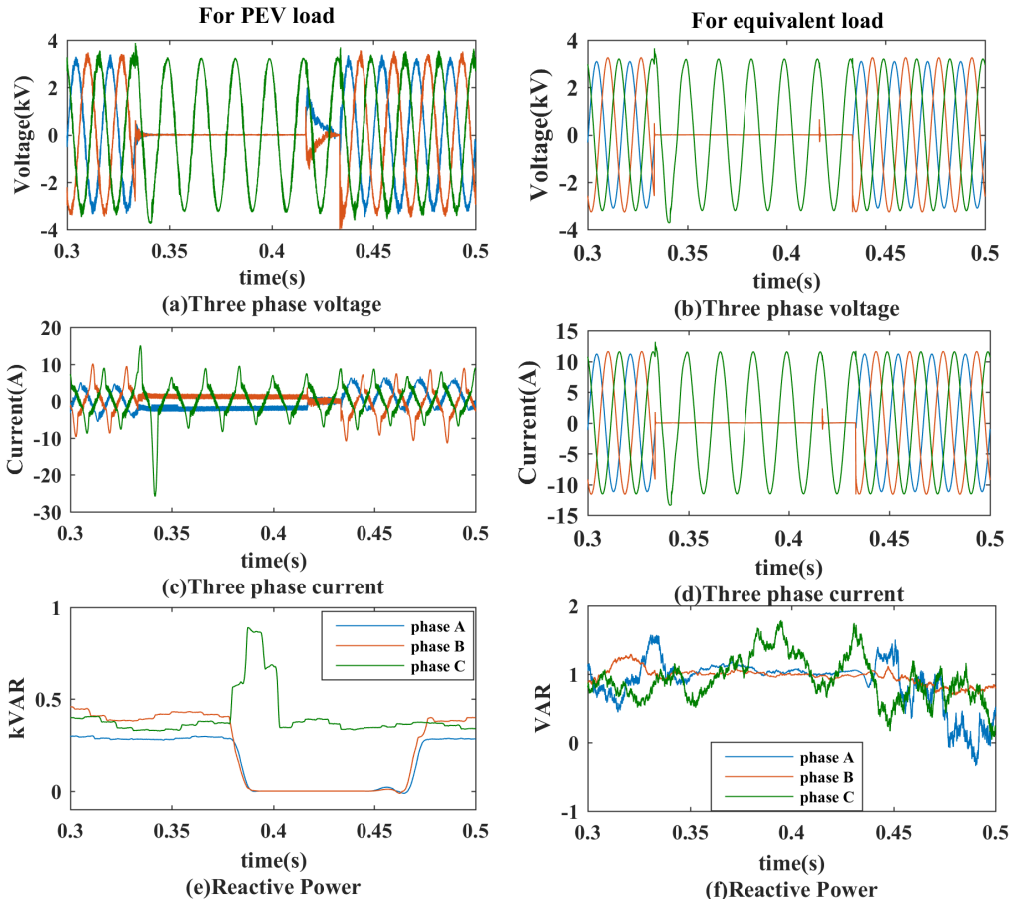

FIGURE 4.5: Impact on voltage, current and reactive power for LLG fault at node 890

equivalent load case as shown in Fig. 4.5(f). For this case the reactive power for the healthy phase C varies between -1 VAR to 2 VAR for the fault duration.

(c) Line to line fault (LL)

Line to line faults are the second most common fault on overhead lines. This fault does not involve path to ground and are least severe in nature. A line to line fault case is simulated involving phase A and phase B in line section 888-890. The fault is applied at 0.33 s into the simulation and removed at 0.42 s. Fig. 4.6(a) and Fig. 4.6(b) shows three phase voltage for PEV load case and for equivalent load case respectively. The voltage, current and the reactive power demand at node 890 are observed. As can be seen from the Fig. 4.6(a) the effects are similar to double

line to ground fault case and a high frequency transient voltage appear during the breaker reclosing period with PEV load whereas in equivalent load case shown in Fig. 4.6(b) no such transient voltage appears during breaker reclosing.

The effect on phase current due to PEV charging load at node 890 is shown in Fig. 4.6(c). The fault current don't show any significant rise in magnitude, only a switching transient current appears in the faulted phases for the fault duration and reclosing period. The fault current in equivalent load case is depicted in Fig. 4.6(d), as can be seen the faulted phase current waveform does not show any transient for fault duration and reclosing period.

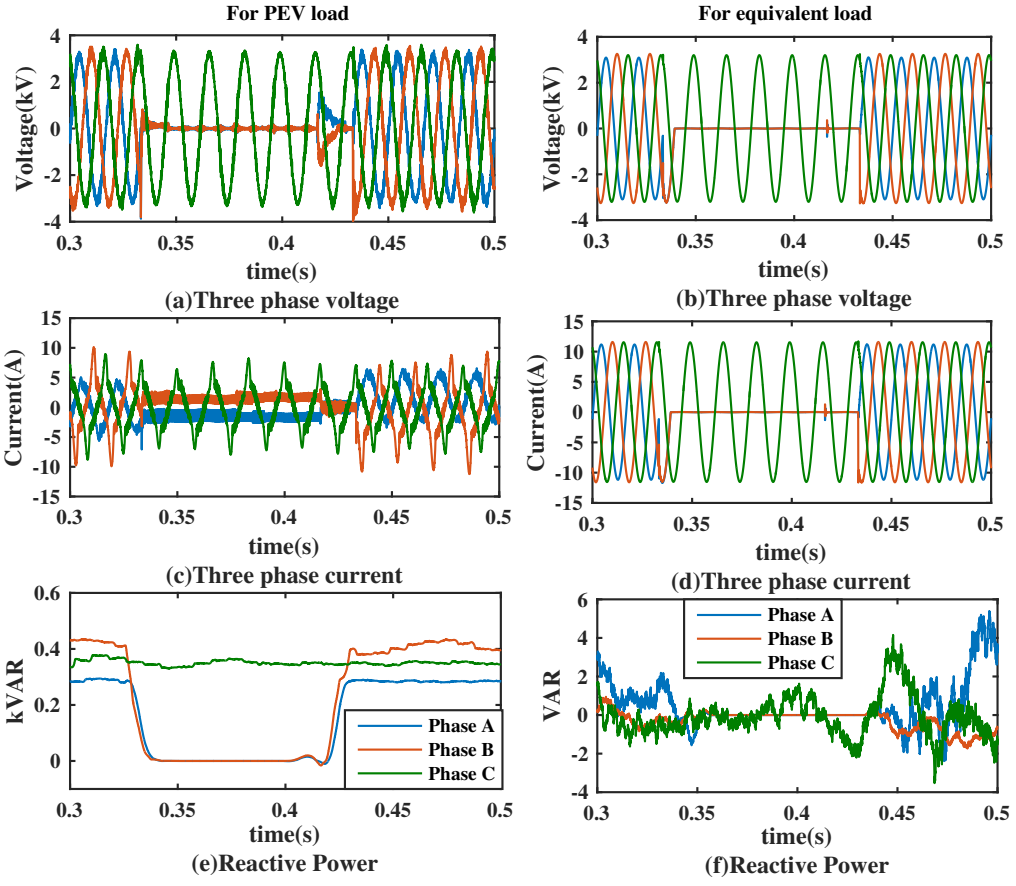

FIGURE 4.6: Impact on voltage, current and reactive power for LL fault at node 890

The reactive power requirement at the faulted node is shown in Fig. 4.6(e) and Fig. 4.6(f) for case 1 and case 2 respectively, no considerable variation in reactive

power requirement is observed for the PEV case and the equivalent load case due to the fault. For the PEV load case the reactive power requirement for faulted phase A and phase B reduces to zero for the fault duration and for the healthy phase C reactive power remains almost constant for the whole fault period and after the fault is removed. Not much variation in reactive power requirement is observed in equivalent load case as well, reactive power for the healthy phase C varies between -3 VAR to 6 VAR for the fault duration.

4.4.2 Balanced Faults

Balanced or symmetrical faults are very severe in nature but are rare in distribution system. To understand the impact of balanced fault on the distribution system, a three-phase fault is applied at 0.33 s between node 888 and node 890 of the distribution feeder with charging electrical vehicle load connected at node 890.

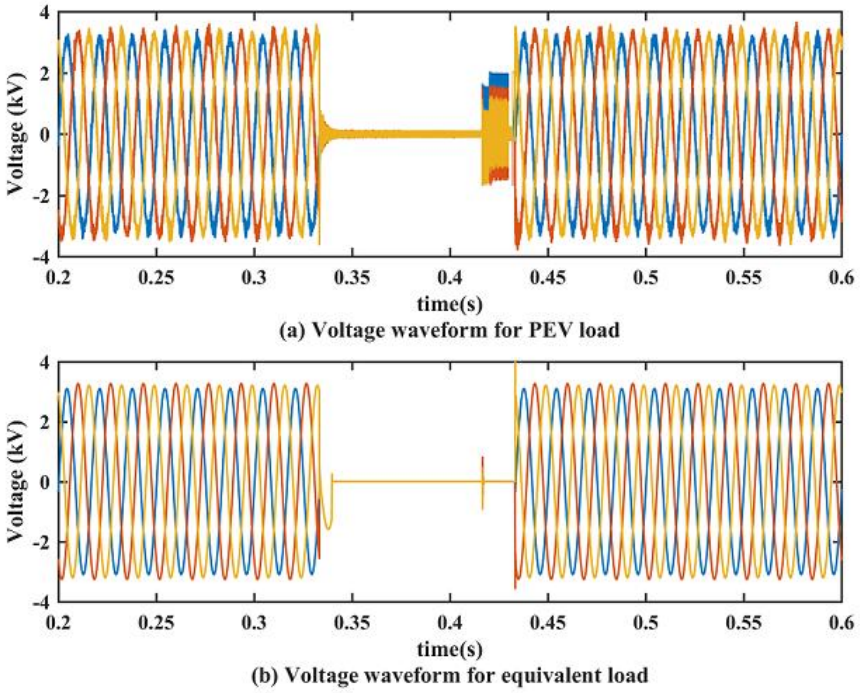

FIGURE 4.7: Impact on three phase voltage for LLL fault at node 890

Fig. 4.7 shows the three-phase voltage waveforms in case of a three-phase fault in the system. The effect shown is similar to single phase fault case and potentially harmful high magnitude transient voltage is observed in all three phases during the fault recovery time for the PEV load connected case, for equivalent load case the effect on voltage waveform is not significant. Phase current and reactive power requirement is not shown in this case because all the three phases have been disconnected by the circuit breaker during the fault.

4.4.3 Open Circuit Faults

Open circuit faults are much more unusual than short circuit faults (both unbalanced and balanced faults), and often they are transformed into short circuits by subsequent events. In terms of the severity of a fault, short circuits faults are of far greater concern than the open circuit faults, although some open circuit faults may present a potential hazard to personnel [115]. An open circuit fault occurs when one or more phases of conductor break on an overhead line. Such faults may also occur in situations where circuit breakers or isolators open but fails to close in one or more phases.

In this work an open conductor fault is simulated by opening phase A at node 888. The fault is applied at 0.33 s and removed at 0.42 s. After occurrence of the open conductor fault, the magnitude of voltage, current and reactive power at the faulted node 890 is shown in Fig. 4.8. It can be seen from this figure that the magnitude of voltage and current of the faulted phase A reduces to almost zero whereas the magnitude of voltage of healthy phase B and phase C does not change significantly.

Fig. 4.8(a) and Fig. 4.8(c) shows voltage and current waveform respectively for case of PEV charging load, the behavior shown is similar to the equivalent load case and no significant change is observed in the voltage and current waveforms of the healthy phases.

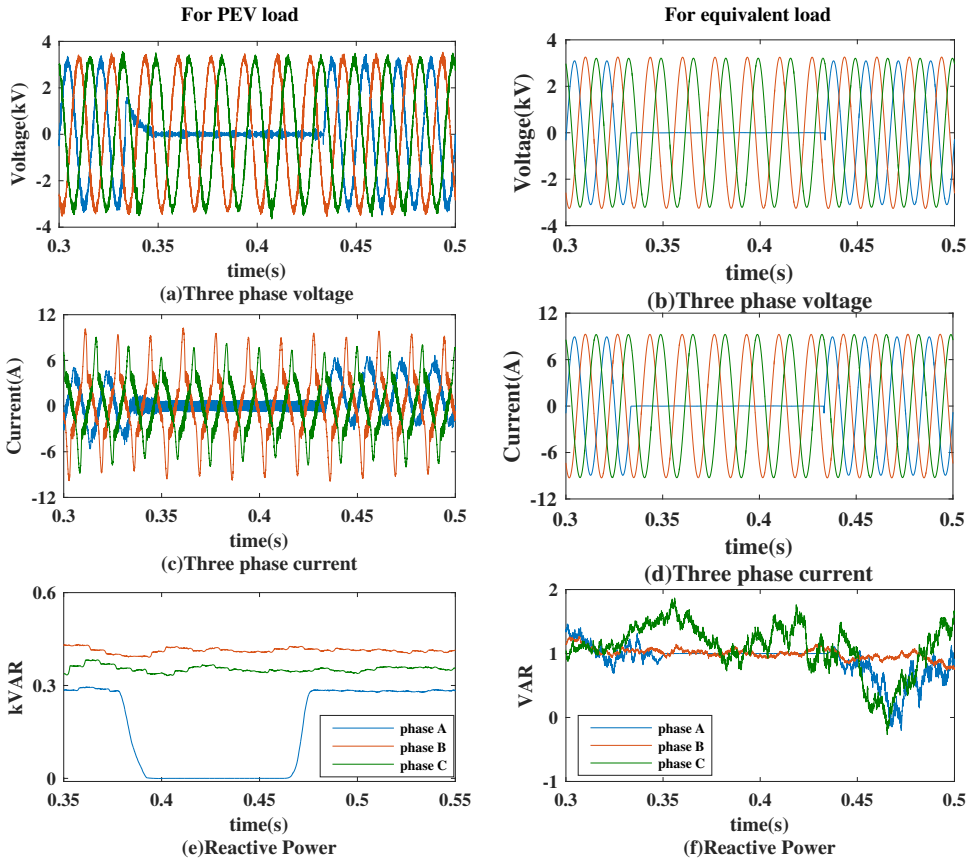

FIGURE 4.8: Impact on voltage, current and reactive power for open circuit fault at node 890

Reactive power requirement for PEV load case is shown in Fig. 4.8(e), as can be seen from the figure, the reactive power requirement remains almost constant for the two healthy phases B and phase C due to open circuit fault. It is only for the open circuited phase A the reactive power drops to 0 VAR for the fault duration. For equivalent load the reactive power requirement is almost zero for the faulted phase A and healthy phase C only phase B show very small reactive power varying between 1 VAR to -1.7 VAR as shown in Fig. 4.8(f).

Hence, from the obtained results it can be concluded that the PEV charging loads do not have any adverse effect on the distribution system for the open circuit fault.

4.5 PEV Charging load Connected to the Main Feeder at Node 840

The analysis shown above was performed on lateral 832-890; this section has the voltage level of 4.16 kV only which is very low compared to the voltage level of main feeder. To see the impact of PEV charging on fault condition in the system on a section at high voltage level, the same analysis is performed on main feeder of the distribution system having nominal voltage rating of 24.9 kV. For this case, the PEV charging load is connected at node 840 of the distribution system on the main feeder.

4.5.1 Unbalanced Faults

(a) Single line to ground faults

With the PEV charging load connected at node 840 of the distribution system on the main feeder a single line to ground fault is applied to phase A at 0.33 s between node 836 and node 840 of the main feeder and the fault is cleared from the system at 0.42 s. The voltage waveform for faulted phase A for PEV load case and equivalent load case is shown in Fig. 4.9(a) and Fig. 4.9(b) respectively. As can be seen when the electrical vehicle charging load is connected at a node of high voltage main feeder the magnitude of voltage transients observed during the period of reconnection of phase A after the fault is cleared from the system is less as compared to the magnitude of voltage transients when the electric vehicle charging load is connected to the low voltage lateral of the distribution system at node 890. Similar improvement appears in the current waveform as well. As can be seen in Fig. 4.9(c), no significant rise in magnitude of phase B current during the fault is observed with charging vehicle load connected to node 840 of the main feeder, as compared to the case when PEVs load is connected to node 890 of the lateral.

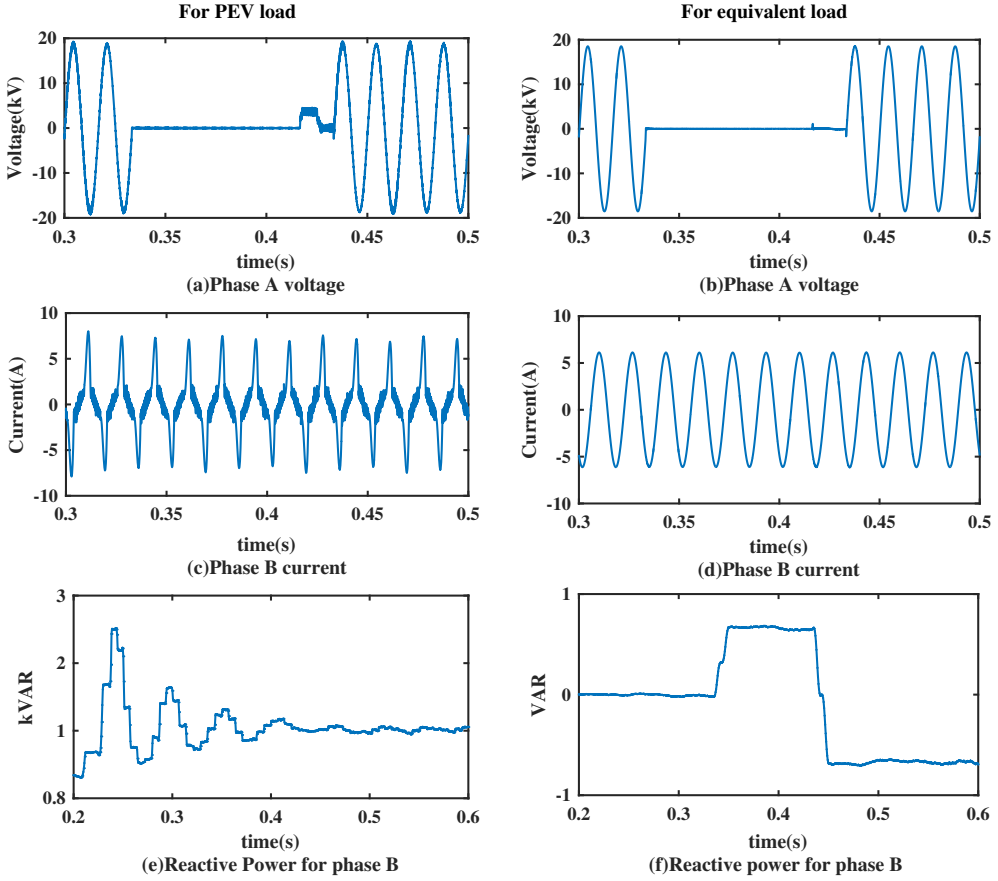

FIGURE 4.9: Impact on voltage, current and reactive power for LG fault at 840

No significant change in the reactive power requirement of phase B is observed during fault when the PEVs charging load is connected to the main feeder as shown in Fig. 4.9(e). Reactive power for the equivalent load case is shown in Fig. 4.9(f). No significant impact in current, voltage and reactive power is observed at other nodes of the distribution system. Hence, it can be said that the effect of PEV load at the time of fault is limited to the faulted node only, because the clearing of fault by the circuit breaker helps in restricting the effect of PEV load to the faulted node only. These results show that the high voltage level of the distribution line minimizes the negative impacts of PEV load on distribution system during the fault.

(b) Double line to ground fault

Fault analysis results for double line to ground fault case on main feeder for a AB phase fault in line section 836-840 is presented in Fig. 4.10.

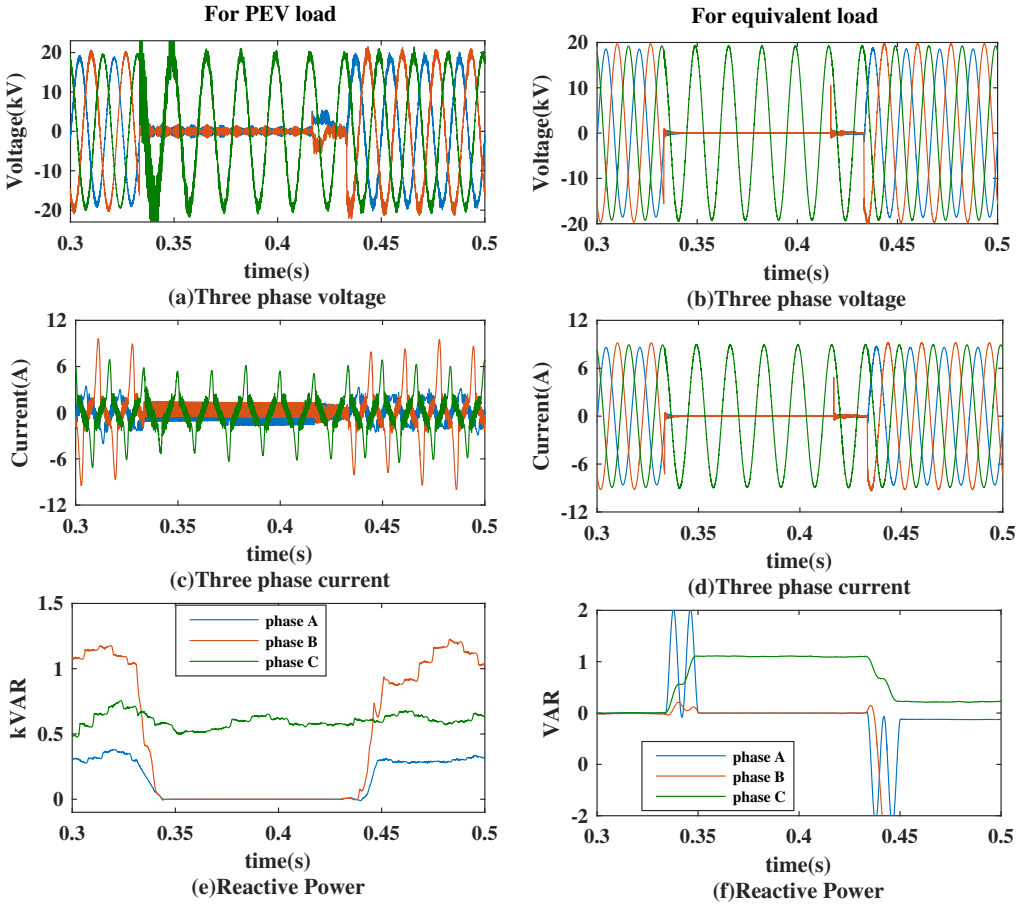

FIGURE 4.10: Impact on voltage, current and reactive power for LLG fault

No significant change is observed in fault current, voltage and reactive power at the faulted node due to the very high voltage level of the distribution feeder compared to the charging station requirements. Fig. 4.10(a) and Fig. 4.10(b) shows the voltage waveform at node 840 for PEV load case and equivalent load case respectively, here, it can be seen that minor voltage transients appear in the waveform for the PEV load case at the time of reclosing whereas in equivalent load case no such transient appears in the waveform. The fault current and reactive power do not show any significant rise in either case.

(c) Line to line faults

Fault analysis for line to line fault case gives similar results as obtained in the double line to ground fault case. Fig. 4.11(a) and Fig. 4.11(b) shows the three phase voltage recorded at node 840, a transient voltage of small magnitude appears in the faulted phase A and phase B for the PEV load case and no such transients in the faulted phases are observed in the equivalent load case. The three phase current at node 840 for the PEV load case and equivalent load case is shown in Fig. 4.11(c) and Fig. 4.11(d) respectively, the fault current does not show any change and the reactive power for the case 1 and case 2 shown in Fig. 4.11(e) and Fig. 4.11(f) respectively also do not show any significant rise.

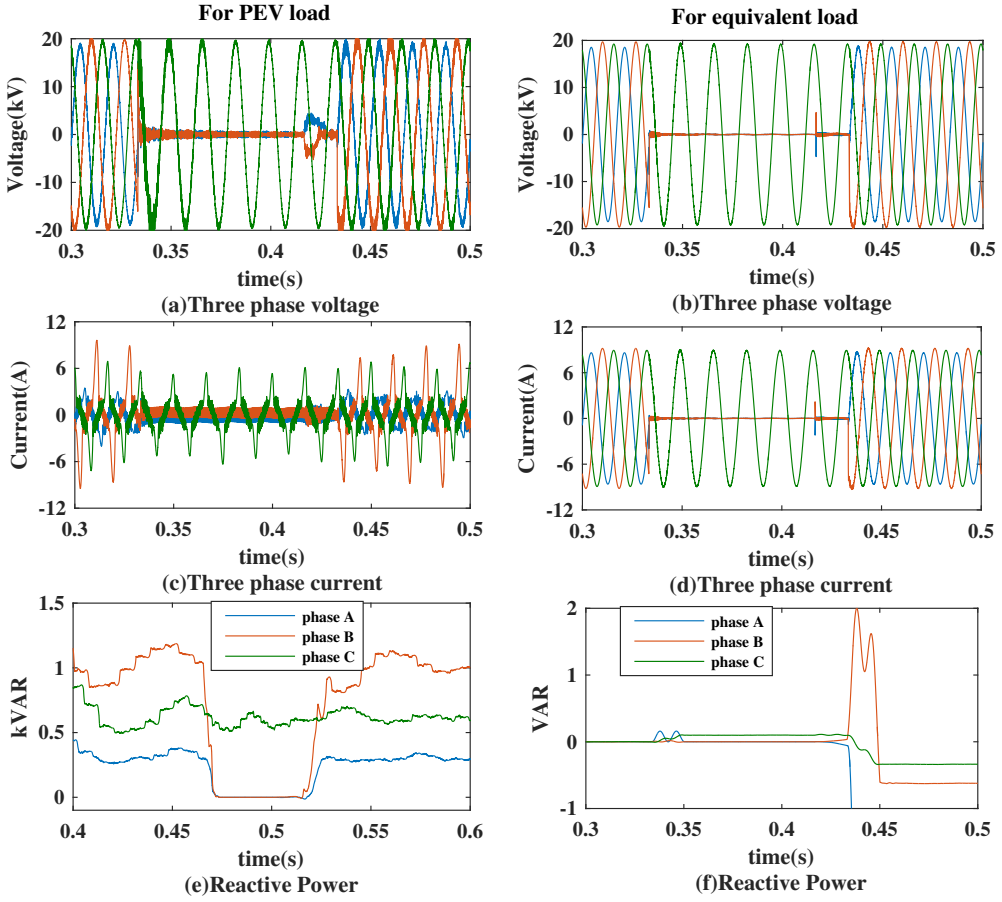

FIGURE 4.11: Impact on voltage, current and reactive power for LL fault at node 840

4.5.2 Balanced Faults

The three phase voltage waveform obtained at node 840 when a three-phase fault is applied at section 836-840 is shown in Fig. 4.12. Fig. 4.12(a) shows the three phase voltage waveform for PEV load case and Fig. 4.12(b) shows three phase voltage waveform for equivalent load case. As can be seen, the magnitude of high-frequency switching transients during the fault recovery time for PEV load case is very low compared to that obtained at node 890 in case of three-phase fault.

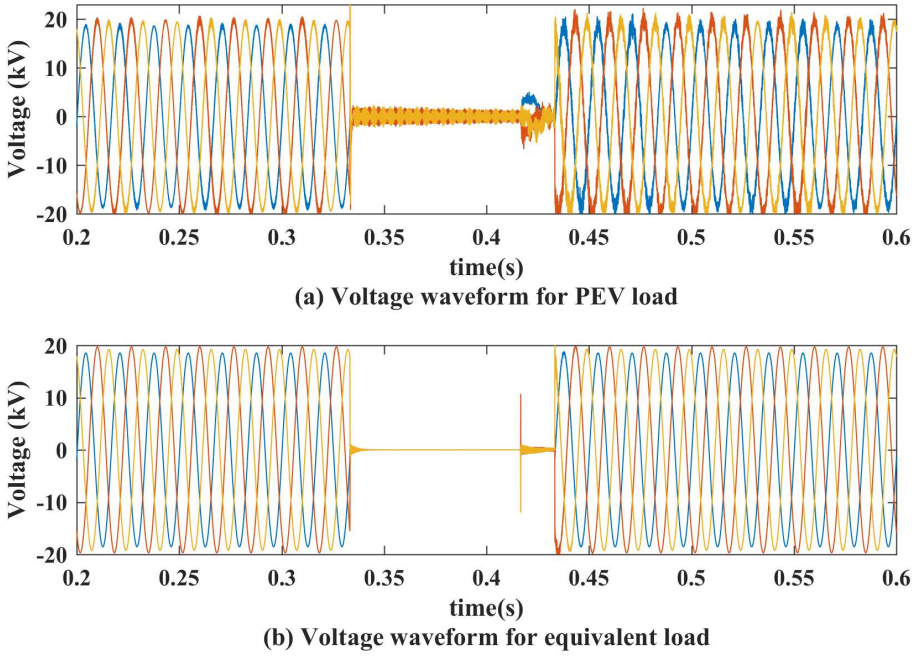

FIGURE 4.12: Impact on three phase voltage for LLL fault at node 840

4.5.3 Open Circuit Faults

The results for open circuit fault on main feeder applied in line section 836-840 are shown in Fig. 4.13. The PEV load does not have any significant effect on the voltage, current and reactive power at the faulted node 840 in comparison to the equivalent load as can be seen in the Fig. 4.13.

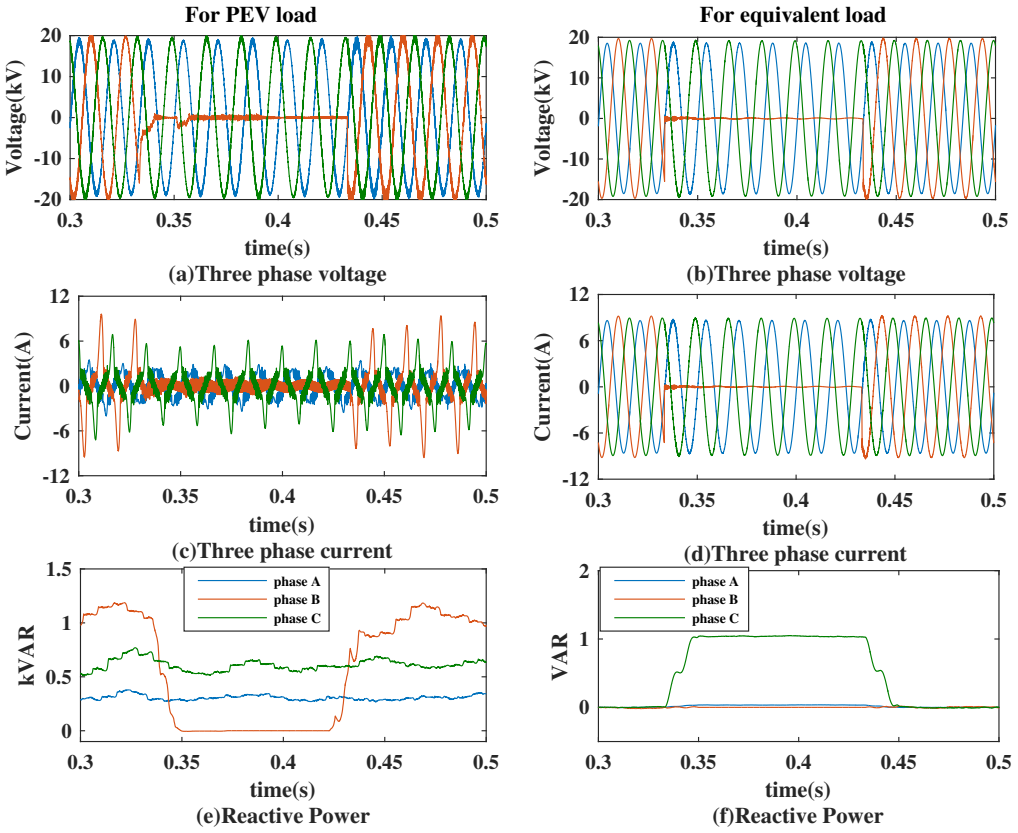

FIGURE 4.13: Impact on voltage, current and reactive power for open circuit fault at node 840

4.6 Conclusion

Electric vehicles are already in the market and their utilization is increasing day by day as electrification of transportation sector provides a promising way to alleviate the pollution caused by the conventional vehicle. Charging of their battery pack requires them to be integrated into distribution system. In this chapter, the impact of PEV charging on distribution network during fault conditions is studied.

The results obtained shows that in case of a fault the PEV load connected node are associated with increase in fault current and reactive power demand as compared to the equivalent constant power load connected to same node in the distribution system. This increase in fault current compared to the equivalent constant power

load is due to energy fed back to the system from the vehicles connected in healthy phase(s) of the distribution system. The increase in reactive power demand can be attributed to the fact that there is a direct relationship between voltage dip and increase in reactive power requirement. Since, there is a voltage collapse at the time of fault hence, the reactive power demand increases in proportion to the voltage dip in the system. When PEVs are integrated into the system a high magnitude transient voltage is observed during the period of re-connection of faulted phase to the system due to the continuous switching of PEV charging system. The impact is highest in case of single line to ground fault and lowest in case of open circuit faults. This high magnitude transient can cause insulation failure and re-ignition of arc in the circuit breaker. The rise in fault current above a safe limit triggers mal-operation of protective device in the distribution system whereas the rise in reactive power demand is associated with increase in system losses and heating of equipment. Suitable topology of charger control and filter type should be determined to mitigate these impacts. The high-frequency voltage transients and increase in current and reactive power during the fault are more significant when the PEVs charging load is connected on a lateral with low voltage level compared to that obtained on the main feeder with high nominal voltage level. Therefore, it can be concluded that the PEV charging load should be connected to a node having high voltage level in a distribution system so that the impact of it on the distribution system during fault conditions could be minimized.

As the important fault parameters such as fault current gets affected due to the presence of EV charging load in the distribution system therefore, the fault location schemes developed in this thesis are tested in presence of EV charging load in distribution system.

Chapter 5

DEVELOPMENT OF FAULT DETECTION AND FAULT CLASSIFICATION SCHEME

5.1 Introduction

This chapter describes the development of fault detection and faults classification scheme for the proposed fault location methods. The proposed fault detection and fault classification method is based on Wavelet Energy Entropy (WEE), magnitude of ground mode current component and algorithm based on decision taking rules.

The voltage and current signal of a network contain distinctive signatures which give the information about the presence or absence of a fault, its type and location in the distribution network [116]. The WEE of DWT detail coefficients obtained from three phase current signal is used by the proposed method in this thesis. The current signal contains important information which can provide detail about the fault status of the distribution network.

Furthermore, this chapter also covers the detail about the signal processing technique and modal transformation used in this thesis. Theories of Wavelet Transform and Modal Transformation are discussed in detail. Modal transformation is used in the proposed travelling wave based fault location methods. The estimation of travelling wave propagation speed which is required for travelling wave based fault location method is also given in this chapter.

5.2 Wavelet Transform

A wavelet is a waveform of effectively limited duration that has an average value of zero. The short time duration of the wavelets helps in achieving the localization in frequency and time. Sinusoids do not have limited duration as they extend from minus to plus infinity. Moreover, sinusoids are smooth and predictable, but wavelets tend to be irregular and asymmetric as shown in Fig. 5.1. As Fourier analysis consists of breaking up a signal into sine waves of various frequencies, wavelet analysis is the breaking up of a signal into shifted and scaled versions of the original (or mother) wavelet. In the wavelet transform (WT), the wavelets are time compressed and expanded. In the wavelet transformation process, each of the wavelet family has the same number of oscillations or cycles as the mother wavelet. The resulting wavelets, called daughter wavelets, are localized both in time and frequency. Thus, wavelet transform provides a local representation of signal in both time and frequency unlike Fourier transform which gives a global representation of signal in terms of frequency.

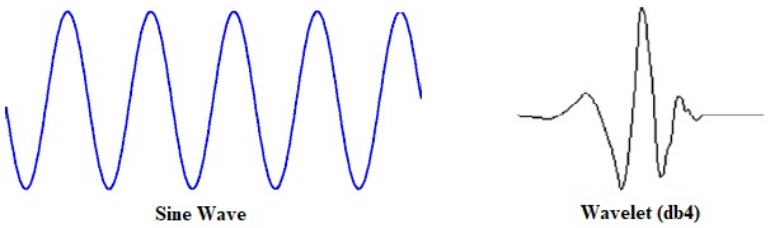

FIGURE 5.1: Comparison of a sinusoid and a sample mother wavelet

Due to the above mentioned properties of wavelet transforms, the WT are suitable for analyzing the compact patterns in transient analysis of power systems [117]. Although the classical Fourier transform is commonly applied in signal processing for frequency analysis, it is suitable to analyze stationary signal where time information is not required. Power system transient, which are typically non-periodic and contains short impulses, can be studied in a better way using WT. Thus, the wavelet transform has been particularly successful in analyzing the power system transients and in protective relaying [118]. Continuous wavelet transform (CWT) and discrete wavelet transform (DWT) are the ways by which wavelet transform can be implemented.

The CWT of a signal $x(t)$ is defined as:

$$CWT_{\psi}x(a,b) = \frac{1}{\sqrt{\mid a \mid}} \int_{-\infty}^{+\infty} x(t)\psi(\frac{t-b}{a})dt \tag{5.1}$$

Where, $\psi(t)$ is the mother wavelet, a and b are scaling parameters which defines the oscillatory frequency, the length of the wavelet and the shifting position respectively. The application of WT in power system generally requires the DWT;

The equation of the DWT is given by:

$$DWT(k,n,m) = \frac{1}{\sqrt{a_o^m}} \sum x[n]\psi(\frac{k - nb_0a_0^m}{a_0^m}) \tag{5.2}$$

Here, $\psi(t)$ is the mother wavelet where m indicates frequency localization and n denotes time localization, the scaling and translation parameter of CWT is replaced by a_0^m and $nb_0a_0^m$ respectively.

In CWT, the scaling parameters a and b are continuous. Therefore, in case of non-stationary signals, huge amount of data is generated. This is not economical in practical situations; the DWT is therefore, introduced in order to solve this problem, where both scaling parameters can be discrete. In DWT, with multi-resolution analysis, the transient signals can be proficiently analyzed and disintegrated using

two filters, one being a high pass filter (HPF) and the other being a low pass filter (LPF). The high pass filter is derived from the mother wavelet function and measures the details in a certain input. On the other hand, the low pass filter provides a smooth account of the input signal and is based on a scaling function linked with the mother wavelet [119]. Fig. 5.2 shows the multi-level disintegration of a signal using DWT.

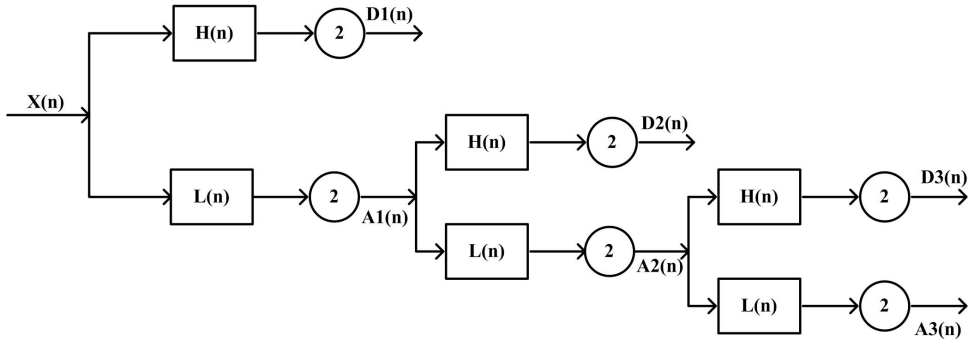

FIGURE 5.2: Wavelet multi-level decomposition

The above figure shows that the DWT has high-pass and low-pass filter banks at each decomposition level. The signal $X[n]$ is decomposed by the high pass and low pass filters into A1(n) and D1(n) at each decomposition level. D1(n) is the detail version of original signal and A1(n) is the smoothed version of original signal which contains only low frequency components.

Fig. 5.3 shows the original signal recorded after fault in the system and the Fig. 5.4 shows the wavelet coefficient's at different decomposition levels. From Fig. 5.4 it is clear that the higher levels give global information and the lower levels provide detail information of the wave.

5.2.1 Wavelet Energy Entropy (WEE)

The Wavelet Energy Entropy gives energy distribution of signals in frequency and time domain [120]. The recorded signal wavelet energy at scale j and instant k

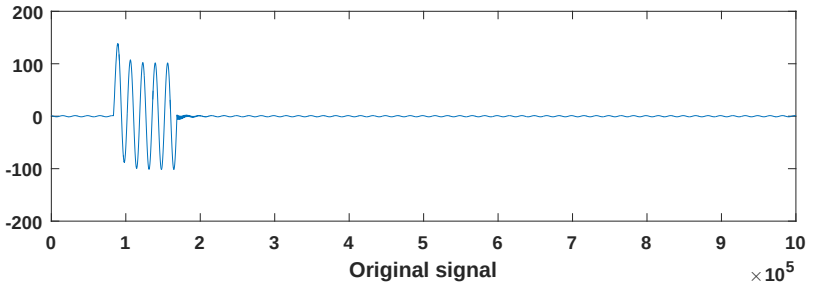

FIGURE 5.3: Original signal after fault

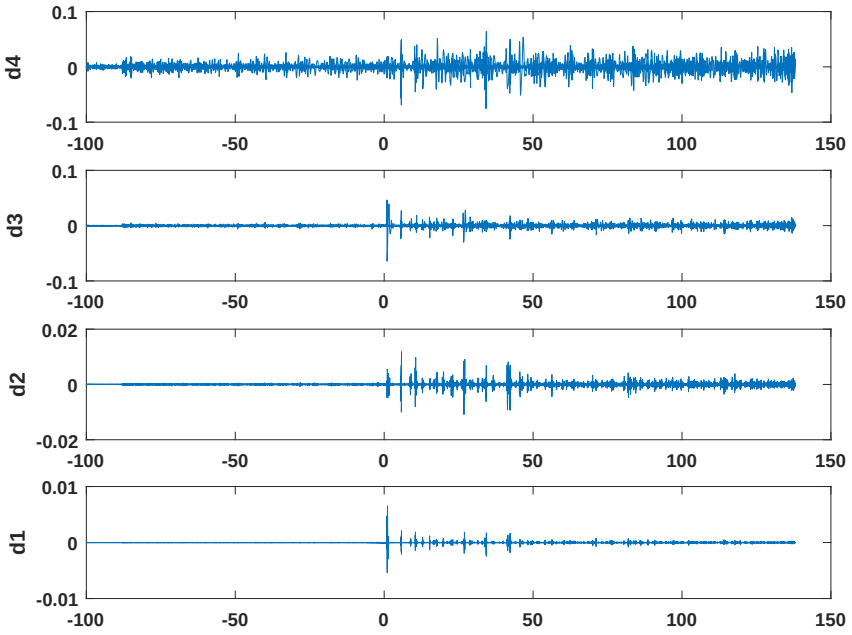

FIGURE 5.4: Wavelet decomposition at level 4

(k = 1, 2, . . . , N) is given as:

$$E_{jk} = \mid D_j(k) \mid^2 \tag{5.3}$$

Where, D_j is the detail coefficient of DWT at scale j. Total energy of signal at scale j s given as:

$$E_j = \sum_{k=1}^{N} E_{jk} \tag{5.4}$$

The relative wavelet energy is given as:

$$P_{jk} = \frac{E_{jk}}{E_j} \tag{5.5}$$

The Wavelet Energy entropy (WEE) at each scale is defined as:

$$WEE = -\sum_{j} P_{jk} \log P_{jk} \tag{5.6}$$

5.2.2 Wavelet Modulus Maxima (WMM)

The modulus maxima at any point (s_0, x_0) of the wavelet transform is defined as a strict local maximum of the modulus if it satisfies the condition:

$$\mid Wf(s_0, x) \mid < \mid Wf(s_0, x_0) \mid \tag{5.7}$$

Where x belongs to either side of x_0.

The modulus maxima represent singularity of a step signal and the point where modulus maxima appear is the point where sharp variation occurs [121]. The wavelet modulus maxima contain all the valuable information of the original signal and the signal can get approximate reconstruction by it.

5.2.3 Selection of Mother Wavelet

In principle, signal processing of fault transients can be performed by any wavelet but it has been observed that the signal processing performance is influenced by the used mother wavelet [122]. There are different family of mother wavelet such as Daubechies wavelets, Symlets, Coiflets and Biorthogonal wavelets which can be used for analysis of fault transients [117]. The best mother wavelet should have a high correlation with the signal of interest [123]. Research performed in [124, 125]

concludes that the Daubechies family wavelets are the best mother wavelet for power system transients. Authors in [123, 126, 127] performed analysis using db1-db8 Daubechies mother wavelets, with db-4 showing best result.

In this thesis, Daubechies family mother wavelets from db1-db8 are considered from which db4 mother wavelet is selected for analysis of fault transients because of its orthogonality, compact support and its good performance in transient analysis of power system as reported in [118].

5.2.4 Selection of Wavelet Detail Scale

The best scale of wavelet decomposition is selected in the same way, which is used in selection of mother wavelet. The optimum scale of wavelet detail coefficients is selected by the analysis of details' spectral energy of the current signal. The spectral energy of each detail component is obtained using the equation 5.3.

In this thesis, travelling wave based methods are used for fault location, which involves high-frequency fault transients. For selecting the travelling wave fault transient scale, the detail scale that has the highest frequency of all scales is usually selected. The range of frequencies for scale 1 to scale 6 for a sampling frequency of 1 MHz is given in Table 5.1.

TABLE 5.1: Frequency decomposition with DWT successive filtering

Detail scale	**Frequency range**
Scale 1	250 kHz- 500 kHz
Scale 2	125 kHz- 250 kHz
Scale 3	62.5 kHz- 125 kHz
Scale 4	31.25 kHz- 62.5 kHz
Scale 5	15.625 kHz- 31.25 kHz
Scale 6	7.8125 kHz- 15.625 kHz

As can be seen from the Table 5.1, for 1MHz sampling frequency scale 1 has highest frequency range but, the wavelet detail coefficients at scale 2 is used in this

work since the coefficient at scale1 has significant amount of noise and measurement error as it corresponds to highest frequency band [128].

5.3 Modal Transformation

Modal transformation is a process in which a certain group of coupled equations are decomposed into decoupled equations by excluding the mutual parts of these equations. By using modal transformation the coupled three phase voltage and current signals can be decomposed into a new set of decoupled voltage and current signals, which can be utilized individually in a manner similar to single phase line. This is illustrated using the impedance matrices of mutually coupled conductors in Fig. 5.5 and by equation 5.8.

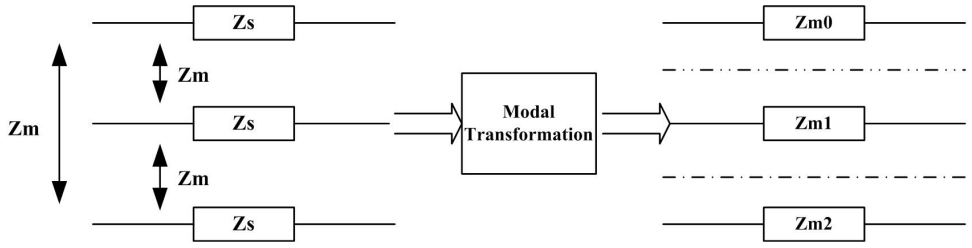

FIGURE 5.5: Modal transformation decomposition

$$\begin{bmatrix} Z_s & Z_m & Z_m \\ Z_m & Z_s & Z_m \\ Z_m & Z_m & Z_s \end{bmatrix} \Rightarrow \begin{bmatrix} Z_{m0} & 0 & 0 \\ 0 & Z_{m1} & 0 \\ 0 & 0 & Z_{m2} \end{bmatrix} \tag{5.8}$$

In this figure Z_{mi} are the modal components for ground mode and two aerial modes ($i = 0,\ 1,\ 2$). Modal transformation can be performed using either Clarke, Karrenbauer or Wedepohl transformation matrix.

The travelling waves based method use travelling wave velocity and its arrival time difference at the terminals to estimate the fault location. Hence, it is required to estimate the speed of travelling waves correctly. But the three-phase overhead

line has strong electromagnetic coupling between the conductors due to which the fault generated travelling waves do not propagate at a uniform speed. Therefore, a modal transformation matrix is required to decompose the three phase voltages or current into three sets of decoupled quantities i.e. modal voltages or current so that a uniform constant speed of travelling wave can be obtained.

The modal voltage and current equation can be represented as:

$$V(x,t) = T_v V_m(x,t) \tag{5.9}$$

$$I(x,t) = T_i I_m(x,t) \tag{5.10}$$

Here, V and I represent modal voltage and current respectively and subscript m represents modal component. T_v and T_i represents transformation matrix.

In this work Clarke's transformation matrix [129] is used to transform the three-phase transients into their modal components:

$$v_{0,1,2} = T^{-1} v_{a,b,c} \tag{5.11}$$

$$i_{0,1,2} = T^{-1} i_{a,b,c} \tag{5.12}$$

$$T^{-1} = \frac{1}{3}\begin{bmatrix} 1 & 1 & 1 \\ 2 & -1 & -1 \\ 0 & \sqrt{3} & -\sqrt{3} \end{bmatrix} \tag{5.13}$$

Here, suffix 1 and 2 represents aerial mode components, 0 represents ground mode component and T^{-1} is the Clarke transformation matrix.

5.4 Overview of Proposed Fault Location Schemes

The proposed fault location schemes comprises of three stages. In the first stage, fault detection and fault type identification task is performed using magnitude

of ground mode component of current and wavelet energy entropy (WEE) per phase. After fault detection and fault type identification the faulted line section is identified using aerial mode component wavelet modulus maxima (WMM) in the next step. The aerial mode WMM is obtained at all the points where laterals are connected to the main feeder. The magnitude of WMM determines the proximity of node to the fault, higher the magnitude of WMM at the node, closer is the node to the fault. Once the faulted section is identified, the actual fault location is estimated along the pre-identified faulted line section in the third and final stage. The proposed single-terminal travelling wave fault location method assumes that the fault data recording are available at the substation node, all the junction point and DG and PEV connected nodes. The proposed two terminal fault location method assumes that the fault data recording are available at both ends of each line section and the incoming samples are time-stamped using GPS. It is assumed that optical current transducers equipped with travelling wave recorders are placed at each end of the line section, and an open communication channel is available through which relay can send fault data to the relay at the remote terminal. Fig. 5.6 shows the schematic overview of proposed fault location schemes.

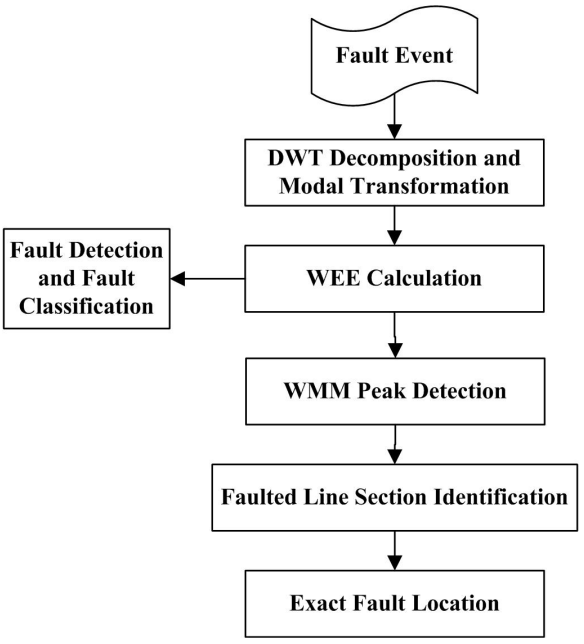

FIGURE 5.6: Schematic overview of proposed fault location schemes

5.5 Fault Detection Algorithm

The developed fault location schemes in this work at first identify the fault condition in the system. This identification is performed using the WEE obtained per phase at scale-2 decomposition level by equation 5.6. The wavelet decomposition is performed using the db4 mother wavelet and detail components at scale-2 are selected due to reasons mentioned in subsection 5.2.3 and in subsection 5.2.4.

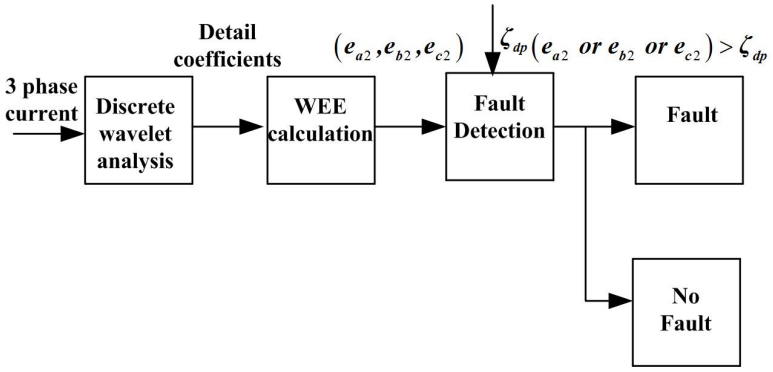

FIGURE 5.7: Fault detection schematic diagram

5.5.1 Rules for Fault Detection Algorithm

The fault condition in the system is detected by comparing the WEE obtained per phase at scale 2. Fig. 5.7 shows the different stages of rule based fault detection algorithm. The three phase current signals serves as the data input to the algorithm. The decomposition of the current signal is carried out using DWT and then the WEE (e_{a2}, e_{b2}, e_{c2}) for each phase at scale-2 is calculated. The calculated WEE for each phase is then compared with the predefined threshold values of each of the respective phase. If the calculated WEE of any phase is greater than the respective threshold value, the fault is detected. The thresholds $\zeta_{dp}, p \in (A, B, C)$ for each phase is decided by several simulations performed on the distribution system under fault and no fault conditions to ensure that the algorithm would be able to discriminate correctly between normal switching events and faults. The rules for fault detection

in the distribution system are:

$$\begin{aligned}(e_{a2}\ or\ e_{b2}\ or\ e_{c2}) > \zeta_{dp} \rightarrow\ & Fault\ is\ detected \\ else \rightarrow\ & No\ fault\end{aligned} \tag{5.14}$$

Here, (e_{a2}, e_{b2}, e_{c2}) are the WEE of phase A, phase B and phase C at scale 2 respectively, and ζ_{dp} is the threshold value of the phase.

5.6 Fault Classification Algorithm

After fault is detected the fault type identification is performed by the proposed method. Each type of fault has its own characteristic features by which the fault classification task is accomplished. Fig. 5.8 shows the flowchart for fault classification and faulted phase selection. This is accomplished in two stages. At first, fault is categorized into grounded or ungrounded fault. The presence of ground path in the fault is determined by looking at the magnitude of ground mode component WMM. If ground mode component is non-zero then fault is identified as a grounded fault otherwise, the fault is identified as an ungrounded fault. Then, the individual phase entropies values are compared for faulted phase selection. The wavelet energy calculated for the faulted phase possess higher energy but the wavelet energy entropy calculated using equation 5.6 uses relative energy therefore, the WEE of faulted phase(s) possess lower energy than non-faulted phase.

5.6.1 Rules for Fault Classification Algorithm

The rules for the fault type identification are listed below; these rules are formulated by observing the patterns during the simulations. Here, the ground mode WMM is represented by $WMMgm$.

Rule 1 : $if\ (e_{a2} < e_{b2}, e_{c2})\ and\ WMMgm \neq 0 \rightarrow A - g\ Fault$

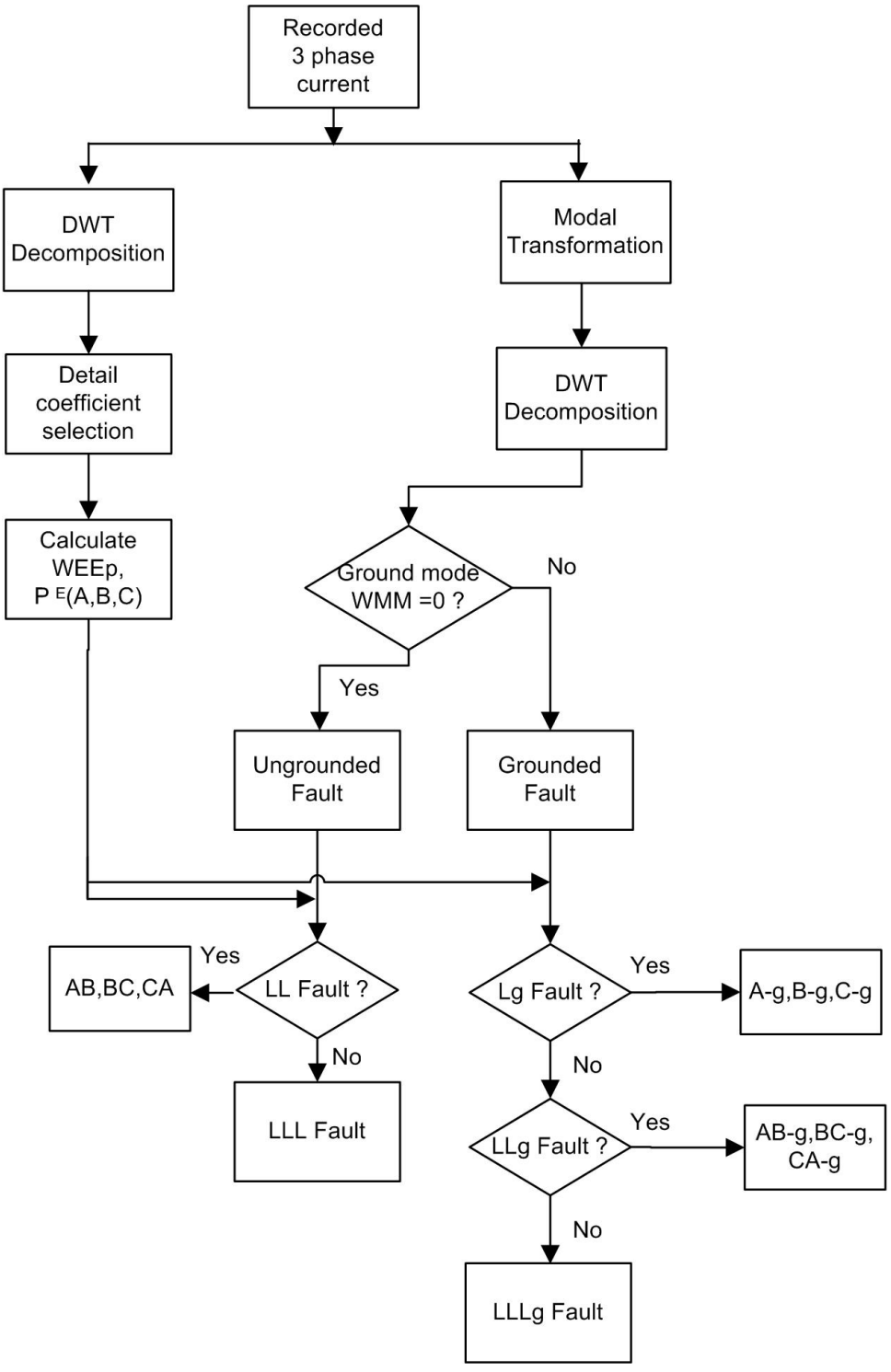

FIGURE 5.8: Flowchart for fault classification

$$Rule\ 2: \ if\ (e_{b2} < e_{a2}, e_{c2})\ and\ WMMgm \neq 0 \rightarrow B - g\ Fault$$

$$Rule\ 3: \ if\ (e_{c2} < e_{a2}, e_{b2})\ and\ WMMgm \neq 0 \rightarrow C - g\ Fault$$

$Rule\ 4: \ if\ (e_{a2}, e_{b2} < e_{c2})\ and\ WMMgm = 0 \rightarrow\ AB\ Fault$

$Rule\ 5: \ if\ (e_{b2}, e_{c2} < e_{a2})\ and\ WMMgm = 0 \rightarrow\ BC\ Fault$

$Rule\ 6: \ if\ (e_{c2}, e_{a2} < e_{b2})\ and\ WMMgm = 0 \rightarrow\ CA\ Fault$

$Rule\ 7: \ if\ (e_{a2}, e_{b2} < e_{c2})\ and\ WMMgm \neq 0 \rightarrow\ AB - g\ Fault$

$Rule\ 8: \ if\ (e_{b2}, e_{c2} < e_{a2})\ and\ WMMgm \neq 0 \rightarrow\ BC - g\ Fault$

$Rule\ 9: \ if\ (e_{c2}, e_{a2} < e_{b2})\ and\ WMMgm \neq 0 \rightarrow\ CA - g\ Fault$

$Rule\ 10: \ else\ (rule\ 1\ to\ 9)\ and\ WMMgm = 0 \rightarrow\ ABC\ Fault$

$Rule\ 11: \ else\ (rule\ 1\ to\ 9)\ and\ WMMgm \neq 0 \rightarrow\ ABC - g\ Fault$

5.7 Conclusion

A fault detection and fault classification scheme is presented in this chapter. The tasks performed by the scheme are the waveform decomposition using DWT, fault event verification and fault type classification. Scale-2 detail coefficients of DWT decomposition of the three phase current and ground mode component WMM of current transients was used as the input source to the algorithms. Wavelet energy entropy of the scale-2 detail coefficient was used as the input to the fault detection algorithm. After fault is detected fault type is identified. The WEE and magnitude of ground mode component WMM serve as the input to the rule-based fault classification algorithm.

The results obtained from the implementation of fault detection and fault classification algorithm on the test system under different operating condition is presented in next chapters.

Chapter 6

TRAVELLING WAVE BASED FAULT LOCATION METHODS

6.1 Introduction

The principle of fault location using travelling wave is based on fault generated high-frequency transient signals which travel away from the fault point towards the line terminals. These transients travel along the lines and are reflected at the line terminals following the rules of Bewley's Lattice Diagrams [66]. The utilization of travelling wave fault location methods in power systems has been till date limited to transmission system only, its use in distribution system has not been explored in depth owing to difficulties such as the requirement of high frequency travelling wave recorders, problem in time synchronization of the recorded data and need of an open communication channel between the terminals. The development in high voltage and current optical transducers technology together with high-frequency transient recorders have overcome the problems encountered in recording of high-frequency transients of fault generated travelling wave and have made travelling wave-based fault location methods more practical [130]. If the time of arrival of the travelling waves at the two ends of the transmission line can be measured precisely, the fault

location then can be determined using arrival time of first peak of either current or voltage travelling wave at the line terminals or the using the time difference between the initial or subsequent wave peaks due to reflection of travelling waves from the fault point. The proposed methods are implemented using transient current signals as input signal. The three-phase current signals are selected as data input for the proposed fault location schemes because the overcurrent protection is the most used form of protection in distribution systems. Hence, the line current signals are readily available. Moreover, the surge in fault current is easier to detect than the voltage collapse during faults and the current travelling wave transients are generally much less distorted than the voltage transients.

6.2 Process of Transient Travelling Waves on Overhead Lines

The occurrence of travelling wave on overhead transmission lines can be explained with a single line to ground fault assumed on single phase overhead line of a two terminal bus network. According to superposition theorem for overhead lines the fault point is superimposed of two equal amplitude and opposite direction voltage source. The pre-fault voltage at fault point has same amplitude as these two voltage sources. The post fault single phase overhead line network can be represented as a superimposed circuit of pre-fault normal operating network and an additional fault component network.

Fig. 6.1 represents the superposition principle for overhead lines [131]. Fig. 6.1(a) presents single line diagram for two terminal overhead line with fault at point F. Fig. 6.1(b) shows equivalent network of Fig. 6.1(a), v_f is the pre-fault voltage at fault point and $-v_f$ is the opposite in direction but equal amplitude pre-fault voltage. Fig. 6.1(c) is the normal operating network in pre-fault condition; v_f is the fault point pre-fault voltage. And the Fig. 6.1(d) is the fault component network.

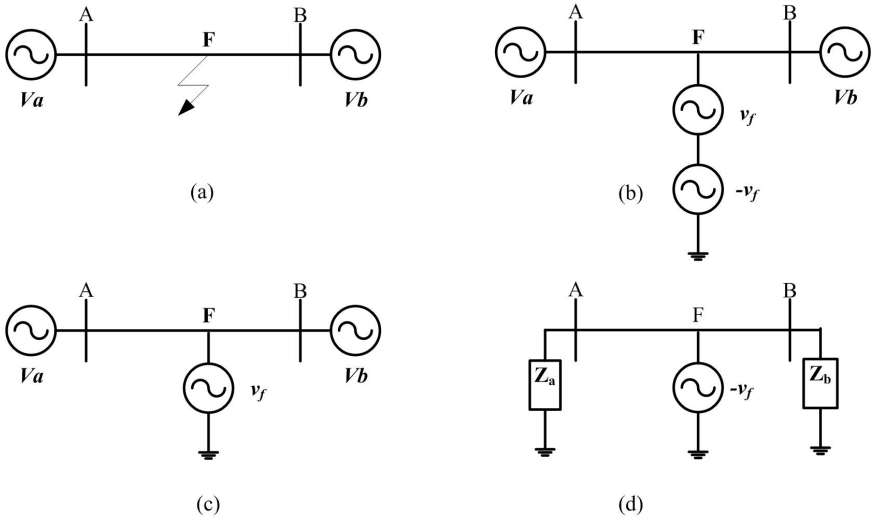

FIGURE 6.1: Superposition principle for overhead lines

The voltage and current transient travelling waves travel toward the end terminals whenever there is a fault on the overhead line. These transient wave signals will continue to bounce back and forth between the fault points and line terminals [1]. The voltage (V) and current (I) equation in partial differential equation for a single-phase lossless overhead transmission line is represented as [1]:

$$\frac{\partial v}{\partial x} = -L\frac{\partial i}{\partial t} \tag{6.1}$$

$$\frac{\partial i}{\partial x} = -C\frac{\partial v}{\partial t} \tag{6.2}$$

In the above equations L and C are the line inductance and capacitance per unit length. The above equations can be further differentiated as:

$$\frac{\partial^2 v}{\partial x^2} = LC\frac{\partial^2 v}{\partial t^2} \tag{6.3}$$

$$\frac{\partial^2 i}{\partial x^2} = LC\frac{\partial^2 i}{\partial t^2} \tag{6.4}$$

In these equations resistance is assumed to be negligible. The solution of equation 6.3 and equation 6.4 is given as:

$$v(x,t) = v_f(x - vt) + v_r(x + vt) \tag{6.5}$$

$$i(x,t) = \frac{1}{Z_c} v_f(x - vt) - \frac{1}{Z_c} v_r(x + vt) \tag{6.6}$$

Here, $Z_c\sqrt{\frac{L}{C}}$ is the characteristic impedance of transmission line and $v = \sqrt{\frac{1}{LC}}$ is the velocity of propagation.

6.2.1 Wave Reflection and Refraction

The buses and transformers act as discontinuities in the path of travelling waves on the overhead lines. When a travelling wave reaches a discontinuity, it suffers both reflection and refraction; part of it reflected back and remaining part passes through. The characteristic impedance of the line and impedance of line beyond the discontinuity decides the magnitude of reflected and refracted waves. Fig. 6.2 shows the Bewley's lattice diagram explaining the phenomena of reflection and refraction of travelling waves.

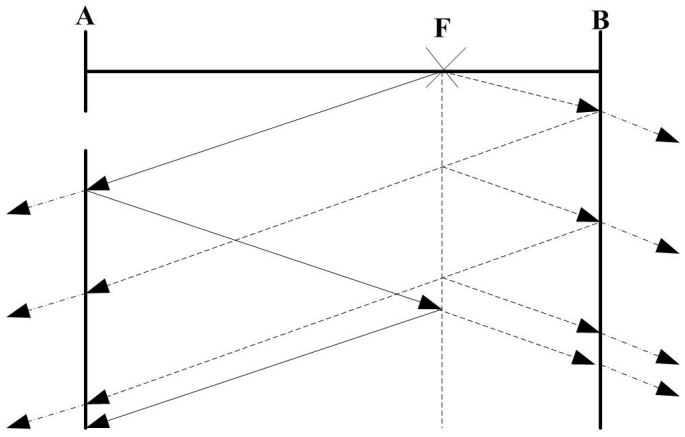

FIGURE 6.2: Bewley's Lattice diagram

The total energy of the incident wave is distributed between the reflected and refracted waves at each discontinuity. The reflection and refraction of travelling wave continue till it loses all the energy and the amplitude become negligible. For a transmission line having characteristic impedance Z_0, the Z_0 in forward and backward direction of fault is given as:

$$Z_0 = \frac{V^+}{I^+} \tag{6.7}$$

$$-Z_0 = \frac{V^-}{I^-} \tag{6.8}$$

Here V^+ and I^+ are the voltage and current in forward direction and V^- and I^- is the voltage and current in backward direction w.r.t. fault point.

The load impedance Z_t at the line termination is given by

$$Z_t = \frac{V^t}{I^t} \tag{6.9}$$

Here, V_t and I_t are reflected voltage and current waves.

Since, voltage and current waves exist at the same time at a junction

$$V^t = V^+ + V^- \tag{6.10}$$

$$I^t = I^+ + I^- \tag{6.11}$$

Substituting equation 6.11 and equation 6.10 in equation 6.9

$$Z_t = \frac{V^+ + V^-}{I^+ + I^-} \tag{6.12}$$

Substituting for I^+ and I^- we get

$$\frac{Z_t}{Z_0} = \frac{V^+ + V^-}{V^+ - V^-} \tag{6.13}$$

Rearranging this equation provides,

$$\frac{V^-}{V_+} = \frac{Z_t - Z_0}{Z_t + Z_0} \tag{6.14}$$

This ratio represented by ρ_v is called voltage reflection factor

$$\rho_v = \frac{Z_t - Z_0}{Z_t + Z_0} \tag{6.15}$$

Similarly, ρ_i represents current reflection factor and is given by

$$\rho_i = \frac{Z_0 - Z_t}{Z_0 + Z_t} \tag{6.16}$$

6.2.2 Estimation of Travelling Wave Velocity

The aerial mode components 1 and 2 have the same velocity V_1, this is called aerial mode velocity. The ground mode component has different velocity than aerial mode component represented by V_0. The accuracy of travelling wave based fault location method is dependent on accuracy of estimated travelling wave propagation speed. The approximated aerial mode and ground mode component has speed near to speed of light but smaller than it. The velocities can be calculated using following equations.

The modal voltage and modal current equations are given as [132]

$$\frac{\partial^2 V_m}{\partial x^2} = S^{-1}LCS\frac{\partial^2 V_m}{\partial t^2} \tag{6.17}$$

$$\frac{\partial^2 I_m}{\partial x^2} = Q^{-1}LCQ\frac{\partial^2 I_m}{\partial t^2} \tag{6.18}$$

$$S^{-1}LCS = Q^{-1}LCQ \begin{bmatrix} L_0C_0 & 0 & 0 \\ 0 & L_1C_1 & 0 \\ 0 & 0 & L_1C_1 \end{bmatrix} \tag{6.19}$$

Thus, the aerial modes have same velocity V_1, and ground mode velocity is V_0

$$V_1 = v_{i_1} = v_{i_2} = \frac{1}{\sqrt{L_1 C_1}} \tag{6.20}$$

$$V_0 = \frac{1}{\sqrt{L_0 C_0}} \tag{6.21}$$

Here, L_1, C_1 are positive sequence line inductance and line capacitance respectively, and L_0, C_0 are zero sequence line inductance and line capacitance respectively. The travelling wave speed is calculated using the system parameters. For this work the system parameters of the used test system are given in Appendix section. Putting the value of those parameters in equation 6.20 and equation 6.21, we get aerial mode and ground mode velocity as:

$V_1 = v_{i_1} = v_{i_2} = 2.9188 \times 10^5\ km/s$

$V_0 = 2.1089 \times 10^5\ km/s$

According to [133] the ground mode impedance is large therefore, the ground mode speed is less than aerial mode speed. Also, the ground mode component is present in case of grounded fault only therefore, it cannot be used for all fault type. Hence, the aerial mode component is selected for fault location in this work.

6.3 Proposed Single-Terminal Fault Location Method

The proposed single-terminal fault location scheme comprises of three stages. In the first stage, the fault detection and classification tasks are performed using Wavelet Energy Entropy (WEE) and magnitude of ground mode component of the current as explained in chapter 5. The identification of faulted line section is done in next stage by comparing the modulus maxima of aerial mode wavelet coefficients obtained at interconnecting point of each line section. The third stage determines the

actual fault location along the faulted line section. In the development of the procedure, it is assumed that the measurements are available at all the interconnecting point of laterals and the measurements need not be synchronized. Optical current transducers equipped with travelling wave recorders are assumed to be placed at the substation and the interconnecting points of each lateral i.e. at nodes 800, 808, 816, 824, 854, 858, 834 and 836 respectively. The following section explains each step of the fault location process in detail.

6.3.1 Faulted Line Section Identification

In a multilateral distribution system the calculated fault location can point to multiple locations in the network from the substation. Hence, for accurate fault location, it is essential to locate the faulted lateral or line section. The identification of faulted lateral is performed by comparing the magnitude of aerial mode WMM obtained at the measurement point where the laterals are connected to the main feeder. From Fig. 6.4 there are 7 such points for IEEE 34 node system, at nodes 808, 816, 824, 854, 858, 834 and 836. Node 832 is also a junction point where lateral is connected but length of the line section 832-888 is 0 feet and it is used only for transformer connection therefore, this node is not used as a measurement point. At the time of fault, the magnitude of WMM is highest for the node closer to the fault and the node at other end has lesser magnitude of WMM than the node which is closer to the fault. All, the other non-faulted line segment node has lesser magnitude of aerial mode WMM compared to the two nodes of faulted line segment. Hence, by comparing them for magnitude, the lateral having highest magnitude of first peak of WMM is identified as the faulted lateral.

6.3.2 Fault Location along the Faulted Line Section

If a fault involving ground occurs in the system, then the backward and forward travelling waves suffers reflections from both the fault point and remote terminals, but in case of balanced or ungrounded fault, there are no significant reflections from remote ends [133]. Thus, the proposed method is developed accordingly, and fault location process for ungrounded and grounded faults is presented separately. The proposed scheme is explained with the help of power system model shown in Fig. 6.3.

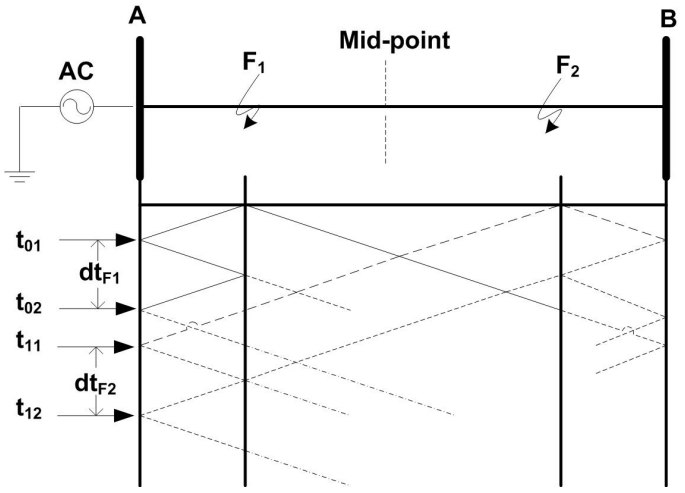

FIGURE 6.3: Lattice diagram for the faults in power system model

Assume faults at point F_1 and F_2 on the power system model at the first half and second half of line section AB from bus A respectively. The distance of F_1 from bus A is same as that of F_2 from bus B. The Bewley lattice diagram for travelling waves produced by fault F_1 and for remote end fault F_2 is shown in Fig. 6.3. For a grounded fault occurred at F_1 the first peak at bus A is due to arrival of backward travelling wave at time t_{01} and the second peak at bus A is due to arrival of backward travelling wave reflected from fault point at time t_{02}. The calculation of fault location is done using the time difference between the first two peaks of aerial

mode wavelet coefficients obtained at bus A, as follows:

$$x = \frac{v \times dt_{F_1}}{2} \tag{6.22}$$

$$dt_{F_1} = t_{02} - t_{01} \tag{6.23}$$

Here v is the propagation velocity of aerial mode and x is the distance to fault.

It can be observed that the difference in time (dt_{F_1} & dt_{F_2}) recorded by the travelling wave fault locator is likely to be identical for the fault F_1 and the fault F_2 for two consecutive transient wavefronts. Therefore, for accurate fault location using travelling wave method an additional discrimination is required. Such discrimination is provided by first identifying the faulted region of the line section. This identification is done by comparing the time difference Δt_0 between the arrival instant of initial peak of modulus maxima of aerial mode and ground mode wavelet coefficients with the difference in time Δt_m obtained between arrival instant of aerial and ground mode wavelet modulus maxima for a fault at the center of the line section. If Δt_0 is lesser than Δt_m then faulted region is recognized as first half of the line section and if Δt_0 is greater than Δt_m then second half of the line section is the faulted region.

Now for a fault at point F_2 the backward travelling wave reaches bus A at time t_{11} and the forward travelling wave reaches at time t_{12}. The fault location is given by equation 6.22 but the time difference is substituted by

$$dt_{F_2} = \frac{2L}{v} - (t_{12} - t_{11}) \tag{6.24}$$

Here, L is the line segment length and $t_{12} - t_{11}$ is the difference in time between two successive peaks of modulus maxima of the aerial mode. Substituting dt_{F_2} in equation 6.22 we get distance to fault x as:

$$x = L - \frac{v - (t_{12} - t_{11})}{2} \tag{6.25}$$

In case of symmetrical and ungrounded fault, the fault location is given by equation 6.22 irrespective of the half in which fault occur, since these faults don't produce any significant reflection from remote end bus.

6.4 Simulation Results

The modified IEEE 34 node distribution system shown in Fig. 6.4 is used as the test system for evaluating the performance of proposed fault location scheme. Detail modelling of the distribution system is presented in chapter 3. In order the consider the effect of DG and PEV charging load, a synchronous generator type DG unit of 350 kW rated power [108] and an PEV charging station are connected to the system at node 840 and node 890 as shown in Fig. 6.4. The synchronous generator DG unit is connected to the end of main section at node 840. Node 890 is selected for adding the charging station because line section 888-890 has nominal voltage rating of 4.16 kV which is suitable for the PEV charging level [SAE Standard J1772, 2010] considered in this thesis. The charging station consists of three PEVs, each with a maximum capacity of drawing 6.6 kW of power from the distribution system. The total extra load due to PEV addition on the system is 19.8 kW. The detail of PEV load modeling is given in chapter 3. All types of shunt fault are simulated at different location on the main feeder and side branches to evaluate the performance of proposed scheme. Simulations are done in MATLAB/SIMULINK at a sampling frequency of 1 MHz.

6.4.1 Fault Detection

The fault detection results of the proposed fault location scheme are presented in this sub-section. Various results covering 'no fault' and fault conditions are given for the test system using Wavelet Energy Entropy (WEE). In order to show the detection capability of the fault detection algorithm, the procedure given in section

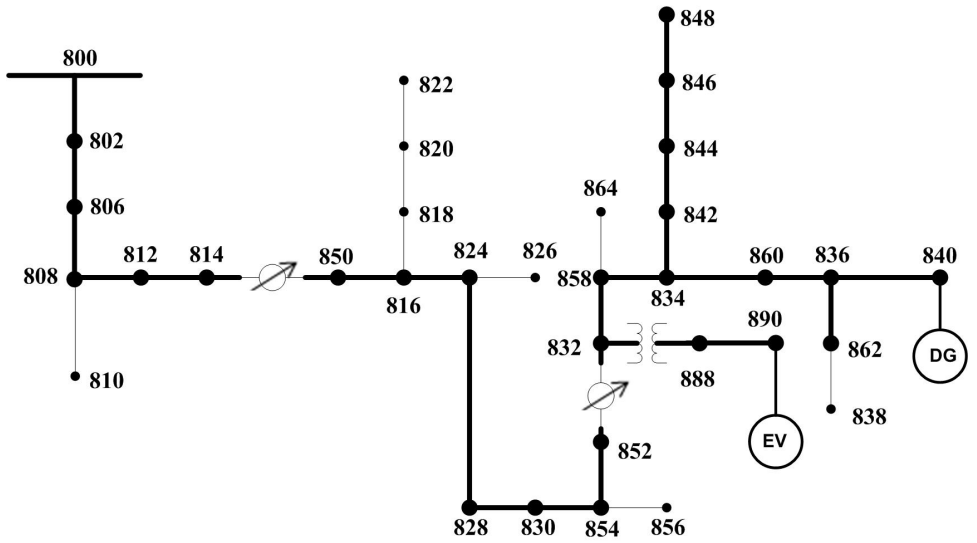

FIGURE 6.4: Lattice diagram for the faults in power system model

5.5 was followed. The fault detection results at the beginning, mid-point and the end of line are presented for the main feeder. The reason behind this is that the magnitude of the current signal changes and diminishes further down the feeder away from the source at the substation.

From the simulation results obtained, the WEE of faulted phase(s) have lowest value. This is because the WEE is computed using relative energy calculation and since, the faulty phase(s) have the highest wavelet energy therefore, the faulted phase(s) have lowest WEE value. Table 6.1 shows WEE values for different phases at no-fault and various fault cases. These simulation results are obtained for 0^0 inception angle and 0 Ω fault resistances at 10% length of main feeder. The WEE in bold text indicates faulted phase, it can be seen the WEE values of fault cases clearly exceeds no-fault case. Table 6.2 shows fault detection results for 45^0 inception angle and 10 Ω fault resistance at 50% length of main feeder. Similarly, the fault detection result for 90% length of main feeder is presented in Table 6.3.

TABLE 6.1: WEE values at 10% of feeder length

Individual phase WEE	**No fault case**	**A-g Fault**	**AB Fault**	**AB-g Fault**	**ABC Fault**	**ABC-g Fault**
e_{a2}	1.7062	**3.6332**	**3.3711**	**2.0140**	**1.8466**	**1.8468**
e_{b2}	1.7063	4.8720	**3.9668**	**2.1027**	**1.9716**	**1.9767**
e_{c2}	1.7062	4.5736	4.4235	3.8276	**2.3199**	**2.3202**

TABLE 6.2: WEE values at 50% of feeder length

Individual phase WEE	**No fault case**	**A-g Fault**	**AB Fault**	**AB-g Fault**	**ABC Fault**	**ABC-g Fault**
e_{a2}	1.6366	**2.8310**	**1.9872**	**3.0077**	**2.1793**	**2.1926**
e_{b2}	1.6364	3.9332	**1.8775**	**3.3840**	**2.7044**	**2.7459**
e_{c2}	1.6362	3.3989	2.8908	4.8704	**2.7075**	**2.8909**

TABLE 6.3: WEE values at 90% of feeder length

Individual phase WEE	**No fault case**	**A-g Fault**	**AB Fault**	**AB-g Fault**	**ABC Fault**	**ABC-g Fault**
e_{a2}	1.6348	**2.6493**	**2.1326**	**2.2283**	**2.0992**	**2.1056**
e_{b2}	1.6365	4.2633	**2.4308**	**2.5983**	**2.2115**	**2.2938**
e_{c2}	1.6366	4.1262	3.6748	3.7737	**2.4109**	**2.3632**

6.4.2 Fault Classification and Faulted Phase Selection

The fault classification and faulted phase selection ability of the proposed scheme is tested using various fault cases. The procedure given in section 5.6 was followed. At first, fault is categorized into grounded or ungrounded fault. The presence of ground path in the fault is determined by looking at the magnitude of ground mode component WMM. Then, the individual phase entropies values are compared for faulted phase selection. Table 6.4 shows the results of fault classification for different fault types using wavelet energy entropy. The WEE shown in bold signify the faulted phase(s). Here, fault classifications for 27 cases are shown in which two cases are misclassified (highlighted text in Table 6.4) and the classification accuracy of 92.59%.

TABLE 6.4: WEE for faults at different locations

Fault Type	WEE per phase	1 Ω /0^0at 10% feeder length	10 Ω /30^0 at 90% feeder length	20 Ω /45^0 on lateral 834-848
A-g	e_{a2}	**1.2163**	1.6196	**0.9572**
	e_{b2}	2.1229	1.5712	1.6235
	e_{c2}	1.7300	1.5768	1.5910
B-g	e_{a2}	3.3576	1.5944	1.3837
	e_{b2}	**1.1355**	**1.4301**	**0.9589**
	e_{c2}	4.6394	1.7349	1.4327
C-g	e_{a2}	3.8934	1.6197	1.0357
	e_{b2}	2.0296	1.1107	1.0052
	e_{c2}	**1.7557**	**0.8528**	**0.9936**
A-B	e_{a2}	**1.3710**	**1.6255**	1.3230
	e_{b2}	**1.2368**	**1.6194**	1.4520
	e_{c2}	1.5759	1.9068	1.0410
B-C	e_{a2}	1.8861	1.6215	1.0933
	e_{b2}	**1.4666**	**1.4596**	**0.8919**
	e_{c2}	**1.6928**	**1.0734**	**0.9134**
C-A	e_{a2}	**1.6963**	**1.4974**	**1.1280**
	e_{b2}	2.6251	2.3673	1.9060
	e_{c2}	**1.3987**	**1.3670**	**0.9376**
AB-g	e_{a2}	**2.0939**	**1.1411**	**1.2913**
	e_{b2}	**1.2690**	**1.1614**	**1.5911**
	e_{c2}	4.5777	1.9215	2.4398
BC-g	e_{a2}	2.6682	1.9542	1.5790
	e_{b2}	**1.3113**	**1.6132**	**1.2733**
	e_{c2}	**2.0557**	**1.4444**	**1.3710**
CA-g	e_{a2}	**4.2007**	**1.4205**	**1.4270**
	e_{b2}	5.3289	2.0632	2.2404
	e_{c2}	**1.5131**	**1.3281**	**1.2114**

6.4.3 Identification of Faulted Line Section

As mentioned in sub-section 6.3.1 the faulted section identification is done by comparing the magnitude of wavelet modulus maxima at scale 2 of aerial mode components. Fig. 6.5 shows the magnitude of aerial mode component obtained at the different nodes for a line to ground fault at a distance 28.62 km from the node 800 for R_f of 1Ω and θ_f of 0^0 in the line section 808-816. The magnitude of aerial mode WMM obtained at node 816 is highest in comparison to other non-faulted section as shown in Table 6.5; hence, the line section 808-816 is identified as faulted line section.

TABLE 6.5: Magnitude of aerial mode WMM

Node	Magnitude of aerial mode WMM
800	4.012×10^{-5}
808	0.63×10^{-2}
816	1.149
824	2.019×10^{-3}
834	2.194×10^{-3}
836	1.057×10^{-6}
858	1.014×10^{-10}

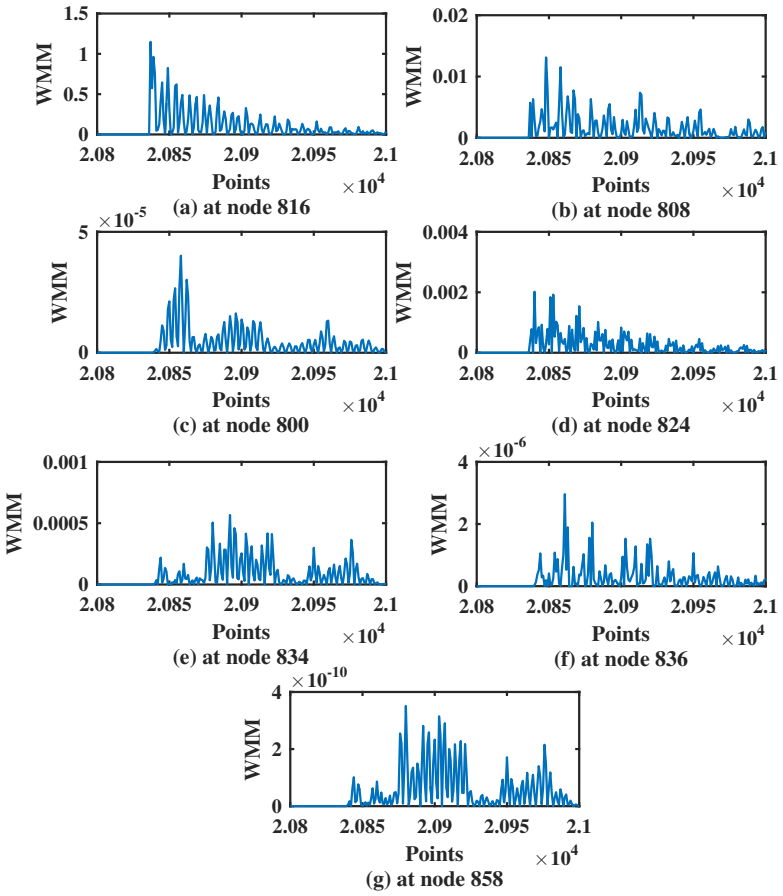

FIGURE 6.5: WMM of aerial mode component obtained at the different node

6.4.4 Fault Location along the Faulted Line Section

Table 6.7 shows the actual fault location obtained along the faulted line section for different fault cases under different R_f and θ_f considering DG and EV load. The faulted half of the line section is decided by comparing Δt_0 and Δt_m, Δt_m for

different line section is shown in Table 6.6. Table 6.7 gives exact fault location for both fault on the main feeder and fault on different laterals. It can be seen from the Table 6.7 that the error in the calculated fault distances is very low. The error is calculated using equation 6.26.

$$error\% = \frac{\mid D_{actual} - D_{calc.} \mid}{l} \times 100 \tag{6.26}$$

Where, D_{actual} and $D_{calc.}$ are actual and calculated distance of fault from substation and l is the length of faulted line section. The maximum error in fault location is 3.39% in the laterals and 1.45% in the main feeder.

TABLE 6.6: Δt_m for faults at the centre of line in different line sections

Distance (km)	Δt_m	**Section**
5.57	5.8	800-808
0.88	0.91	808-810
10.29	10.70	808-816
9.69	10.10	816-822
1.55	1.61	816-824
0.46	0.47	824-826
3.32	3.45	824-854
3.55	3.69	854-856
5.61	5.83	854-832
1.60	1.66	832-890
0.75	0.78	832-858
0.25	0.26	858-864
0.88	0.91	858-834
0.89	0.92	834-848
0.72	0.75	834-836
0.78	0.81	836-838
0.13	0.14	836-840

TABLE 6.7: Fault location result in different sections

Fault type	R_f & θ_f	**Distance from node 800 (km)**	**Faulted section**	**Calculated distance (km)**	**Error** (%)
A-g	$10\Omega/30^0$	1.81	800-808	1.47	0.58
B-g	$1\Omega/0^0$	38.27	824-854	37.43	1.45
C-g	$20\Omega/45^0$	56.25	834-848	56.19	3.39
AB	$1\Omega/0^0$	28.62	808-816	28.37	0.43
BC	$30\Omega/90^0$	35.05	816-824	35.22	-0.29
CA	$10\Omega/30^0$	46.52	854-858	45.80	1.24
AB-g	$20\Omega/45^0$	25.50	808-816	25.13	0.63
BC-g	$1\Omega/0^0$	54.97	858-834	55.65	-1.17
CA-g	$30\Omega/90^0$	43.83	816-822	44.37	-2.78
ABC	$10\Omega/135^0$	6.50	800-808	6.22	0.48
ABC-g	$20\Omega/30^0$	55.10	832-890	55.00	3.11

6.5 Sensitivity Studies

6.5.1 Effect of different types of DG on Fault Location Scheme

The fault current level increases or decreases depending upon the type of DG used and location of fault. Hence, the severance of transient current recorded at the measurement point changes. The fault current level is maximum in case of synchronous generator type of source and minimum in case of inverter based sources [8]. To evaluate the accuracy of proposed method against the contribution to fault current by different types of DG sources, the proposed fault location method is also tested with a 100 kW PV (inverter based) source [109] connected at node 840 and the results are compared with the results of fault in the absence of any source at the node and in the presence of 350 kW synchronous generator type DG at the same node. As can be seen from the obtained results shown in Fig. 6.6(a), Fig. 6.6(b) and Fig. 6.6(c) without DG case, with synchronous generator case and with PV case respectively, for a line to ground fault in line section 834-840 with a R_f of 10Ω and θ_f of 30^0 at a distance 1.5 km from the node 834 the first two peak of WMM occur at same time instants in all the three cases and hence the time difference between the first two peaks of WMM, which is used for calculating fault distance remains

unaltered and only the peak magnitude changes due to the change in fault level. As the proposed method uses only time information from the WMM profile for fault location estimation, the proposed method accuracy is not affected by the presence of different types of DG sources.

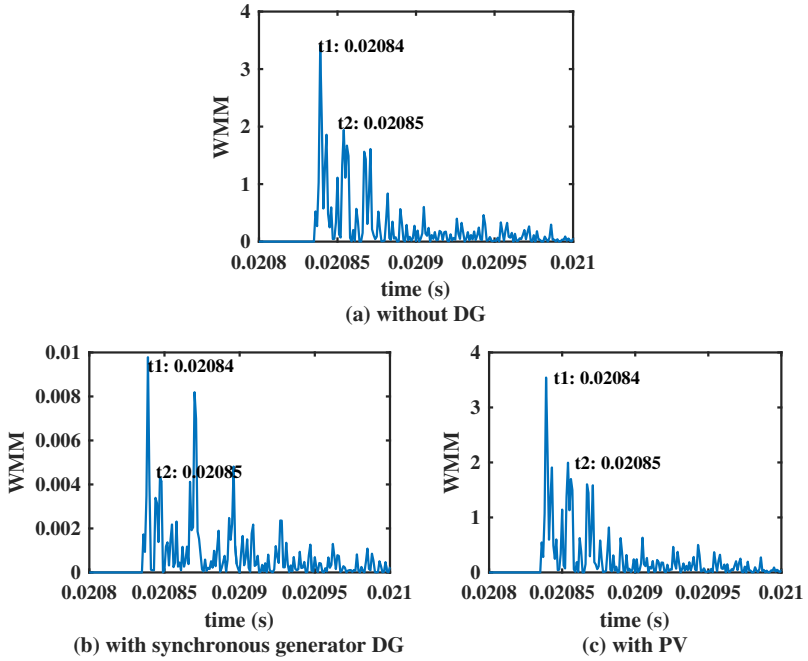

FIGURE 6.6: WMM for aerial mode current with DGs

6.5.2 Effect of Presence of PEV Load on Fault Location Scheme

Electric Vehicles use is increasing day by day as it provides viable alternate to concern associated with the conventional vehicles, but the integration of PEVs to the distribution system for charging purpose will create operational challenges to the utility grid. To understand the effect of PEV charging load on fault location algorithm, PEV charging station consisting three PEVs are connected to the distribution system. The effects are similar to that shown by DG. The pattern of the wavelet modulus maxima of current signal remains same only the magnitude changes

as shown in Fig. 6.7(a) and Fig. 6.7(b) for a line to ground fault in section 832-890 at a distance of 2.22 km from node 832. Hence, the presence of PEV charging load doesn't affect the accuracy of proposed fault location scheme.

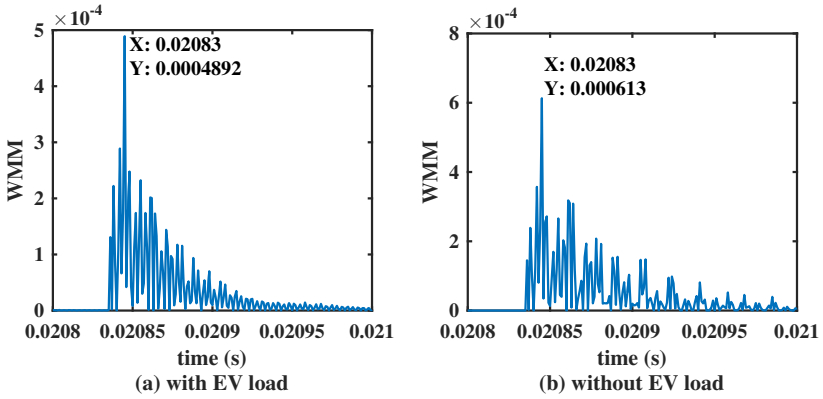

FIGURE 6.7: WMM for aerial mode current with PEV

6.5.3 Effect of different R_f and θ_f on Fault Location Scheme

Fault resistance (R_f) and fault inception angle (θ_f) affect the magnitude of fault transients especially the fault current transients and this could lead to error in calculated fault distances. Several simulation tests were performed to evaluate the accuracy of proposed scheme under different combination of R_f and θ_f . The fault location results shown in Table 6.7 along the identified faulted section are obtained for fault inception angle of 0^0, 30^0, 45^0, 90^0, 135^0 and the assumed fault resistances are 1Ω, 10Ω, 20Ω and 30Ω. The result shown indicates that error increase with the increase in fault resistances. However, the highest error is 3.39% in the laterals and 1.45% in main feeder. Hence the proposed scheme shows good accuracy under variety of R_f and θ_f .

6.5.4 Comparison with Previous Methods

In order to verify the accuracy and effectiveness of the proposed fault location scheme the average error obtained in the proposed scheme is compared with the average error reported in existing fault location methods available in literature. As can be seen from Table 6.8 the proposed fault location scheme is more accurate as compared to the previous works giving less error in exact fault location in a multilateral distribution system with DG and EV Charging load. The test system used in [134] does not contain any DG whereas method presented in [71] is tested only against line to ground fault. The radial distribution network used in [68] is small and simple without any laterals. The method in [135] shows good accuracy but fault detection and classification is not clearly mentioned and the method in [77] is not applied in multilateral distribution networks. None of the method mentioned above is tested against the presence of EV charging load in the distribution network and fault detection and classification are not performed in most of the works.

Table 6.8: Comparison with Previous Methods

Method	**Network used**	**DG**	**EV**	**Avg. error**
Continuous-Wavelet Transform [134]	IEEE 34 bus network	No	No	NA
Wavelet transform and neural [71]	6-bus distribution system	No	No	132.26 m
BP neural network and wavelet [68]	Radial distribution network of 110kV	No	No	380 m
Multi-measurements point and wavelet [135]	IEEE 34 bus network	Yes	No	1.081 km
Graph theory and wavelet maxima [77]	DC Network	No	No	0.176%
Proposed method	**IEEE 34 bus network**	**Yes**	**Yes**	**395 m (1.41%)**

6.6 Proposed Two-Terminal Fault location Method

The single-terminal methods are capable of providing fast fault location with good accuracy and don't require any data synchronization. But the single-terminal methods sometime face challenges in recognizing between travelling waves reflected from the fault and from line terminals, which reduces the reliability of fault location algorithm. Therefore, a two-terminal travelling wave based method is proposed in this thesis. The two-terminal fault location scheme also comprises of three stages of fault detection and classification, faulted line segment identification and exact fault location along the identified faulted line segment. The working of the first two stages is same as mentioned in section (5.5, 5.6) and in subsection 6.8.2 that is used in single-terminal method. The exact fault location process along the identified faulted line section in this method uses arrival time of first wave peak at the two ends of the faulted line segment. The proposed fault location assumes that the fault data recording are available at both ends of each line section and the incoming samples are time-stamped using GPS. It is assumed that optical current transducers equipped with travelling wave recorders are placed at each end of the line section, and an open communication channel is available through which relay can send fault data to the relay at the remote terminal.

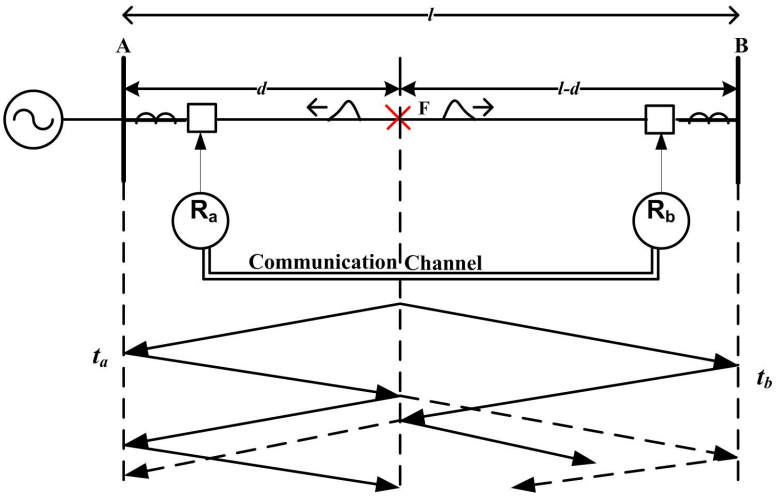

FIGURE 6.8: Time space diagram of travelling waves

6.6.1 Exact Fault Location

The exact fault location along the identified faulted line section is explained with the help of Fig. 6.8, where a line section is connected by bus A and bus B. The travelling wave recorder is located at both ends of the line. The recorded signals are transformed into modal components and then DWT decomposition is performed. If WMM spikes are detected by the relay then the time corresponding to the arrival of the waves is recorded and fault location is calculated. Fig. 6.9 gives each step of the exact fault location estimation process. The incoming signals are time-stamped using Global Positioning System (GPS). A communication channel is used to communicate between the relays. Fault is assumed to occur at point F from a distance d from the bus A; the fault originated travelling waves propagates away from the fault towards the terminal A and B. The time information recorded by the relays at the remote terminal is sent to the other relay. Therefore, the time difference recorded can be given as:

$$t_d = \mid t_a - t_b \mid \tag{6.27}$$

Where, t_a is the time recorded by the relay, R_a, and t_b is the time recorded by the relay R_b. The time taken by the travelling wave to travel the length of line is given by:

$$t = \frac{l}{v} \tag{6.28}$$

Where, l is the length of faulted line segment and v is the propagation velocity of travelling waves. The fault distance from relay R_a is calculated as:

$$d_1 = \left((t_a - t_b) + \left(\frac{l}{v}\right)\right) \times \frac{v}{2} \tag{6.29}$$

And fault distance from relay R_b can be calculated as

$$d_2 = \left(\left(\frac{l}{v}\right) - (t_a - t_b)\right) \times \frac{v}{2} \tag{6.30}$$

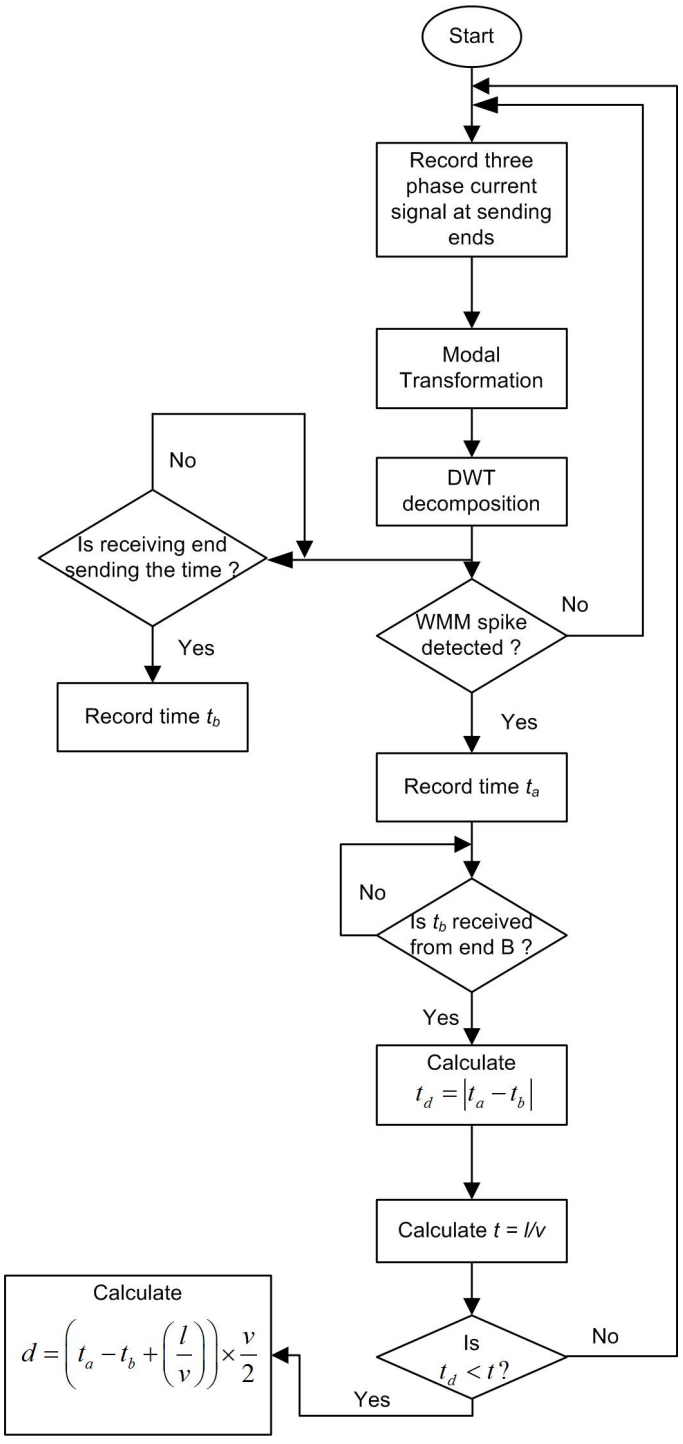

FIGURE 6.9: Flowchart for exact fault location

6.7 Case Study

The effectiveness of the proposed fault location scheme is tested using modified IEEE 34 node distribution system as shown in Fig. 6.10. The nominal voltage level of this network is 24.9 kV and it has 8 single phase node and 26 three-phase node. Since, some of the lines sections are made up of very short lines therefore for simplification purpose the line section having length less than one km is merged with the adjacent lines and line sections between any two interconnecting point are merged to form a single line section. In this way the total number of nodes is reduced to 21 nodes, of which 14 nodes are three phase node and 7 nodes are single phase node. Simulations are performed at a sampling rate of 1 MHz in SIMULINK at different location on the main feeder and side branches to evaluate the performance of proposed scheme.

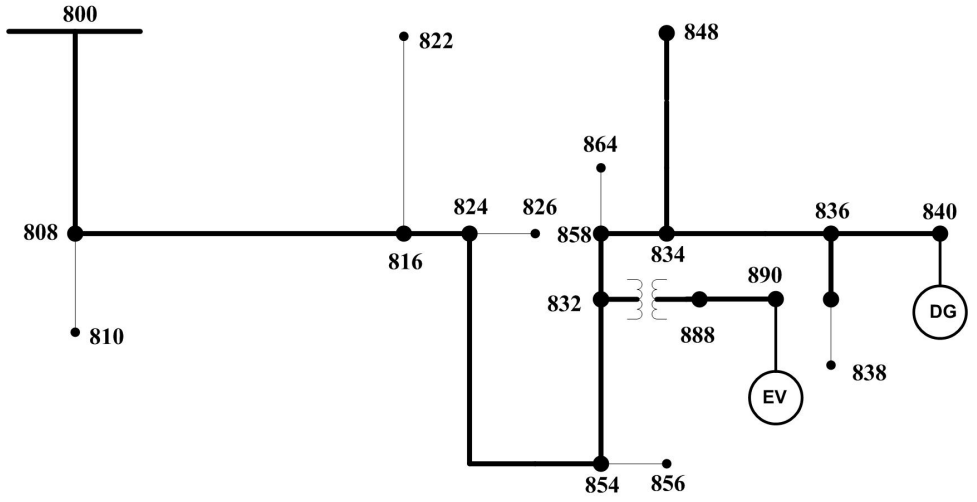

FIGURE 6.10: Modified IEEE 34 node distribution system

6.8 Simulation Results

The fault location estimations are obtained by faults generated at various points along the line from the starting of the feeder to the end of the feeder because the current signal magnitude varies and reduces towards the end of feeder. The results are obtained by several simulation cases considering effect of various fault conditions such as fault inception angle, fault resistance, fault distance and integration of DG and EV charging load.

6.8.1 Fault Detection and Faulted Phase Identification

The proposed scheme fault detection and faulted phase identification ability is tested using various fault cases. Table 6.9 shows the results of fault classification for different fault types using wavelet energy entropy. The WEE shown in bold signify the faulted phase(s). Here, fault classifications for 27 cases are shown in which one case is misclassified (highlighted text in Table 6.9) and the classification accuracy is 96.29%.

6.8.2 Faulted Line Section Identification

The faulted line section identification is performed by comparing the magnitude of aerial mode component WMM obtained at scale 2. A single line to ground fault is created at R_f of 10Ω and θ_f of 45^0 with phase 'A' being the faulted phase. The distance of fault from node 800 is 28.62 km. Fig. 6.11 show the magnitude of aerial mode WMM obtained at the interconnecting points of all the laterals. The magnitude of aerial mode WMM obtained at node 816 and 808 is highest in comparison to other non-faulted section as shown in Table 6.10 therefore; the line section 808-816 is recognized as the faulted line section.

TABLE 6.9: WEE for faults at different locations

Fault Type	**WEE per phase**	**1Ω/45^0 at 10% feeder length**	**10Ω/60^0 at 90% feeder length**	**20Ω/30^0 on lateral 834-848**
A-g	e_{a2}	**0.8955**	**0.8146**	**2.0748**
	e_{b2}	2.0070	1.8762	3.8286
	e_{c2}	1.2537	1.8530	3.8838
B-g	e_{a2}	2.2115	2.0500	3.6176
	e_{b2}	**0.9694**	**1.2309**	**2.7339**
	e_{c2}	1.4784	1.7851	3.6125
C-g	e_{a2}	2.4599	2.2874	3.5899
	e_{b2}	2.3971	2.1556	3.6085
	e_{c2}	**0.9277**	**1.1976**	**2.7033**
AB	e_{a2}	**0.8926**	1.4261	**1.5947**
	e_{b2}	**0.9146**	1.7055	**1.8962**
	e_{c2}	4.2671	1.6374	4.9148
BC	e_{a2}	1.7633	5.7367	4.5164
	e_{b2}	**1.4125**	**1.3070**	**1.8627**
	e_{c2}	**1.1321**	**1.1831**	**1.5208**
CA	e_{a2}	**0.9081**	**0.8788**	**1.6617**
	e_{b2}	1.6364	1.7129	4.7888
	e_{c2}	**0.8837**	**1.1536**	**1.6103**
AB-g	e_{a2}	**0.8836**	**0.8290**	**3.8931**
	e_{b2}	**0.9171**	**1.0104**	**1.9791**
	e_{c2}	4.4538	2.0014	5.0080
BC-g	e_{a2}	2.5796	4.5554	4.9347
	e_{b2}	**0.9977**	**1.4323**	**1.6443**
	e_{c2}	**1.6076**	**1.0966**	**1.5875**
CA-g	e_{a2}	**0.8895**	**0.8771**	**3.4472**
	e_{b2}	2.9290	1.8501	5.0275
	e_{c2}	**0.8779**	**1.0870**	**1.7482**

6.8.3 Exact Fault Location

A line to ground fault is applied at a distance of 16.30 km from node 808. Fig. 6.12 (a and b) shows the WMM of aerial mode current signal at scale 2 recorded at node 808 and at node 816 respectively. In this case, the WMM peak at node 808 occurs at t1 = 0.41667 ms and at node 816 at t2 = 0.41709 ms, thus yielding the time difference td = 0.42 ms. The fault location is calculated using equation 6.29

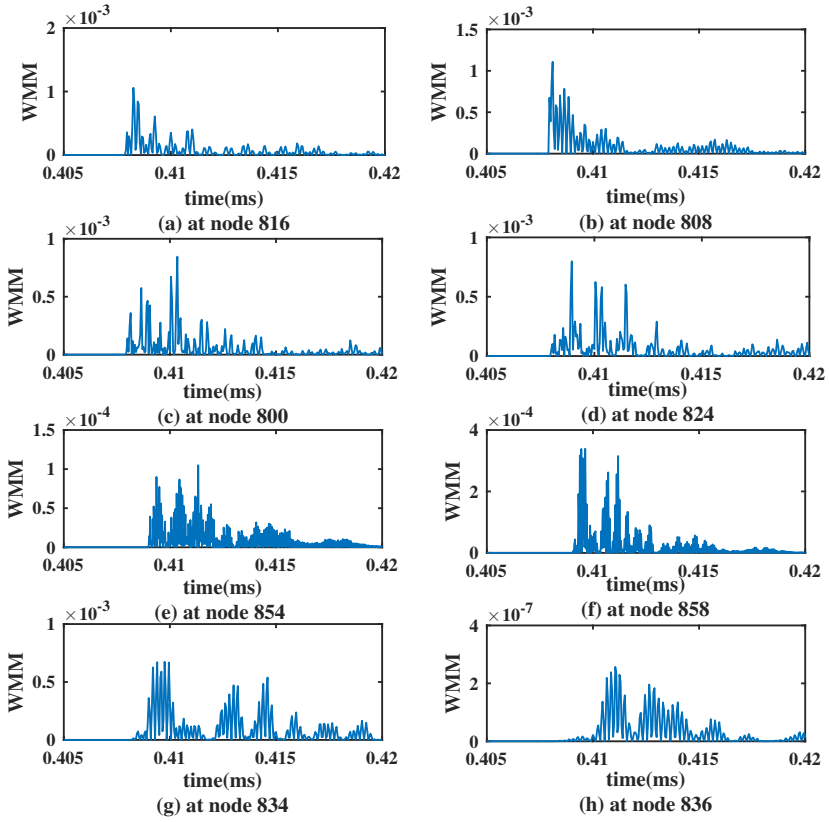

FIGURE 6.11: WMM of aerial mode at different nodes

TABLE 6.10: Magnitude of aerial mode WMM

Node	Magnitude of aerial mode WMM
816	1.058×10^{-3}
808	1.108×10^{-3}
800	8.456×10^{-4}
824	7.99×10^{-4}
854	1.526×10^{-4}
858	1.528×10^{-4}
834	6.712×10^{-4}
836	2.568×10^{-7}

as: $d_1 = 16.47$ km. Similarly, the exact fault location obtained for fault both on the side laterals and on the main feeder is shown in Table 6.11. From the table it can be seen that the maximum error in fault location is 2.82% in the laterals and 0.38% in the main feeder. The error is calculated using the equation 6.26.

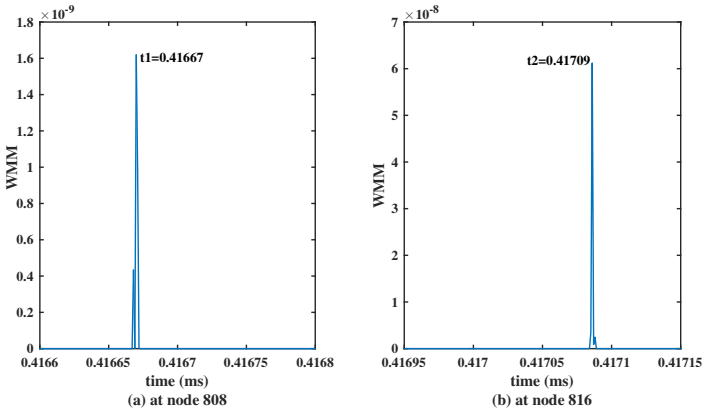

FIGURE 6.12: WMM of aerial mode at different nodes

TABLE 6.11: Fault location result in different sections

Fault type	R_f & θ_f	**Distance from node 800 (km)**	**Faulted section**	**Calculated distance (km)**	**Error (%)**
A-g	$10\Omega/30^0$	1.75	800-808	1.58	0.29
B-g	$1\Omega/0^0$	38.00	824-854	37.88	0.21
C-g	$20\Omega/45^0$	56.25	834-848	56.20	2.82
AB	$1\Omega/0^0$	28.90	808-816	29.05	0.26
BC	$30\Omega/90^0$	35.10	816-824	35.18	0.14
CA	$10\Omega/30^0$	46.20	854-858	45.98	0.38
AB-g	$20\Omega/45^0$	25.50	808-816	25.41	0.15
BC-g	$1\Omega/0^0$	54.97	858-834	55.11	0.24
CA-g	$30\Omega/90^0$	43.50	824-854	43.39	0.19
ABC	$10\Omega/135^0$	6.50	800-808	6.41	0.15
ABC-g	$20\Omega/30^0$	55.10	832-890	55.03	2.17

6.9 Sensitivity Studies

6.9.1 Effect of Different Type of DG on Fault Location Scheme

The type of DG integrated to the system and the location of fault with respect to the DG determines the level of fault current in the network. Hence, the intensity of recorded current transient changes accordingly. According to [8] the synchronous generator type of DG contribution to fault current is maximum whereas an inverter based sources which does not contains any rotating part contributes minimum to the fault current. Therefore, in addition to the synchronous generator DG [108], the

proposed method is also tested in presence of an inverter based 100 kW PV source [109] connected at node 840. Fig. 6.13 (a, b and c) shows the results obtained for without DG, synchronous generator DG and PV respectively for a two phase fault with phase A and phase B as faulted phase in line section 834-840 with a R_f of 20Ω and θ_f of 45^0 at a distance 1.4 km from the node 834, the peak of WMM occur at same time instant in all the three cases. Hence, the presence of different type of DG does not affect the time profile of WMM peak only the peak magnitude changes due to change in fault level. As the proposed method uses only time information from the WMM profile for fault location estimation, the proposed method accuracy is not affected by the presence of different types of DG sources.

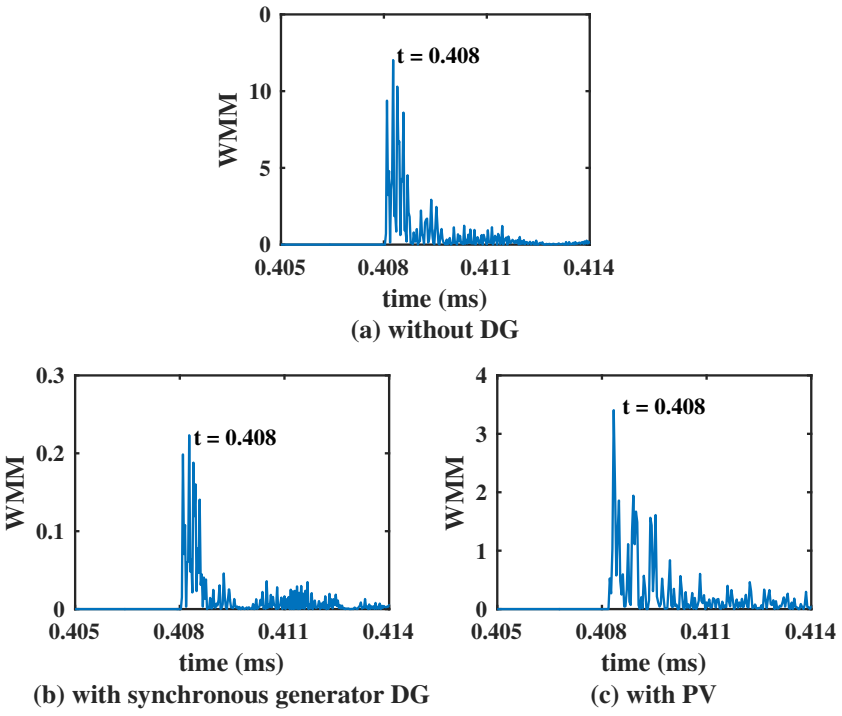

FIGURE 6.13: Aerial mode current WMM with DGs

6.9.2 Effect of EV Load on Fault Location Scheme

Due to environmental concerns and depletion of fossil fuels the electric vehicles are becoming popular with each passing day. Therefore, to understand the effect of EV charging load on the proposed fault location algorithm, simulations are performed in a similar way that is used in single-terminal method. A EV charging station consisting of three EVs are connected to the distribution network. The effects are similar to that shown in single terminal method. The pattern of the WMM of current signal stays same only the magnitude changes as shown in Fig. 6.14 (a and b) for a three phase fault in section 832-890 at a distance of 2.1 km from node 832. Hence, the presence of EV charging load doesn't affect the accuracy of proposed two-terminal fault location scheme.

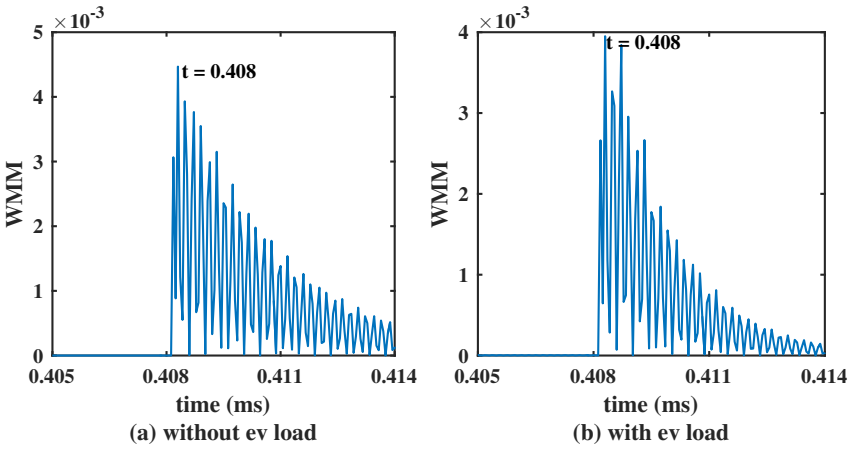

FIGURE 6.14: Aerial mode current WMM with EV load

6.9.3 Effect of Noise on Fault Location Scheme

The fault inception angle affects the sharpness of fault originated travelling waves. The signal to noise ratio (SNRs) of the arriving wave decreases with decrease in fault inception angle. This result in difficulty in travelling wave detection and consequently the fault location estimation becomes more challenging. From the Fig.

6.15 which is the enlarged version of Fig. 6.11(d) shown below it can be seen that the peaks of WMM can be detected easily in presence of noise in the signal. Therefore, the proposed method can accurately locate fault in noisy signal. The influence of noise on the fault location accuracy of the proposed method is also tested in presence of different noise level. The input current signal is contaminated with 30, 50, 80, 100 dB of white Gaussian noises respectively for the illustrative single line to ground fault case in subsection 6.8.2. The aerial mode signal, its associated wavelet coefficients and WMM for 50 dB noise case at node 808 are shown in Fig. 6.16.

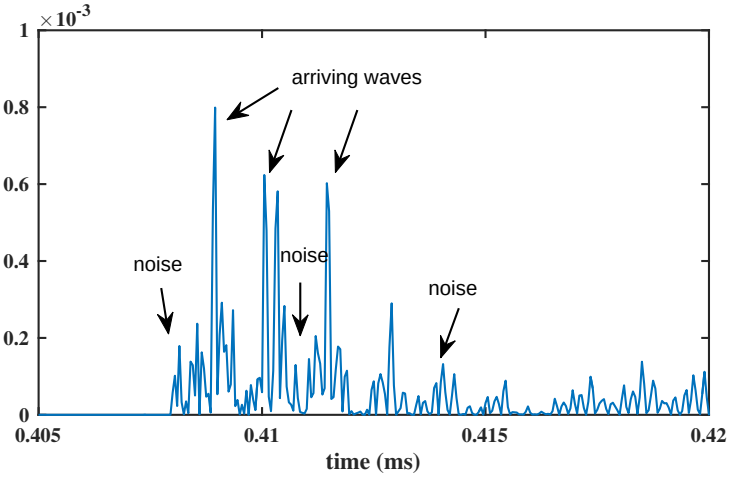

FIGURE 6.15: WMM of aerial mode at node 824

As can be seen from the Fig. 6.16 the maximum detail wavelet coefficients and WMM is unaffected by the presence of high level of noise in the signal. The wavelet coefficients at the instances not corresponding to the travelling wave arrivals have nonzero values but the amplitudes of maximum detail wavelet coefficients and WMM are always larger than those of noises. The similar results were obtained for the signal contaminated with 30 dB, 80 dB and 100 dB of noise. The simulation proves that the fault location results accuracy are not affected by noise condition.

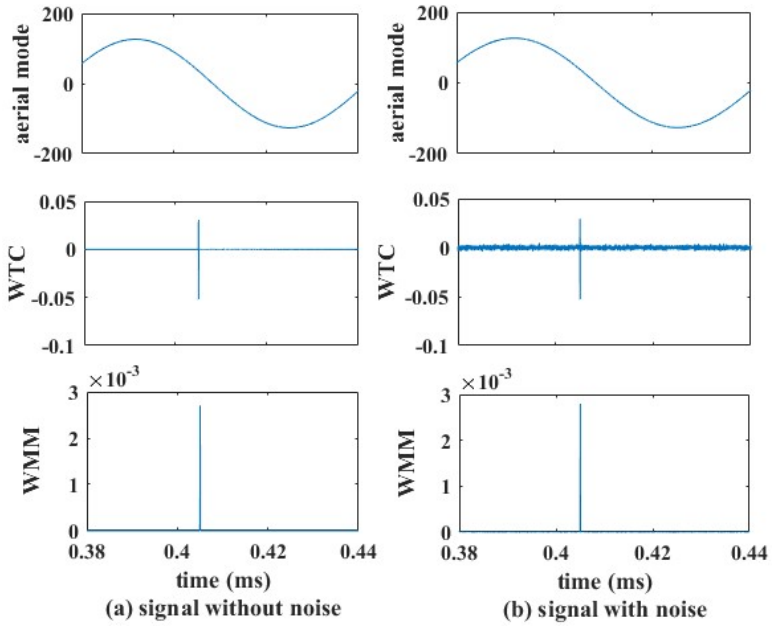

FIGURE 6.16: Aerial mode signals and associated WTC and WMM

6.9.4 Comparison with Previous Methods

A comparison of the average error reported in the previous methods to the average error in fault location of the proposed method is presented in Table 6.12. The comparison clearly shows that the proposed method is more accurate and detects, classify and locates the fault with an average fault location error of 117.27 m which is much less as compared to other methods proposed previously. The fault location method proposed in [69] is not tested for all fault types and uses a very high sampling rate of 1 GHz and the method presented in [71] is tested only against line to ground fault. The method proposed in [68] shows good accuracy but fault detection and classification is not proposed in this work. The proposed method gives accurate fault location in a multilateral distribution system with DG and EV charging load whereas the radial distribution network used in [74] does not contain any lateral and DG. None of the method mentioned above is tested against the presence of EV charging load in the distribution network and fault detection and classification are not performed in most of the works.

TABLE 6.12: Comparison with previous methods

Method	**Network used**	**Sampling rate**	**Average error (m)**
Continuous-Wavelet Transform [69]	IEEE 34 bus network	1 GHz	NA
WT and ANN [71]	11-bus distribution system	750 KHz	132.26 m
Data fusion and asynchronous voltage measurements [68]	IEEE 30 bus system	I MHz	380 m
Network topology and reclosing superimposed travelling waves [74]	10 kV radial distribution network	1 MHz	342 m
Proposed method	**IEEE 34 bus network**	**1 MHz**	**117.27 m**

6.10 Conclusion

A novel single-terminal and a two-terminal travelling wave based schemes for fault location for a multilateral distribution network are presented in this chapter. Based on the simulation results obtained, following conclusions can be drawn.

- The proposed single-terminal and two-terminal approaches for fault detection, classification, faulted section identification and location based on travelling wave method for a multilateral distribution network is able to perform the above mentioned task with good accuracy.
- The robustness of proposed schemes is tested against any change in topology of the system both in terms of feeders and in terms of connected sources.
- The accuracy of the proposed schemes is tested for various fault cases for different fault resistance, fault inception angle and fault distances.
- The above two proposed fault location methods are found to be accurate in the presence of different types of DG and EV charging load.
- From the obtained fault location results it is observed that the accuracy of two-terminal method is higher than the single-terminal method.

Chapter 7

HYBRID METHOD FOR FAULTED SECTION IDENTIFICATION AND FAULT LOCATION

7.1 Introduction

The hybrid methods for fault identification and location are adopted to develop a novel method which exploits the benefits provided by the incorporation of more than one method. The idea is to utilize the strengths of individual methods while restraining their shortcomings. Few techniques using hybrid methods for fault location in distribution systems have been proposed till now [96–105]. These methods generally use artificial intelligence techniques along with some advanced signal processing techniques to extract fault information from the recorded signals and to locate fault. Therefore, these techniques require training of data sets for estimation of fault location. These data sets are dependent on system operating conditions

and network topology, any change in such condition requires regeneration of training data otherwise the accuracy of fault location estimation gets affected. To avoid such problems, a novel hybrid method combining high-frequency transient method and impedance based method is proposed in this work. This method uses the fault-generated high-frequency signals for identifying the faulted line section only thus negating the problem of discrimination between multiple reflections of the travelling wave from bus-bars and the fault point, as is seen in the travelling wave based fault location methods. Once the faulted line segment is identified, the exact fault location along the identified faulted line segment is determined using the impedance base method. As the faulted line segment is already identified in the first stage, this eliminates the problem of multiple fault location associated with the single-terminal impedance based method in a multilateral distribution system.

7.2 Proposed Hybrid Fault Location Scheme

The main idea of the proposed hybrid fault location scheme is to combine the individual strength of high-frequency transient method and impedance based method. The high-frequency components which are used in travelling wave based methods to identify the arrival time of travelling wave peaks at the line terminals requires very high sampling rate of the order of MHz for data acquisition so that a very high time resolution for the travelling wave peaks can be obtained. But the proposed hybrid method uses high-frequency transients for faulted line segment identification only therefore, it doesn't require very high sampling rate for obtaining high time resolution for travelling wave peaks. Furthermore, as the impedance based method is employed for exact fault location only after identification of faulted line segment, this eliminates the problem of multiple fault location candidates in a multi-lateral distribution network. The requirements for the implementation of the proposed scheme are as follows: (1) Measurements should be available at all the

junction points, i.e., the points where laterals are connected to the main feeder. (2) Measurements should be available at the DG connection point.

The flowchart for the proposed fault location scheme is shown in Fig. 7.1, with the following steps:

1. Transient three-phase currents are recorded at all the junction points, substation node and DG terminal.
2. DWT decomposition using db-4 is done at all the measurement points to get WEE per phase at scale 2.
3. Fault in the distribution feeders is detected using WEE of each phase.
4. Modal transformation is performed on recorded current signal using Clarke's transformation matrix to obtain modal components of current signal.
5. Aerial and ground mode WMM is calculated from wavelet detail coefficients for faulted lateral identification and fault type identification purpose.
6. Fault current direction is determined at different nodes.
7. Faulted line segment is identified using magnitude of WMM and fault current direction.
8. Fault type identification using WEE of each phase and magnitude of ground mode component WMM.
9. Calculation of fault location using equation 7.6.

The proposed fault location scheme consists of four stages namely fault detection, fault type identification/faulted phase selection, faulted line segment identification followed by exact fault location. The working principle of first two stages are same as mentioned in section 5.5 and in section 5.6.

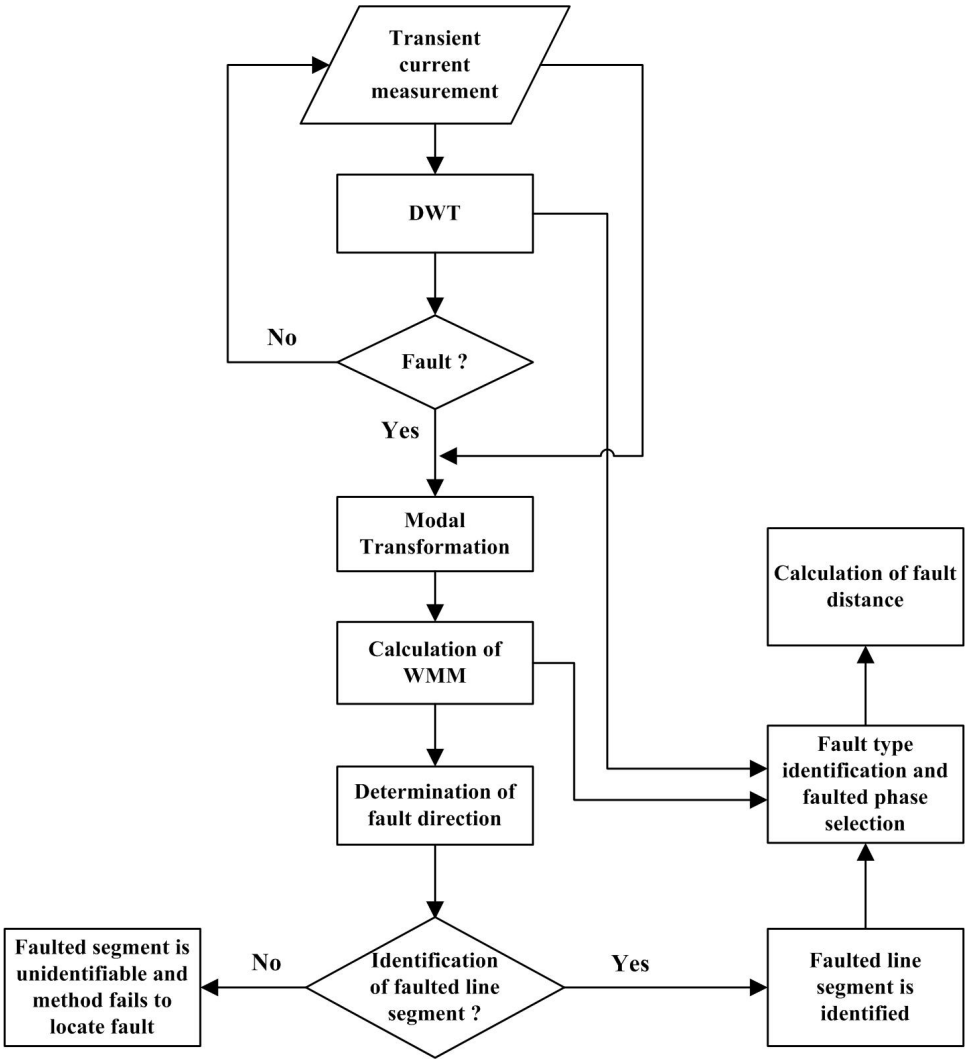

FIGURE 7.1: Flowchart of the proposed hybrid fault location scheme

7.2.1 Identification of Faulted Line Segment

The proposed hybrid fault location scheme performs identification of faulted line segment of the system by comparing the magnitude of aerial mode WMM and by monitoring the direction of fault current at the junction point of the laterals. This is explained with the help of a simple distribution system shown in Fig. 7.2. Current transformers (CTs) are installed at each end of a line section. Thus, three CTs are installed at node 2 where three lines are interconnected, to measures the current leaving the respective nodes.

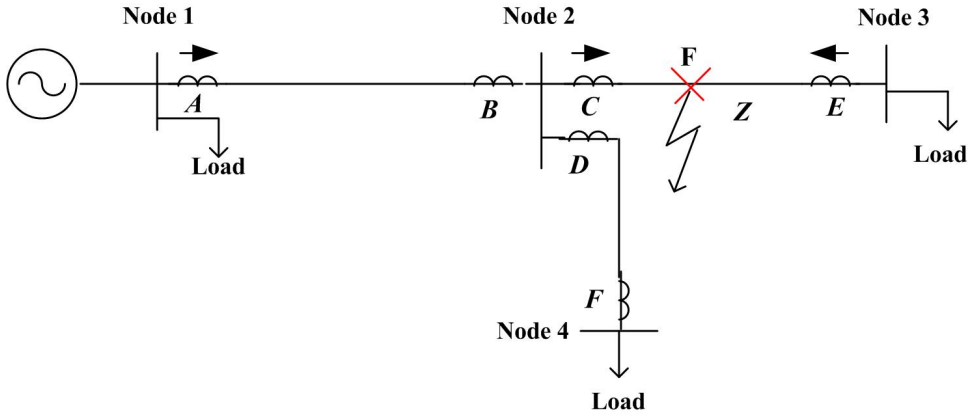

FIGURE 7.2: Simple distribution system model

For a fault F in section Z, between node 2 and node 3, the high-frequency transients are observed by the CTs at all measurement points located at different nodes. The CT on the faulted branch will observe both the incident current surges plus the reflections whereas the CTs on the other feeders will observe the transmitted component. The recorded three phase current transients at the measurement points are transformed into their modal component using Clarke's transformation. From the obtained modal components, wavelet modulus maxima (WMM) of aerial mode component are calculated. The magnitude of WMM determines the proximity of node to the fault, higher the magnitude of WMM at the node, closer is the node to the fault. For the fault in section Z the magnitude of WMM obtained at different measurement points is shown in Fig. 7.3. Here the magnitude of WMM is highest at node 2 (point B and point C) followed by magnitude of WMM at node 3 (point E). Point B and point C has same magnitude of WMM as they correspond to the same node. The magnitude of WMM at all other non-faulted line segment node has lesser magnitude in comparison to these two nodes. Hence, the lateral Z having highest magnitude of aerial mode WMM is identified as the faulted lateral. Table 7.1 shows the magnitude of WMM obtained at all the measurement points.

This identification of faulted line segment is further confirmed by monitoring the direction of fault current. The transients recorded at the faulted lateral shows

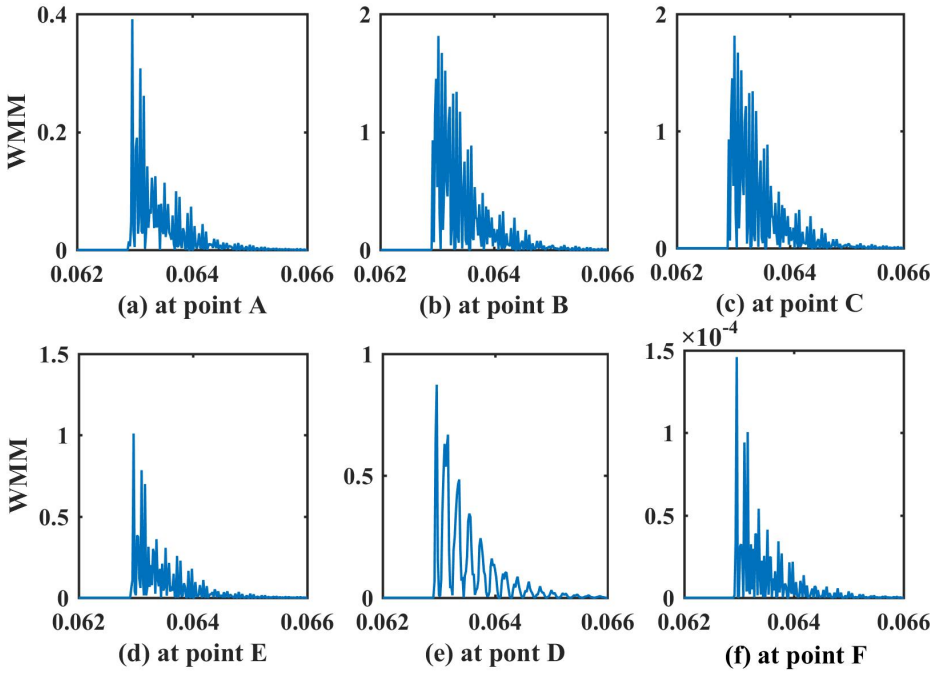

FIGURE 7.3: Magnitude of aerial mode WMM at different measurement points

TABLE 7.1: Magnitude of Aerial Mode WMM

Point	**Magnitude of WMM**
Point A	0.3923
Point B	1.7823
Point C	1.7823
Point E	1.01
Point D	0.81
Point F	1.46×10^{-4}

opposite sign compared to those obtained on the non-faulted laterals. The cross-correlation between the wavelet coefficients of aerial mode 1 and mode 2 signals of current transients are used to determine whether the coefficients are of same sign or not. One signal is selected as the reference signal and cross-correlation coefficients of the reference signal and other signal for different time instants are calculated. If the highest values of all the cross-correlation coefficients are positive then the coefficients are of same sign, otherwise they are of opposite sign. Fig. 7.4 shows the measured three phase current at point C and point E for fault F on line segment Z, this figure also shows their aerial mode-1 component and its corresponding wavelet coefficients. The cross-correlation coefficients of the wavelet coefficients of aerial

mode components obtained at faulted lateral show opposite sign. Therefore, the relay at node 2 identifies fault in forward direction whereas relay at node 3 identifies fault in backward direction. From the fault current direction obtained (shown by arrow) at different measurement point in Fig. 7.3 section Z is clearly identified as faulted line section.

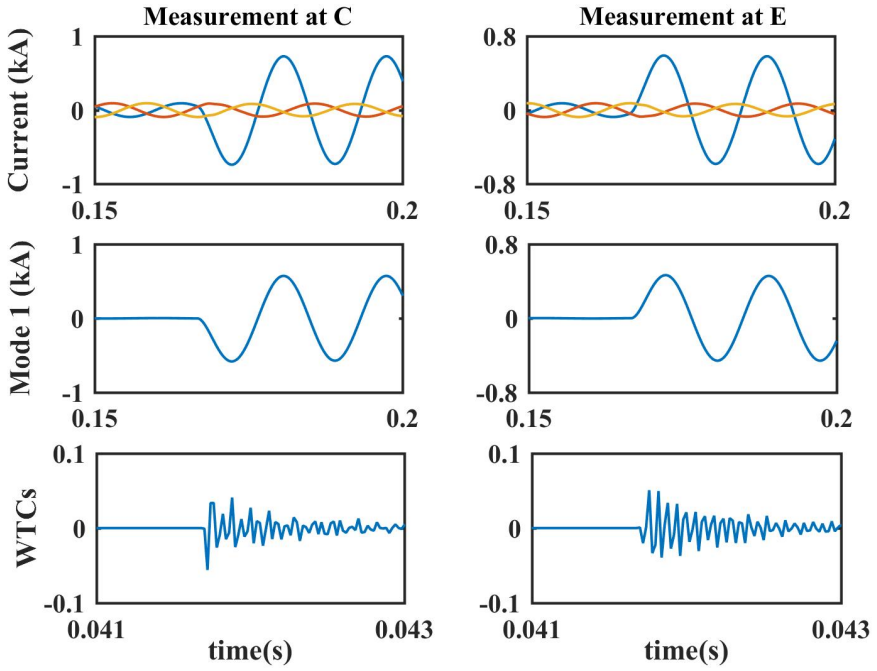

FIGURE 7.4: Three phase current, corresponding aerial mode 1 and their WTCs

7.2.2 Exact Fault Distance Location

The actual fault distance calculated along the identified faulted line section is based on impedance measurement technique. The proposed method takes into account the unequal mutual coupling and unbalanced loading condition in the system. The process of actual fault distance calculation is illustrated with the help of a single line to ground fault assumed on phase A, of the network shown in Fig. 7.5.

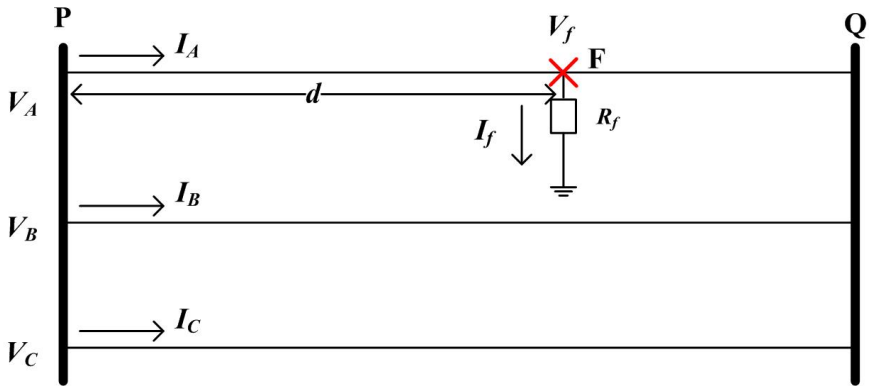

FIGURE 7.5: Single line to ground fault in a line section

The three phase voltage at node P can be represented as:

$$\begin{bmatrix} V_A \\ V_B \\ V_C \end{bmatrix} = d \begin{bmatrix} Z_{AA} & Z_{AB} & Z_{AC} \\ Z_{BA} & Z_{BB} & Z_{BC} \\ Z_{CA} & Z_{CB} & Z_{CC} \end{bmatrix} \begin{bmatrix} I_A \\ I_B \\ I_C \end{bmatrix} + \begin{bmatrix} V_{FA} \\ V_{FB} \\ V_{FC} \end{bmatrix} \tag{7.1}$$

Here, d is the fault distance, Z terms are elements of impedance matrix, V_A, V_B, V_C are the three phase voltages, I_A, I_B, I_C are the three phase currents and V_{FA}, V_{FB}, V_{FC} are the phase voltages at the fault point.

The voltage of phase A at node P is:

$$V_A = d(I_A Z_{AA} + I_B Z_{AB} + I_C Z_{AC}) + V_{FA} \tag{7.2}$$

The fault point voltage can be given as:

$$V_F = I_f \times R_f \tag{7.3}$$

Here, V_F is the fault point voltage, I_f is the fault current and R_f is the fault resistance. Putting the value of V_F in equation 7.2, we get

$$V_A = d(I_A Z_{AA} + I_B Z_{AB} + I_C Z_{AC}) + I_f R_f \tag{7.4}$$

In the above equation, fault distance, fault resistance and fault current are all unknown quantities. Using Fig. 7.5 the fault current (I_f) can be estimated as:

$$I_f = I_A - I_{Apf} \tag{7.5}$$

Here, I_{Apf} denotes prefault phase A current. Substituting the value of I_f in equation 7.4 and separating the real and imaginary part, we get fault distance and R_f as:

$$d = \frac{V_A^r I_f^i - V_A^i I_f^r}{a I_f^i - b I_f^r} \tag{7.6}$$

$$R_f = \frac{V_A^r b - V_A^i a}{b I_f^r - a I_f^i} \tag{7.7}$$

Here, $a = real(I_A Z_{AA} + I_B Z_{AB} + I_C AC)$

$b = imag(I_A Z_{AA} + I_B Z_{AB} + I_C AC)$

$V_A^r = real(V_A),\ V_A^i = imag(V_A)\ and$

$I_f^r = real(I_f),\ I_f^i = imag(I_f)$

For other types of fault the value of fault current and fault voltage will be different, which is given in Table 7.2.

TABLE 7.2: Fault voltage and current for different fault type

Fault Type	**Fault Voltage**	**Fault Current**
$A-G$	V_{AF}	I_{Af} - I_{Apf}
$B-G$	V_{BF}	I_{Bf} - I_{Bpf}
$C-G$	V_{CF}	I_{Cf} - I_{Cpf}
AB, $AB-G$, ABC	V_{AF} - V_{BF}	(I_{Af} - I_{Apf}) – (I_{Bf} - I_{Bpf})
BC, $BC-G$, ABC	V_{BF} - V_{CF}	(I_{Bf} - I_{Bpf}) – (I_{Cf} - I_{Cpf})
CA, $CA-G$, ABC	V_{CF} - V_{AF}	(I_{Cf} - I_{Cpf}) – (I_{Af} - I_{Apf})

7.2.2.1 Compensation for Loads in the System

The equations given above do not account for load taps in the distribution feeder. Therefore, if load taps are present between the fault point and the measuring point then the estimated fault distance will contain error. To eliminate this error and obtain a more accurate fault location in presence of load taps the voltage and current equations are modified to obtain voltage and current at the load near to the fault.

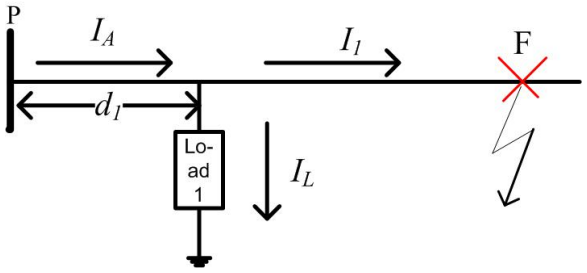

FIGURE 7.6: Compensation for load in the system

Fig. 7.6 shows phase A in which a load 1 is connected at a distance d_1 from node P.

Voltage at this load bus 1 is calculated as:

$$\begin{bmatrix} V_{A1} \\ V_{B1} \\ V_{C1} \end{bmatrix} = \begin{bmatrix} V_A \\ V_B \\ V_C \end{bmatrix} - d_1 \begin{bmatrix} Z_{AA} & Z_{AB} & Z_{AC} \\ Z_{BA} & Z_{BB} & Z_{BC} \\ Z_{CA} & Z_{CB} & Z_{CC} \end{bmatrix} \begin{bmatrix} I_A \\ I_B \\ I_C \end{bmatrix} \tag{7.8}$$

Here, V_{A1}, V_{B1}, V_{C1} are the three phase voltages at the load bus, I_A, I_B, I_C are the three phase current from node P and V_A, V_B, V_C are the three phase voltages at the node P.

And the current leaving load bus 1 is calculated as:

$$I_1 = I_A - I_L \tag{7.9}$$

The current drawn by the load (I_L) is given by

$$I_L = \frac{V_{A1}}{Z_L} \tag{7.10}$$

Here, Z_L is the impedance of load bus 1.

With the help of new value of voltage and current the fault distance can be calculated from the new location of load bus 1.

7.2.2.2 Fault Location in Presence of DG

It is necessary to have certain information about the presence of DG on a system during fault for accurate fault location. The proposed method in this work assumes that the knowledge of location of DG and current and voltage signals data is available at the DG terminal. As shown in Fig. 7.7 the fault current in case of DG is calculated as:

$$I_f = I_A + I_G \tag{7.11}$$

Here, I_G is the current from DG.

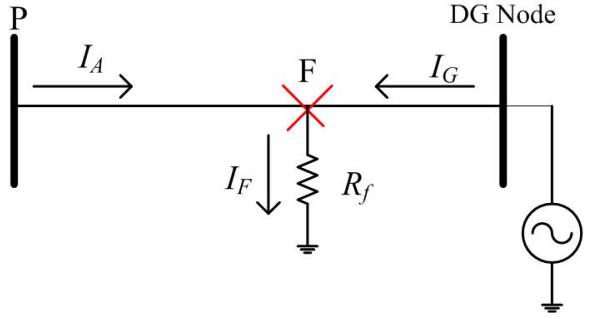

FIGURE 7.7: Compensation for DG in the system

The following steps is used to calculate the fault distance in presence of DG in the system.

1. Voltage of faulted phase is calculated using equation 7.1 to 7.4.

2. Fault current is calculated using equation 7.5 and 7.11.

3. Fault location is estimated using equation 7.6.

7.3 Simulation Results

The proposed fault location scheme is also tested using the modified IEEE 34 node distribution system shown in Fig. 6.10. In addition to the modifications two DGs have been added to the system, DG-1 is a 350 kW synchronous generator [31] connected at node 840 in the system and DG-2 is a 100 kW inverter based PV source [32] connected at node 848. Detail specifications of DGs are given in AppendixB. A sampling rate of 50 kHz is used to record the fault data.

7.3.1 Identification of Faulted Line Segment

A three phase to ground fault is applied in the line section 824-854 at a distance of 5 km from the node 824, the fault inception angle (θ_f) is 45^0 and fault resistance (R_f) is 20 Ω. The WMM of wavelet coefficients of the aerial mode current signal extracted at all the junction point is shown in Fig. 7.8. Table 7.3 gives the peak magnitude of WMM obtained at all the measurement points. As can be seen from the Table 7.3 the magnitude of WMM obtained at node 854 is highest and at 824 is second highest and from the fault current direction identified using cross-correlation of aerial mode WTCs, the line section 824-854 is identified as the faulted line segment. Fig. 7.9 shows the fault current direction and WTCs at node 824 and node 854.

In order to verify the accuracy of the proposed faulted lateral identification scheme, a number of faults are simulated at different locations for various R_f and θ_f. Magnitude of aerial mode WMM obtained at different locations for these fault cases is listed in Table 7.4, here the WMM in bold indicates magnitude at the two

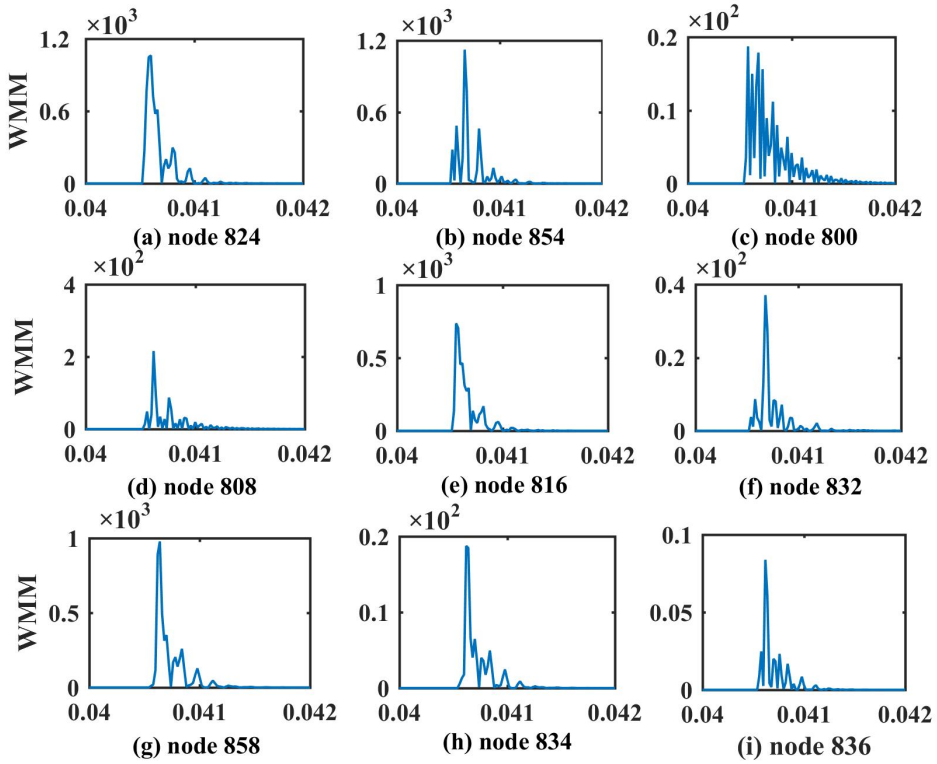

FIGURE 7.8: WMM at different nodes

TABLE 7.3: Magnitude of aerial mode WMM

Node	Magnitude of WMM
824	1.061×10^3
854	1.123×10^3
800	0.18×10^2
808	2.15×10^2
816	0.73×10^3
832	0.37×10^2
858	0.97×10^2
834	0.18×10^2
836	0.084

end nodes of the faulted line segments. The fault direction identified at different location for these fault cases is also shown in Table 7.4, in this table FR denotes forward fault and BW denotes backward fault.

TABLE 7.4: Magnitude of aerial mode WMM at different locations and fault direction

Fault Type	**Section**	**800**	**808**	**816**	**824**	**854**	**832**	**858**	**834**	**836**	**Fault Direction**	
											FR	**BW**
ABC	808-816	39.1	**1.19** $\times 10^2$	**3.19** $\times 10^2$	31.14	15.50	5.32	5.11	1.21	1.1 $\times 10^{-2}$	808	816
A-G	816-824	71.4	4.823	**1.59** $\times 10^3$	**2.69** $\times 10^2$	15.87	39.78	33.56	8.54	1.03 $\times 10^{-2}$	816	824
ABC-G	808-816	40.3	**65.91**	**1.25** $\times 10^2$	52.45	33.21	8.79	7.61	2.45	1.33 $\times 10^{-2}$	808	816
B-G	800-808	**1.41** $\times 10^2$	**67.53**	10.05	11.65	3.674	7.57	0.7036	12.08	7.99 $\times 10^{-5}$	800	808
C-G	808-816	8.64	**15.72**	**10.88**	7.78	8.15	2.455	2.55	1.992	1.82 $\times 10^{-3}$	808	816
BC	800-808	**82.05**	**26.2**	1.91 $\times 10^{-2}$	8.712 $\times 10^{-2}$	2.05 $\times 10^{-3}$	1.395 $\times 10^{-3}$	1.618 $\times 10^{-4}$	3.10 $\times 10^{-3}$	8.66 $\times 10^{-5}$	800	808
AB	808-816	39.88	**1.18** $\times 10^2$	**38.17**	11.43	9.75	9.162	9.05	26.18	4.02 $\times 10^{-3}$	808	816
BC-G	824-854	1.87	3.985	75.09	**96.41**	**2.26** $\times 10^2$	80.55	89.82	19.2	8.23 $\times 10^{-3}$	824	854
CA	854-832	4.124	4.643	30.6	34.3	**69.99**	**1.90** $\times 10^2$	56.9	11.3	2.1 $\times 10^{-2}$	854	832
CA-G	834-836	9.97	0.946	51.82	49.24	6.039	10.65	15.89	**2.77** $\times 10^2$	**1.138** $\times 10^2$	834	836
AB-G	824-854	35.64	20.04	3.63 $\times 10^2$	**5.20** $\times 10^2$	**1.428** 10^3	4.28 $\times 10^2$	3.58 $\times 10^2$	57.7	3.95 $\times 10^{-2}$	824	854

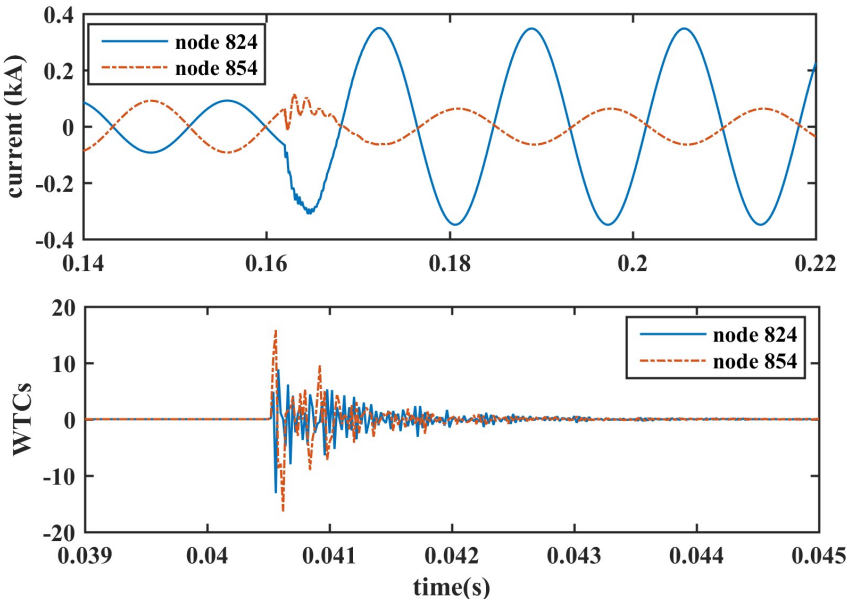

FIGURE 7.9: Fault current and its WTCs at the two end nodes

7.3.2 Exact Fault Location along the Faulted Line Section

After the faulted line section is identified, the exact fault location along the faulted line segment is estimated. Error in the estimated fault distance is calculated by equation 6.26 recommended in [1, 2].

For the three phase to ground fault case mentioned in subsection 7.3.1, once the correct faulted line segment is identified the exact fault location along this line segment is evaluated as 5.022 km. Thus the fault location algorithm identifies the fault location with an error of 0.038%. However to check the robustness of exact fault location technique, all type of shunt faults were simulated at different locations of the distribution system. Fault location results for different types of fault are presented below individually.

7.3.2.1 Single Phase to Ground Faults

Several fault cases for line to ground fault are simulated across the distribution feeder. Fig. 7.10 shows the fault location error for single phase to ground fault cases.

The fault location error ranges from 6 meter to 82 meter. The highest error of 82 meters in exact fault location which is 0.14% occurs in phase B at a distance of 23 km from the node 800. The mean error is 36.23 meter and standard deviation is 16.6 meter.

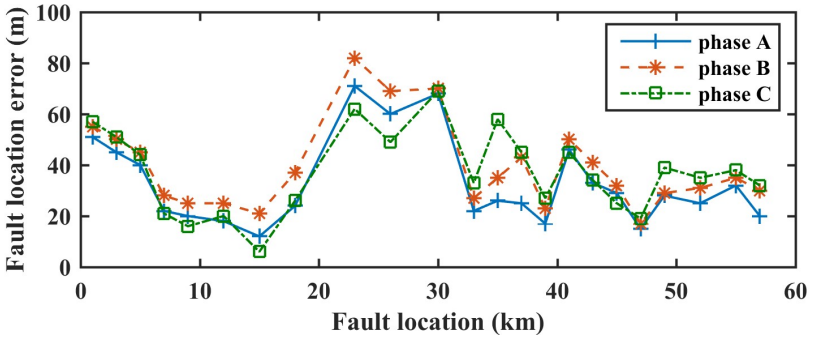

FIGURE 7.10: Error in fault location for single phase to ground faults

7.3.2.2 Phase to Phase Faults

Fig. 7.11 presents error in fault location for phase to phase fault cases. The error ranges from 15 meter to 135 meter, with the highest error being 0.23% obtained in BC phase fault case. The mean error and standard deviation in fault location is 60.91 meter and 29.22 meter respectively. Similarly, the fault location error in case of double phase to ground fault is shown in Fig. 7.12. In this case, the highest fault location error is 124 meter and the error ranges from 23 to 124 meter (0.04% to 0.21%). The mean error and standard deviation in fault location is 55.98 meter and 20.85 meter respectively.

7.3.2.3 Three Phase Faults

Fig. 7.13 and Fig. 7.14 show the fault location error in case of three phase faults and three phases to ground faults respectively. The fault location error lies from 9 meter to 105 meter (0.01% to 0.18%) for three phase fault cases. The mean

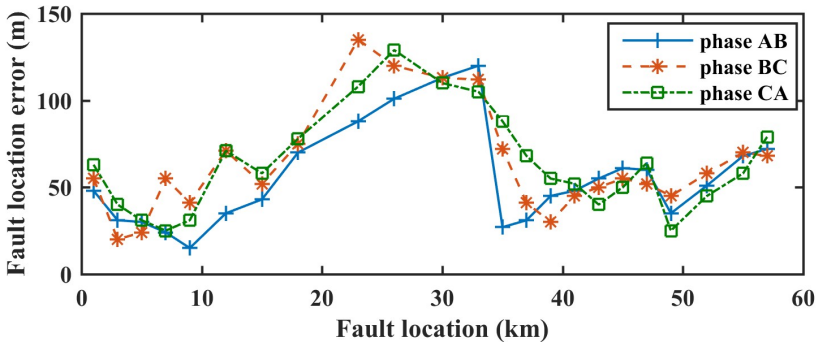

FIGURE 7.11: Error in fault location for phase to phase faults

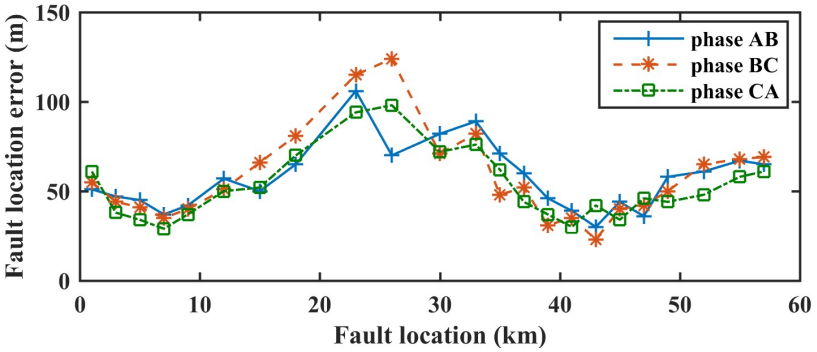

FIGURE 7.12: Error in fault location for two phase to ground faults

error is 53.73 meter and standard deviation is 22.84 meter. For three phases to ground fault the fault location error ranges from 22 meter to 111 meter (0.03% to 0.19%), with mean error being 63.40 meter and standard deviation of 25.38 meter.

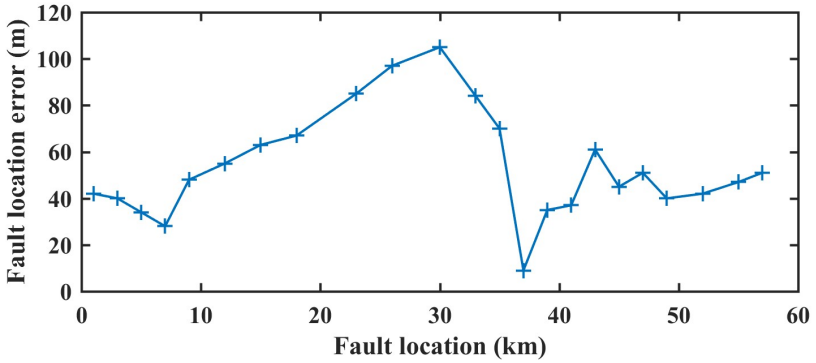

FIGURE 7.13: Error in fault location for three phase to faults

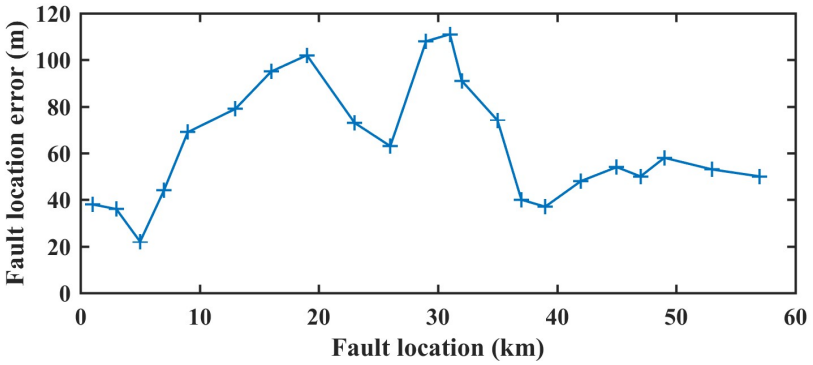

FIGURE 7.14: Error in fault location for three phase to ground fault

7.4 Sensitivity Assessment

The sensitivity of the proposed algorithm is evaluated in this section using the following parameters: variation in fault resistance, fault inception angle and variation in fault distance. The sensitivity of proposed hybrid scheme is also tested in presence of PEV charging load in distribution system.

7.4.1 Effect of Variation in Fault Resistance

Different value of R_f is used to evaluate the performance of proposed fault location scheme. The magnitude of fault generated high frequency transient changes slightly with change in R_f but the polarity of fault current remains unchanged. The magnitude of WMM obtained for fault cases with different R_f follows the WMM magnitude pattern discussed in subsection 7.2.1. Therefore, the change in R_f doesn't affect the accuracy of faulted line segment identification by the proposed hybrid fault location scheme. As the change in fault resistance changes the fault current hence, the fault location estimation of impedance based method gets affected by change in fault resistance. Fig. 7.15 shows the error in fault location due to change in fault resistance. Fault resistances of 10Ω, 30Ω, 60Ω and 100Ω are used to test the accuracy of fault location algorithm for faults in line section 808-816. The fault location error increases with increase in R_f. As expected highest error is obtained

in case of 100Ω fault resistance. However, the fault location error in this case ranges from 1.39% to 3.19% which is not very high for a large and unbalanced distribution network.

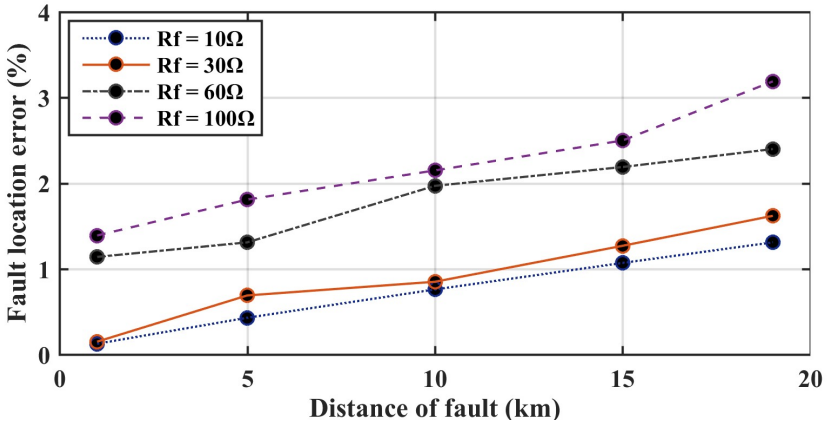

FIGURE 7.15: Fault location error for different fault resistances

7.4.2 Effect of Variation in Fault Inception Angle

Fault inception angle affects the severity of fault generated high frequency transients. As the inception angle decreases detection of these transients become more challenging. Fig. 7.16(a) and Fig. 7.16(b) shows the magnitude and polarity of fault transients at different inception angle for a line to ground fault in line section 800-808.

As can be seen from the results the magnitudes of transients are affected by the fault inception angle but the polarity remains unchanged. Despite change in transient's magnitude the pattern of WMM magnitude and fault current direction follows the principles discussed in subsection 7.2.1. B therefore, the fault location scheme is able to identify the faulted line segment at different fault inception angles. The fault location using impedance based method remains unaffected by the change in fault inception angle.

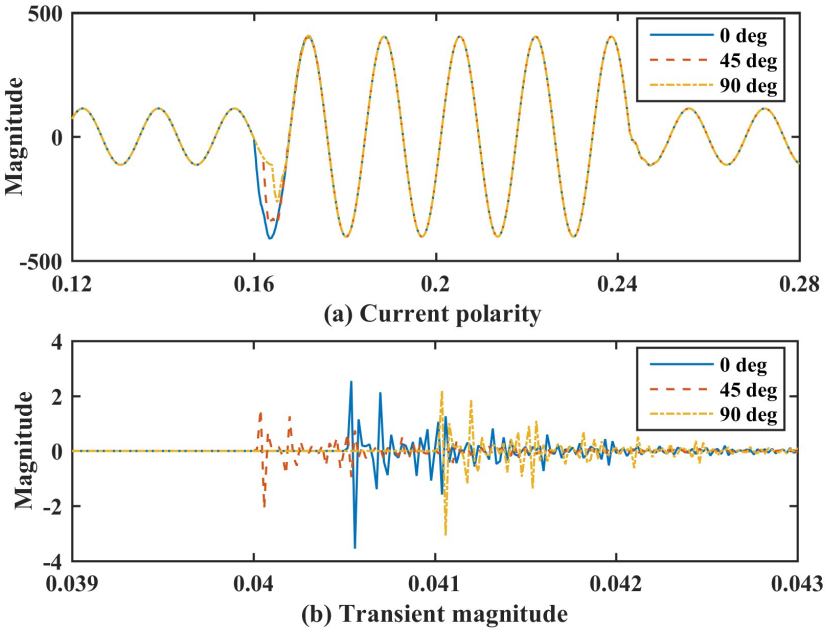

FIGURE 7.16: Polarity and magnitude of fault transients at different inception angle

7.4.3 Effect of Variation in Fault Distance

The response of proposed fault location scheme has been analyzed for faults at different locations across the length of the distribution feeder. Critical fault cases like faults occurring near the line terminals have been included in the analysis. Different fault type at different fault resistances were simulated at various locations on the main feeder. The fault location results for an A-g fault with R_f of 10Ω and 20Ω is depicted in Fig. 7.17. It can be seen from Fig. 7.17 that there is not much variation in error in fault location across the entire length of main feeder. This is because the proposed scheme locates fault after identification of faulted line segment and the fault location is calculated from the fault data recorded at the nearest terminal behind the fault. The maximum errors for the two mentioned cases were 0.76% and 0.8%, respectively which is very low for a long distribution feeder. This result shows that the proposed scheme is not significantly affected by the variation in fault distance. Change in fault distance has no effect on the accuracy of faulted line segment identification.

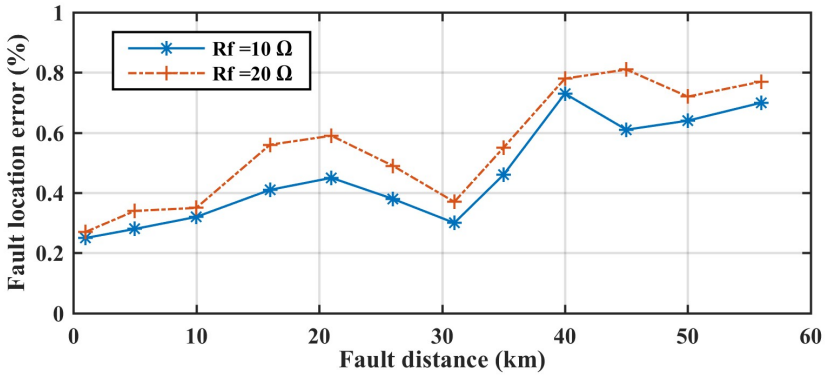

FIGURE 7.17: Effect of variation in fault distance on fault location error

7.4.4 Effect of PEV Charging load on Fault Location

The effect of presence of PEV charging load in the distribution system on fault location algorithm is checked in a similar way that is used in travelling wave based methods. To illustrate the effect of PEV charging load on fault location accuracy, fault location is calculated when PEV charging load is connected to the system and results are compared with those results which are obtained when PEV load is not connected to the system. Fig.7.18 shows the comparison of fault location error for with PEV and without PEV case. These results are obtained for line to ground fault cases in line section 808-816.

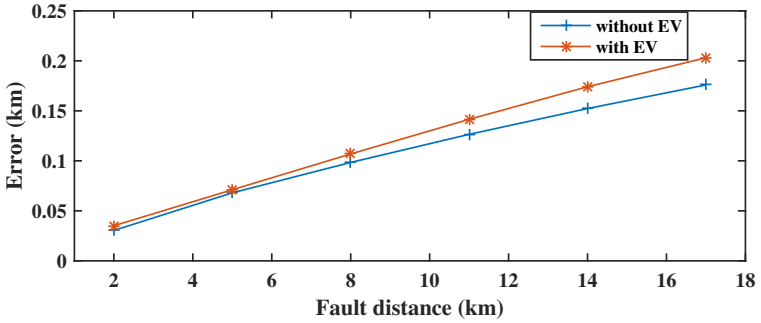

FIGURE 7.18: Effect of PEV charging load on fault location error

As can be seen from the Fig. 7.18 the error is slightly higher in case of PEV charging load but the highest difference between the fault location errors is 27.2

meter and the average difference is 13.38 meter only. Hence, the presence of PEV load does not affect the fault location accuracy significantly.

7.5 Conclusion

A new hybrid fault location scheme which combines the accuracy of high-frequency transient method and simplicity of impedance based method is presented in this thesis to overcome the challenges in fault location in a multi-lateral distribution network. Based on the results obtained, following conclusions can be drawn.

- The proposed scheme for faulted line segment identification using aerial mode WMM and fault current direction is effective in accurately identifying the faulted line segment in a multi-lateral distribution network.
- The impedance based technique utilized for exact fault location along the identified faulted line segment is able to locate the fault without facing the problem of multiple fault location as observed in case of single ended impedance based technique.
- Simulations carried out under different R_f and θ_f shows that the proposed fault location scheme presents a high level of accuracy and dependability in an unbalanced multi-lateral distribution network.

Chapter 8

CONCLUSION AND FUTURE SCOPE

8.1 Introduction

The penetration of DGs and PEV charging loads are growing in distribution systems, which is changing the system condition both in normal operating conditions and during fault conditions. The presence of DG alters the passive nature of distribution system to active one with non-radial power flow direction. The motive of this work is to develop effective fault location methods for multi-lateral distribution network embedded with DGs and PEV charging loads with increased focus on reducing the power outage time. A fast and accurate fault handling at active multi-lateral distribution system is required to reduce the outage times to improve the system reliability, and the first step in this direction is to have fault location methods capable of implementation in such systems. Three methods for fault location are presented in this thesis, intended for application in active multi-lateral distribution systems.

The PEV charging load is new type of load at the distribution system level and its effect on distribution system during fault condition is largely unknown. Therefore, at first, fault analysis is carried out on a distribution system embedded with PEV charging load to understand its impact on distribution system fault conditions. In this regard, a single-phase AC Level 2 bidirectional charger for PEV load charging is modeled in SIMULINK.

Fault location in distribution systems is a difficult task due to the presence of laterals and the non-homogeneous nature of the lines. The presence of laterals causes multiple fault position when fault location is estimated from the substation node. To eliminate this problem, the fault location process has been divided into different stages to avoid the occurrence of multiple fault location positions. Instead of calculating the distance of fault point and then trying to eliminate some of the possible fault locations, the proposed methods firstly identifies the faulted line section or lateral of the distribution system after a fault is detected in the system. This ensures that the faulted section or lateral of the system is correctly identified before the distance of fault point is estimated.

In the proposed fault location schemes, DWT is used for feature extraction of a particular type of shunt fault, and then WEE of wavelet detail coefficients are calculated to detect and identify the fault type. The magnitude of ground mode component WMM is used for classifying the fault into grounded fault and ungrounded fault. The rules for fault detection and fault type identification are formed after performing several simulations and observing the energy pattern of each phases under fault and no fault conditions so that the algorithm is able to discriminate correctly between fault and no fault conditions.

Two fault location methods based on travelling wave is proposed in this thesis, one is a single-terminal travelling wave based method and other is a two-terminal travelling wave based fault location method. The proposed travelling wave based methods are implemented using transient current signals as the input signal. The

three-phase current signals are selected as data input for the proposed fault location schemes because the overcurrent protection is the most used form of protection in distribution networks. Hence, the line current signals are readily available. Moreover, the surge in fault current is easier to detect than the voltage collapse during faults. The developed fault location schemes identify the faulted line section by comparing the Wavelet Modulus Maxima (WMM) of aerial mode wavelet coefficients, obtained at interconnecting point of each line section. After that exact fault location is estimated along the faulted line section. The simulations are performed on the modified IEEE 34 node distribution system for evaluating the performance of proposed fault location scheme. In order to consider the effect of Distributed Generation (DG) and Electric Vehicle charging load, a DG unit and a PEV charging station is integrated to the distribution system. Both the synchronous generator type and inverter based DGs are considered in simulations. All types of shunt fault are simulated at different location on the main feeder and side branches to evaluate the performance of proposed scheme.

A hybrid method for fault location is also proposed in this thesis. The main idea of the hybrid fault location scheme is to combine the individual strengths of the high-frequency transient methods and the impedance based methods of fault location. The proposed hybrid method uses high-frequency transients for faulted line segment identification only, therefore, it does not require very high sampling rate for obtaining the high time resolution for travelling wave peaks. Furthermore, as the impedance based method is employed only for determining exact fault location, once the faulted line segment is identified, this eliminates the problem of multiple fault location candidates in a multi-lateral distribution network.

Overall, the major contributions of this thesis addresses most, if not all of the short-comings of previous methods of fault location and the proposed methods have been carefully developed to overcome any issues that can occur when the fault location scheme is deployed in a real active multi-lateral distribution system.

8.2 Summary of Important Findings

In Chapter 3 a single phase AC level 2 bi-directional charger is modeled and tested for its performance in MATALB/SIMULINK. The charging system modeled consists of a bi-directional AC-DC converter and a bi-directional DC-DC converter. The DC-DC converter is used for charging the battery in buck mode and for discharging it works in boost mode. A unipolar method of switching is used in the control of single phase bi-directional AC-DC converter and PWM technique is applied for controlling the battery charging and discharging using bi-directional DC-DC converter. IEEE 34 node distribution system is also modeled and simulated in the Chapter 3. Details of various components used in modelling the test feeder are presented in the chapter and the simulation results are validated by comparing the load flow results for the simulated system to the benchmark IEEE distribution subcommittee results. The distributed parameter line model has been used to model all the line segments.

Chapter 4 evaluates the impact of PEV charging load on an unbalanced distribution system during fault conditions. Simulations are carried out on the IEEE 34 node system in MATLAB/SIMULINK. The impact is investigated for the PEV charging load connected at a node of the main feeder and also at a node on the low voltage lateral in the distribution system respectively under both unbalanced and balanced fault conditions. In order to compare the impact of charging load to the impact of other loads on the distribution system during fault conditions, two cases were simulated on this test system with PEV charging load and equivalent constant power load respectively. The impact of PEV charging on distribution system during fault condition is determined by observing the voltage, active power, reactive power and the fault current at all major nodes of the system. The main findings of the work carried out in Chapter 4 are as follows:

1. The results obtained show that in case of a fault, node at which the PEV charging load in connected is associated with increase in fault current and

reactive power demand as compared to the equivalent constant power load connected to same node in the distribution system.

2. When PEVs are integrated into the system a high magnitude transient voltage is observed during the period of reconnection of faulted phase to the system.

3. These impacts are seen to be highest in case of single line to ground faults.

4. The impact is more significant when the PEV charging load is connected on a lateral with low voltage level as compared to that obtained with the PEV charging load connected to the main feeder with high nominal voltage level.

A fault detection and fault classification algorithm has been proposed in Chapter 5. The fault condition is detected in the network by comparing the WEE obtained per phase at scale-2 to the predefined threshold value for each of the respective phase. The thresholds value for each phase is decided by several simulations performed on the distribution network under fault and no fault conditions to ensure that the algorithm would be able to discriminate correctly between normal switching events and faults. Once the fault is detected, fault classification is done in accordance to the algorithm based on decision taking rules which are formulated using individual phase entropy values WEE and magnitude of ground mode current component. The main contributions of this Chapter are following:

1. Fault detection is proposed using WEE of wavelet detail coefficient's at scale-2.

2. Rule based fault type identification is proposed using WEE and magnitude of ground mode component WMM.

In Chapter 6 a single-terminal and a two-terminal travelling wave based fault location methods are proposed. The proposed single-terminal method is implemented using transient current signals as the input signal. The three-phase current signals are selected as data inputs for the proposed fault location scheme because the

overcurrent protection is the most used form of protection in distribution networks. Hence, the line current signals are readily available. Moreover, the surge in fault current is easier to detect than the voltage collapse during faults. The developed fault location scheme comprises of three stages. In the first stage, the fault detection and classification tasks are performed using WEE and magnitude of ground mode component of the current. The identification of faulted line section is done in the next stage by comparing the WMM of aerial mode wavelet coefficients, obtained at interconnecting point of each line section. The third stage determines the exact fault location along the faulted line section. It is assumed that the measurements are available at all the interconnecting point of laterals. Optical current transducers equipped with travelling wave recorders are assumed to be placed at the interconnecting points of each lateral in the network. The simulations are performed on the modified IEEE 34 node distribution system for evaluating the performance of proposed fault location scheme. In order to consider the effect of DG and Electric Vehicle charging load, a DG unit and an Electric Vehicles charging station are integrated to the distribution system. Both the synchronous generator type and inverter based DGs are considered in simulation. All types of shunt fault are simulated at different location on the main feeder and side branches to evaluate the performance of proposed scheme. The single-terminal method is capable of providing fast fault location with good accuracy and don't require any data synchronization. But single-terminal methods of fault location sometimes face challenges in differentiating between travelling waves reflected from the fault and the travelling waves reflected from line terminals, which reduces the reliability of fault location algorithm. Therefore, a two-terminal travelling wave based method is also proposed in this Chapter. The two-terminal fault location scheme also comprises of three stages of fault detection and classification, faulted line segment identification and exact fault location along the identified faulted line segment. The fault detection and classification and faulted line segment identification is same as that of single terminal method, but the exact fault location along the identified faulted line section uses arrival time of first wave peak at the two ends of the faulted line segment. The travelling wave recorders

are assumed to be located at both ends of the line. The effectiveness of the proposed fault location scheme is also tested using modified IEEE 34 node distribution system. The key contributions of the Chapter 6 are following:

1. A novel single-terminal and a two-terminal travelling wave based schemes for fault locations in a multilateral distribution network are proposed.
2. The robustness of the proposed schemes is tested against any change in topology of the system both in terms of feeders and in terms of connected sources.
3. The accuracy of the proposed schemes is tested for various fault cases for different fault resistance, fault inception angle and fault distances.
4. The above two proposed fault location methods are found to be accurate in the presence different types of DG and EV charging load.
5. From the obtained fault location results it is observed that the accuracy of two-terminal method is higher than the single-terminal method.

In Chapter 7 a hybrid method for fault location is proposed. The main idea of the hybrid fault location scheme is to combine the individual strengths of the high-frequency transient methods and the impedance based methods of fault location. The proposed hybrid method uses high-frequency transients for faulted line segment identification only therefore, it does not require very high sampling rate for obtaining the high time resolution for travelling wave peaks. Furthermore, as the impedance based method is employed only for determining exact fault location, once the faulted line segment is identified, this eliminates the problem of multiple fault location candidates in a multi-lateral distribution network. The proposed method takes into account the unequal mutual coupling and unbalanced loading condition in the system. The contributions of work done in Chapter 7 are following:

1. Faulted line segment identification using magnitude of aerial mode WMM and fault current direction.

2. Exact fault location along the identified faulted line segment using impedance based technique.

3. Low sampling rate requirement for faulted line segment identification and exact fault location.

4. Simulations carried out under different R_f and θ_f shows that the proposed fault location scheme presents a high level of accuracy and dependability in an unbalanced multi-lateral distribution network.

8.3 Future Scope

Research and development is a continuous process. Each step of research work opens many avenues for future research. As a consequence of the investigations carried out, a variety of issues pertaining to fault location in active multi-lateral distribution system has been handled with consideration of DGs and PEV charging loads. Though there are several inter-related issues to be resolved, some require urgent attention due to their wide implications. Following are some of the aspects, identified as a promising area for future research work in the area of fault location:

- Developing high-frequency models of Current transformers (CTs) for application in fault location using travelling waves.

- Developing advanced signal processing techniques for analyzing travelling wave signals.

- More detailed analysis of the travelling wave speeds for ground and aerial modes based on frequency-dependent transmission line models.

- Hardware implementation and field tests of proposed methods in the thesis.

Appendix A

DATA FOR IEEE 34 NODE TEST FEEDER

Overhead Line Configurations (Config.)

Config.	Phasing	Phase ACSR	Neutral ACSR	Spacing ID
300	B A C N	1/0	1/0	500
301	B A C N	#2 6/1	#2 6/1	500
302	A N	#4 6/1	#4 6/1	510
303	B N	#4 6/1	#4 6/1	510
304	B N	#2 6/1	#2 6/1	510

Transformer Data

	kVA	kV-high	kV-low	R - %	X - %
Substation:	2500	69 - D	24.9 -Gr. W	1	8
XFM -1	500	24.9 - Gr.W	4.16 - Gr. W	1.9	4.08

Line Segment Data

Node A	Node B	Length(ft.)	Config.
800	802	2580	300
802	806	1730	300
806	808	32230	300
808	810	5804	303
808	812	37500	300
812	814	29730	300
814	850	10	301
816	818	1710	302
816	824	10210	301
818	820	48150	302
820	822	13740	302
824	826	3030	303
824	828	840	301
828	830	20440	301
830	854	520	301
832	858	4900	301
832	888	0	XFM-1
834	860	2020	301
834	842	280	301
836	840	860	301
836	862	280	301
842	844	1350	301
844	846	3640	301
846	848	530	301
850	816	310	301
852	832	10	301
854	856	23330	303
854	852	36830	301
858	864	1620	302
858	834	5830	301
860	836	2680	301
862	838	4860	304
888	890	10560	300

Spot Loads

Node	Load Model	Ph-1 kW	Ph-1 kVAr	Ph-2 kW	Ph-2 kVAr	Ph-3 kW	Ph-4 kVAr
860	Y-PQ	20	16	20	16	20	16
840	Y-I	9	7	9	7	9	7
844	Y-Z	135	105	135	105	135	105
848	D-PQ	20	16	20	16	20	16
890	D-I	150	75	150	75	150	75
830	D-Z	10	5	10	5	25	10
Total		344	224	344	224	359	229

Distributed Loads

Node A	Node B	Load Model	Ph-1 kW	Ph-1 kVAr	Ph-2 kW	Ph-2 kVAr	Ph-3 kW	Ph-3 kVAr
802	806	Y-PQ	0	0	30	15	25	14
808	810	Y-I	0	0	16	8	0	0
818	820	Y-Z	34	17	0	0	0	0
820	822	Y-PQ	135	70	0	0	0	0
816	824	D-I	0	0	5	2	0	0
824	826	Y-I	0	0	40	20	0	0
824	828	Y-PQ	0	0	0	0	4	2
828	830	Y-PQ	7	3	0	0	0	0
854	856	Y-PQ	0	0	4	2	0	0
832	858	D-Z	7	3	2	1	6	3
858	864	Y-PQ	2	1	0	0	0	0
858	834	D-PQ	4	2	15	8	13	7
834	860	D-Z	16	8	20	10	110	55
860	836	D-PQ	30	15	10	6	42	22
836	840	D-I	18	9	22	11	0	0
862	838	Y-PQ	0	0	28	14	0	0
842	844	Y-PQ	9	5	0	0	0	0
844	846	Y-PQ	0	0	25	12	20	11
846	848	Y-PQ	0	0	23	11	0	0
Total			262	133	240	120	220	114

Shunt Capacitors

Node	Ph-A kVAr	Ph-B kVAr	Ph-C kVAr
844	100	100	100
848	150	150	150
Total	250	250	250

Regulator Data

Regulator ID:	1		
Line Segment:	814 - 850		
Location:	814		
Phases:	A - B -C		
Connection:	3-Ph,LG		
Monitoring Phase:	A-B-C		
Bandwidth:	2.0 volts		
PT Ratio:	120		
Primary CT Rating:	100		
Compensator Settings:	Ph-A	Ph-B	Ph-C
R - Setting:	2.7	2.7	2.7
X - Setting:	1.6	1.6	1.6
Volltage Level:	122	122	122
Regulator ID:	2		
Line Segment:	852 - 832		
Location:	852		
Phases:	A - B -C		
Connection:	3-Ph,LG		
Monitoring Phase:	A-B-C		
Bandwidth:	2.0 volts		
PT Ratio:	120		
Primary CT Rating:	100		
Compensator Settings:	Ph-A	Ph-B	Ph-C
R - Setting:	2.5	2.5	2.5
X - Setting:	1.5	1.5	1.5
Volltage Level:	124	124	124

Appendix B

DATA FOR DGs

Table B.1: Specification of Synchronous Generator DG

Vrated (V)	480	Xd (pu)	1.76
Prated (kW)	350	Xq (pu)	1.66
kVArated	410	X1d (pu)	0.21
Qmax(pu)	0.5	X1q (pu)	0.18
Qmin (pu)	-0.25	X11d (pu)	0.13
pf	0.85	X11q (pu)	0.11

Table B.2: Specification of PV

Prated (kW)	100
Open circuit voltage (V)	64.2
Short circuit current (A)	5.96
Transformer connection	100-kVA 260V/24.9kV

Appendix C

Publications

The following research papers have been published, accepted for publications and communicated out of this thesis work.

International Journals

1. Ranjeet Kumar, D. Saxena, ***"Impact of Plug-In Electric Vehicles on Faulted Distribution System"***, Arabian Journal for Science and Engineering, Springer, 2019.

2. Ranjeet Kumar, D. Saxena, ***"A Literature Review on Methodologies of Fault Location in Distribution System with Distributed Generation"***, Energy Technology, Wiley, 2019.

3. Ranjeet Kumar, D. Saxena, ***"Fault Location in Distribution Network using Travelling Waves"***, International Journal of Energy Sector Management, 2018.

4. Ranjeet Kumar, D. Saxena, ***"Fault Location in Multi-Lateral Distribution Network with Electric Vehicle Charging Load"***, Energy Storage, Wiley, 2019.

5. Ranjeet Kumar, D. Saxena, ***"Fault Location in a Multi-lateral Distribution Network using Hybrid Method"***, Communicated in Energy Technology, Wiley.

International Conferences

1. Ranjeet Kumar, D. Saxena, ***"A Traveling Wave Based Method for Fault Location in Multi-Lateral Distribution Network with DG"*** *IEEE PES Innovative Smart Grid Technologies Asia (ISGT Asia 2018)*, pp. 7-12, May 22-25 2018, Singapore.

2. Ranjeet Kumar, D. Saxena, ***"A Traveling Wave Based Method For Fault Location In Multi-Lateral Distribution Network"***, *IEEE International Conference on Emerging Trends in Engineering, Science and Technology (PICC)*, pp. 1-5, January 18-20, 2018, Thrissur.

3. Ranjeet Kumar, D. Saxena, ***"Fault Analysis of a Distribution System Embedded with Plug-in Electric Vehicles"***, *IEEE International Conference on Recent Developments in Control, Automation and Power Engineering (RDCAPE)*, pp. 1-5,26-27 October 2017, Noida.

4. Ranjeet Kumar, D. Saxena, ***"Fault Location in Distribution Network with Distributed Generation: An Overview and Key Issues"***, *IEEE PIICON)*, pp. 1-5, 25-27 Nov, 2016, Bikaner.

Bibliography

[1] M. M. Saha, J. J. Izykowski, and E. Rosolowski, *Fault location on power networks*. Springer Science & Business Media, 2009.

[2] A. Muir and J. Lopatto, "Final report on the august 14, 2003 blackout in the united states and canada: causes and recommendations," 2004.

[3] L. Lawton, M. Sullivan, K. Van Liere, A. Katz, and J. Eto, "A framework and review of customer outage costs: Integration and analysis of electric utility outage cost surveys," Lawrence Berkeley National Lab.(LBNL), Berkeley, CA (United States), Tech. Rep., 2003.

[4] M. Hoel and S. Kverndokk, "Depletion of fossil fuels and the impacts of global warming," *Resource and energy economics*, vol. 18, no. 2, pp. 115–136, 1996.

[5] T. Ackermann, G. Andersson, and L. Söder, "Distributed generation: a definition," *Electric power systems research*, vol. 57, no. 3, pp. 195–204, 2001.

[6] A. R. Bergen, *Power systems analysis*. Pearson Education India, 2009.

[7] W. Wang, Z.-C. Pan, W. Cong, C.-G. Yu, and F. Gu, "Impact of distributed generation on relay protection and its improved measures," in *2008 China International Conference on Electricity Distribution*. IEEE, 2008, pp. 1–5.

[8] K. Kauhaniemi and L. Kumpulainen, "Impact of distributed generation on the protection of distribution networks," 2004.

[9] L. Kumpulainen and K. Kauhaniemi, "Aspects of the effects of distributed generation in single-line-to-earth faults," in *2005 International Conference on Future Power Systems.* IEEE, 2005, pp. 5–pp.

[10] E. Ungar and K. Fell, "Plug in, turn on, and load up," *IEEE Power and Energy Magazine*, vol. 8, no. 3, pp. 30–35, 2010.

[11] D. Sperling and D. Gordon, *Two billion cars: driving toward sustainability.* Oxford University Press, 2010.

[12] R. Walling, R. Saint, R. C. Dugan, J. Burke, and L. A. Kojovic, "Summary of distributed resources impact on power delivery systems," *IEEE Transactions on power delivery*, vol. 23, no. 3, pp. 1636–1644, 2008.

[13] E. C. Senger, G. Manassero, C. Goldemberg, and E. L. Pellini, "Automated fault location system for primary distribution networks," *IEEE Transactions on Power Delivery*, vol. 20, no. 2, pp. 1332–1340, 2005.

[14] M. Lehtonen, S. Pettissalo, and J.-H. Etula, "Calculational fault location for electrical distribution networks," in *1991 Third International Conference on Power System Monitoring and Control.* IET, 1991, pp. 38–43.

[15] J. P. Lopes, N. Hatziargyriou, J. Mutale, P. Djapic, and N. Jenkins, "Integrating distributed generation into electric power systems: A review of drivers, challenges and opportunities," *Electric power systems research*, vol. 77, no. 9, pp. 1189–1203, 2007.

[16] S. M. Brahma and A. A. Girgis, "Microprocessor-based reclosing to coordinate fuse and recloser in a system with high penetration of distributed generation," in *2002 IEEE Power Engineering Society Winter Meeting. Conference Proceedings (Cat. No. 02CH37309)*, vol. 1. IEEE, 2002, pp. 453–458.

[17] S. M. Brahmaa and A. A. Girgis, "Development of adaptive protection scheme for distribution systems with high penetration of distributed generation," *IEEE Transactions on power delivery*, vol. 19, no. 1, pp. 56–63, 2004.

[18] I. S. Board, *IEEE Standard for Interconnecting Distributed Resources with Electric Power Systems: 1547-2003*. IEEE, 2003.

[19] T. D. C. Huayllas, D. Ramos, and R. Vasquez-Arnez, "Microgrid systems: Current status and challenges," in *2010 IEEE/PES Transmission and Distribution Conference and Exposition: Latin America (T&D-LA)*. IEEE, 2010, pp. 7–12.

[20] I. Xyngi and M. Popov, "An intelligent algorithm for the protection of smart power systems," *IEEE Transactions on smart grid*, vol. 4, no. 3, pp. 1541–1548, 2013.

[21] N. Schäfer, T. Degner, A. Shustov, T. Keil, and J. Jäger, "Adaptive protection system for distribution networks with distributed energy resources," 2010.

[22] L. P. Fernandez, T. G. San Román, R. Cossent, C. M. Domingo, and P. Frias, "Assessment of the impact of plug-in electric vehicles on distribution networks," *IEEE transactions on power systems*, vol. 26, no. 1, pp. 206–213, 2010.

[23] M. C. Kisacikoglu, B. Ozpineci, and L. M. Tolbert, "Reactive power operation analysis of a single-phase ev/phev bidirectional battery charger," in *8th International Conference on Power Electronics-ECCE Asia*. IEEE, 2011, pp. 585–592.

[24] A. Dubey, S. Santoso, and M. P. Cloud, "Understanding the effects of electric vehicle charging on the distribution voltages," in *2013 IEEE Power & Energy Society General Meeting*. IEEE, 2013, pp. 1–5.

[25] M. C. Kisacikoglu, B. Ozpineci, and L. M. Tolbert, "Examination of a phev bidirectional charger system for v2g reactive power compensation," in *2010 Twenty-Fifth Annual IEEE Applied Power Electronics Conference and Exposition (APEC)*. IEEE, 2010, pp. 458–465.

[26] C. Dharmakeerthi, N. Mithulananthan, and T. K. Saha, "Overview of the impacts of plug-in electric vehicles on the power grid," in *2011 IEEE PES Innovative Smart Grid Technologies*. IEEE, 2011, pp. 1–8.

[27] R. C. Green II, L. Wang, and M. Alam, "The impact of plug-in hybrid electric vehicles on distribution networks: A review and outlook," *Renewable and sustainable energy reviews*, vol. 15, no. 1, pp. 544–553, 2011.

[28] A. D. Hilshey, P. D. Hines, P. Rezaei, and J. R. Dowds, "Estimating the impact of electric vehicle smart charging on distribution transformer aging," *IEEE Transactions on Smart Grid*, vol. 4, no. 2, pp. 905–913, 2012.

[29] Q. Yan and M. Kezunovic, "Impact analysis of electric vehicle charging on distribution system," in *2012 North American Power Symposium (NAPS)*. IEEE, 2012, pp. 1–6.

[30] G. Razeghi, L. Zhang, T. Brown, and S. Samuelsen, "Impacts of plug-in hybrid electric vehicles on a residential transformer using stochastic and empirical analysis," *Journal of Power Sources*, vol. 252, pp. 277–285, 2014.

[31] H. Wang, Q. Song, L. Zhang, F. Wen, and J. Huang, "Load characteristics of electric vehicles in charging and discharging states and impacts on distribution systems," 2012.

[32] H.-l. Li, X.-m. Bai, and W. Tan, "Impacts of plug-in hybrid electric vehicles charging on distribution grid and smart charging," in *2012 IEEE International Conference on Power System Technology (POWERCON)*. IEEE, 2012, pp. 1–5.

[33] P. Richardson, D. Flynn, and A. Keane, "Impact assessment of varying penetrations of electric vehicles on low voltage distribution systems," in *IEEE PES General Meeting*. IEEE, 2010, pp. 1–6.

[34] V.-L. Nguyen, T. Tran-Quoc, and S. Bacha, "Harmonic distortion mitigation for electric vehicle fast charging systems," in *2013 IEEE Grenoble Conference*. IEEE, 2013, pp. 1–6.

[35] S. Han, S. Han, and K. Sezaki, "Development of an optimal vehicle-to-grid aggregator for frequency regulation," *IEEE Transactions on smart grid*, vol. 1, no. 1, pp. 65–72, 2010.

[36] E. Sortomme and M. A. El-Sharkawi, "Optimal scheduling of vehicle-to-grid energy and ancillary services," *IEEE Transactions on Smart Grid*, vol. 3, no. 1, pp. 351–359, 2011.

[37] S. Lin, Z. He, T. Zang, and Q. Qian, "Impact of plug-in hybrid electric vehicles on distribution systems," in *2010 International Conference on Power System Technology*. IEEE, 2010, pp. 1–5.

[38] A. D. Clarke, H. A. Bihani, E. B. Makram, and K. A. Corzine, "Analysis of the impact of different pev battery chargers during faults," *Journal of Power and Energy Engineering*, vol. 2, no. 08, p. 31, 2014.

[39] C. R. Mason, *The art and science of protective relaying*. John Wiley and Sons, 1956.

[40] R. M. Rifaat, "Critical considerations for utility/cogeneration inter-tie protection scheme configuration," *IEEE Transactions on Industry Applications*, vol. 31, no. 5, pp. 973–977, 1995.

[41] S. H. Horowitz and A. G. Phadke, *Power system relaying*. John Wiley & Sons, 2008, vol. 22.

[42] S. Chaitusaney and A. Yokoyama, "Reliability analysis of distribution system with distributed generation considering loss of protection coordination," in *2006 International Conference on Probabilistic Methods Applied to Power Systems*. IEEE, 2006, pp. 1–8.

[43] S. Favuzza, M. Ippolito, F. Massaro *et al.*, "An investigation of protection devices coordination effects on distributed generators capacity in radial distribution systems," in *2013 International Conference on Clean Electrical Power (ICCEP)*. IEEE, 2013, pp. 686–692.

[44] A. Naiem, Y. Hegazy, A. Abdelaziz, and M. Elsharkawy, "A classification technique for recloser-fuse coordination in distribution systems with distributed generation," *IEEE Transactions on Power Delivery*, vol. 27, no. 1, pp. 176–185, 2011.

[45] S. Shen, D. Lin, H. Wang, P. Hu, K. Jiang, D. Lin, and B. He, "An adaptive protection scheme for distribution systems with dgs based on optimized thevenin equivalent parameters estimation," *IEEE Transactions on Power Delivery*, vol. 32, no. 1, pp. 411–419, 2015.

[46] H. Cheung, A. Hamlyn, L. Wang, G. Allen, C. Yang, and R. Cheung, "Network-integrated adaptive protection for feeders with distributed generations," in *2008 IEEE Power and Energy Society General Meeting-Conversion and Delivery of Electrical Energy in the 21st Century.* IEEE, 2008, pp. 1–8.

[47] H. B. Funmilayo and K. L. Butler-Purry, "An approach to mitigate the impact of distributed generation on the overcurrent protection scheme for radial feeders," in *2009 IEEE/PES Power Systems Conference and Exposition.* IEEE, 2009, pp. 1–11.

[48] Z. Bo, X. Dong, R. Xu, and A. Klimek, "A new integrated protection scheme for distributed generation systems," in *2008 China International Conference on Electricity Distribution.* IEEE, 2008, pp. 1–7.

[49] G. Kaur and M. Vaziri, "Effects of distributed generation (dg) interconnections on protection of distribution feeders," in *2006 IEEE Power Engineering Society General Meeting.* IEEE, 2006, pp. 8–pp.

[50] P. H. Shah and B. R. Bhalja, "New adaptive digital relaying scheme to tackle recloser–fuse miscoordination during distributed generation interconnections," *IET Generation, Transmission & Distribution*, vol. 8, no. 4, pp. 682–688, 2014.

[51] A. Hamlyn, H. Cheung, L. Wang, C. Yang, and R. Cheung, "Adaptive protection and control strategy for interfacing wind-power electricity generators to distribution grids," in *2008 IEEE Power and Energy Society General Meeting-Conversion and Delivery of Electrical Energy in the 21st Century.* IEEE, 2008, pp. 1–8.

[52] W. Lewis and L. Tippett, "Fundamental basis for distance relaying on 3-phase systems," *Transactions of the American Institute of Electrical Engineers*, vol. 66, no. 1, pp. 694–709, 1947.

[53] E. O. Schweitzer, "A review of impedance-based fault locating experience," in *Proceedings of the 15th Annual Western Protective Relay Conference, Spokane, WA*, vol. 24, 1988, p. 27.

[54] R. Aggarwal, Y. Aslan, and A. Johns, "An interactive approach to fault location on overhead distribution lines with load taps," 1997.

[55] D. Penkov, B. Raison, C. Andrieu, J.-P. Rognon, and B. Enacheanu, "Dg impact on three phase fault location. dg use for fault location purposes?" in *2005 International Conference on Future Power Systems.* IEEE, 2005, pp. 6–pp.

[56] F. Abo-Shady, M. Alaam, and A. M. Azmy, "Impedance-based fault location technique for distribution systems in presence of distributed generation," in *2013 IEEE International Conference on Smart Energy Grid Engineering (SEGE).* IEEE, 2013, pp. 1–6.

[57] J. J. Mora-Flórez, R. A. Herrera-Orozco, and A. F. Bedoya-Cadena, "Fault location considering load uncertainty and distributed generation in power distribution systems," *IET Generation, Transmission & Distribution*, vol. 9, no. 3, pp. 287–295, 2015.

[58] M. T. Hagh, M. M. Hosseini, and S. Asgarifar, "A novel phase to phase fault location algorithm for distribution network with distributed generation," 2012.

[59] A. S. Bretas and R. H. Salim, "Fault location in unbalanced dg systems using the positive sequence apparent impedance," in *2006 IEEE/PES Transmission & Distribution Conference and Exposition: Latin America.* IEEE, 2006, pp. 1–6.

[60] J. Nunes and A. Bretas, "A impedance-based fault location technique for unbalanced distributed generation systems," in *2011 IEEE Trondheim PowerTech.* IEEE, 2011, pp. 1–7.

[61] S. F. Alwash, V. K. Ramachandaramurthy, and N. Mithulananthan, "Fault-location scheme for power distribution system with distributed generation," *IEEE Transactions on Power Delivery*, vol. 30, no. 3, pp. 1187–1195, 2014.

[62] S. M. Brahma, "Fault location in power distribution system with penetration of distributed generation," *IEEE transactions on power delivery*, vol. 26, no. 3, pp. 1545–1553, 2011.

[63] Z. Bo, R. Aggarwal, A. Johns, and P. Moore, "Accurate fault location and protection scheme for power cable using fault generated high frequency voltage transients," in

Proceedings of 8th Mediterranean Electrotechnical Conference on Industrial Applications in Power Systems, Computer Science and Telecommunications (MELECON 96), vol. 2. IEEE, 1996, pp. 777–780.

[64] P. Gale, P. Crossley, X. Bingyin, G. Yaozhong, B. Cory, and J. Barker, "Fault location based on travelling waves," in *1993 Fifth International Conference on Developments in Power System Protection*. IET, 1993, pp. 54–59.

[65] H. Dommel and J. Michels, "High speed relaying using travelling wave transient," *IEEE PES WM, New York, Jan, 1978*, pp. 1–7.

[66] L. Bewley, "Traveling waves on transmission systems," *Transactions of the American Institute of Electrical Engineers*, vol. 50, no. 2, pp. 532–550, 1931.

[67] S. Rajendra and P. McLaren, "Travelling-wave techniques applied to the protection of teed circuits:-multi-phase/multi-circuit system," Cambridge University Engineering Dept., Cambridge, Tech. Rep., 1985.

[68] R. Liang, G. Fu, X. Zhu, and X. Xue, "Fault location based on single terminal travelling wave analysis in radial distribution network," *International Journal of Electrical Power & Energy Systems*, vol. 66, pp. 160–165, 2015.

[69] A. Borghetti, M. Bosetti, C. Nucci, M. Paolone, and A. Abur, "Integrated use of time-frequency wavelet decompositions for fault location in distribution networks: Theory and experimental validation," *IEEE Transactions on Power Delivery*, vol. 25, no. 4, pp. 3139–3146, 2010.

[70] A. Dwivedi and X. Yu, "Fault location in radial distribution lines using travelling waves and network theory," in *2011 IEEE International Symposium on Industrial Electronics*. IEEE, 2011, pp. 1051–1056.

[71] M. Pourahmadi-Nakhli and A. A. Safavi, "Path characteristic frequency-based fault locating in radial distribution systems using wavelets and neural networks," *IEEE transactions on power delivery*, vol. 26, no. 2, pp. 772–781, 2010.

[72] K. Jia, T. Bi, Z. Ren, D. W. Thomas, and M. Sumner, "High frequency impedance based fault location in distribution system with dgs," *IEEE Transactions on Smart Grid*, vol. 9, no. 2, pp. 807–816, 2016.

[73] M. Goudarzi, B. Vahidi, R. Naghizadeh, and S. Hosseinian, "Improved fault location algorithm for radial distribution systems with discrete and continuous wavelet analysis," *International Journal of Electrical Power & Energy Systems*, vol. 67, pp. 423–430, 2015.

[74] S. Shi, Z. Hu, Z. Ma, and X. Dong, "Travelling waves-based identification of sub-health condition of feeders in power distribution system," *IET Generation, Transmission & Distribution*, vol. 12, no. 5, pp. 1067–1073, 2017.

[75] J. Ding, L. Li, Y. Zheng, C. Zhao, H. Chen, and X. Wang, "Distributed travelling-wave-based fault location without time synchronisation and wave velocity error," *IET Generation, Transmission & Distribution*, vol. 11, no. 8, pp. 2085–2093, 2017.

[76] D. Wang, H. Gao, G. Zou, and S. Luo, "Ultra-high-speed travelling wave directional protection based on electronic transformers," *IET Generation, Transmission & Distribution*, vol. 11, no. 8, pp. 2065–2074, 2017.

[77] Q. Lin, G. Luo, and J. He, "Travelling-wave-based method for fault location in multi-terminal dc networks," *The Journal of Engineering*, vol. 2017, no. 13, pp. 2314–2318, 2017.

[78] M. Begovic and D. Novosel, "On wide area protection," in *2007 IEEE Power Engineering Society General Meeting.* IEEE, 2007, pp. 1–5.

[79] M. Zima, M. Larsson, P. Korba, C. Rehtanz, and G. Andersson, "Design aspects for wide-area monitoring and control systems," *Proceedings of the IEEE*, vol. 93, no. 5, pp. 980–996, 2005.

[80] J. Bertsch, C. Carnal, D. Karlson, J. Mcdaniel, and K. Vu, "Wide-area protection and power system utilization," *Proceedings of the IEEE*, vol. 93, no. 5, pp. 997–1003, 2005.

[81] H. Nazaripouya and S. Mehraeen, "Optimal pmu placement for fault observability in distributed power system by using simultaneous voltage and current measurements," in *2013 IEEE Power & Energy Society General Meeting*. IEEE, 2013, pp. 1–6.

[82] S. Geramian, H. A. Abyane, and K. Mazlumi, "Determination of optimal pmu placement for fault location using genetic algorithm," in *2008 13th International Conference on Harmonics and Quality of Power*. IEEE, 2008, pp. 1–5.

[83] K. Mazlumi, H. A. Abyaneh, S. Sadeghi, and S. Geramian, "Determination of optimal pmu placement for fault-location observability," in *2008 Third International Conference on Electric Utility Deregulation and Restructuring and Power Technologies*. IEEE, 2008, pp. 1938–1942.

[84] R. A. F. Pereira, L. G. W. Da Silva, and J. R. S. Mantovani, "Pmus optimized allocation using a tabu search algorithm for fault location in electric power distribution system," in *2004 IEEE/PES Transmision and Distribution Conference and Exposition: Latin America (IEEE Cat. No. 04EX956)*. IEEE, 2004, pp. 143–148.

[85] J. Cordova and M. O. Faruque, "Fault location identification in smart distribution networks with distributed generation," in *2015 North American Power Symposium (NAPS)*. IEEE, 2015, pp. 1–7.

[86] M. Xu, Y. Sun, K.-J. Li, W. Xiao, H. Li, and H. Gao, "A wide area protection scheme for smart distribution network with dg," in *2015 IEEE Industry Applications Society Annual Meeting*. IEEE, 2015, pp. 1–5.

[87] A. M. El-Zonkoly, "Fault diagnosis in distribution networks with distributed generation," *Electric Power Systems Research*, vol. 81, no. 7, pp. 1482–1490, 2011.

[88] J. Ghorbani, M. A. Choudhry, and A. Feliachi, "Fault location and isolation using multi agent systems in power distribution systems with distributed generation sources," in *2013 IEEE PES Innovative Smart Grid Technologies Conference (ISGT)*. IEEE, 2013, pp. 1–6.

[89] N. Perera, A. Rajapakse, and A. Gole, "Wavelet-based relay agent for isolating faulty sections in distribution grids with distributed generators," 2006.

[90] G. Celli and F. Pilo, "An innovative transient-based protection scheme for mv distribution networks with distributed generation," 2008.

[91] M. Figueroa and E. Orduna, "Ultra-high-speed protection for medium voltage distribution networks with distributed generation," in *2008 IEEE/PES Transmission and Distribution Conference and Exposition: Latin America*. IEEE, 2008, pp. 1–8.

[92] H. Zayandehroodi, A. Mohamed, H. Shareef, and M. Farhoodnea, "A novel neural network and backtracking based protection coordination scheme for distribution system with distributed generation," *International Journal of Electrical Power & Energy Systems*, vol. 43, no. 1, pp. 868–879, 2012.

[93] H. Zayandehroodi, A. Mohamed, M. Farhoodnea, and M. Mohammadjafari, "An optimal radial basis function neural network for fault location in a distribution network with high penetration of dg units," *Measurement*, vol. 46, no. 9, pp. 3319–3327, 2013.

[94] S. A. M. Javadian and M. Massaeli, "A fault location method in distribution networks including dg," *Indian Journal of Science and Technology*, vol. 4, no. 11, pp. 1446–1451, 2011.

[95] R. Agrawal and D. Thukaram, "Identification of fault location in power distribution system with distributed generation using support vector machines," in *2013 IEEE PES Innovative Smart Grid Technologies Conference (ISGT)*. IEEE, 2013, pp. 1–6.

[96] M. Dehghani, M. H. Khooban, and T. Niknam, "Fast fault detection and classification based on a combination of wavelet singular entropy theory and fuzzy logic in distribution lines in the presence of distributed generations," *International Journal of Electrical Power & Energy Systems*, vol. 78, pp. 455–462, 2016.

[97] A. Rafinia and J. Moshtagh, "A new approach to fault location in three-phase underground distribution system using combination of wavelet analysis with ann and fls," *International Journal of Electrical Power & Energy Systems*, vol. 55, pp. 261–274, 2014.

[98] D. Thukaram, H. Khincha, and H. Vijaynarasimha, "Artificial neural network and support vector machine approach for locating faults in radial distribution systems," *IEEE Transactions on Power Delivery*, vol. 20, no. 2, pp. 710–721, 2005.

[99] E. Koley, S. K. Shukla, S. Ghosh, and D. K. Mohanta, "Protection scheme for power transmission lines based on svm and ann considering the presence of non-linear loads," *IET Generation, Transmission & Distribution*, vol. 11, no. 9, pp. 2333–2341, 2017.

[100] S. Beheshtaein, M. Savaghebi, J. C. Vasquez, and J. M. Guerrero, "A hybrid algorithm for fault locating in looped microgrids," in *2016 IEEE Energy Conversion Congress and Exposition (ECCE)*. IEEE, 2016, pp. 1–6.

[101] S. H. Mortazavi, Z. Moravej, and S. M. Shahrtash, "A hybrid method for arcing faults detection in large distribution networks," *International Journal of Electrical Power & Energy Systems*, vol. 94, pp. 141–150, 2018.

[102] R. Pérez and C. Vásquez, "Fault location in distribution systems with distributed generation using support vector machines and smart meters," in *2016 IEEE Ecuador Technical Chapters Meeting (ETCM)*. IEEE, 2016, pp. 1–6.

[103] A. C. Adewole, R. Tzoneva, and S. Behardien, "Distribution network fault section identification and fault location using wavelet entropy and neural networks," *Applied soft computing*, vol. 46, pp. 296–306, 2016.

[104] M. Daisy and R. Dashti, "Single phase fault location in electrical distribution feeder using hybrid method," *Energy*, vol. 103, pp. 356–368, 2016.

[105] A. Pathirana, A. Rajapakse, and N. Perera, "Development of a hybrid protection scheme for active distribution systems using polarities of current transients," *Electric Power Systems Research*, vol. 152, pp. 377–389, 2017.

[106] D. T. Feeders, "Ieee pes distribution system analysis subcommittee," *OnlineAvailable: http://www. ewh. ieee. org/soc/pes/dsaco m/testfeeders/index. html*, 2011.

[107] W. Kersting and R. Green, "The application of carson's equation to the steady-state analysis of distribution feeders," in *2011 IEEE/PES Power Systems Conference and Exposition*. IEEE, 2011, pp. 1–6.

[108] J. A. Silva, H. B. Funmilayo, and K. L. Bulter-Purry, "Impact of distributed generation on the ieee 34 node radial test feeder with overcurrent protection," in *2007 39th North American Power Symposium*. IEEE, 2007, pp. 49–57.

[109] P. Giroux, G. Sybille, C. Osorio, and S. Chandrachood, "Grid-connected pv array," *Mathworks Co*, 2012.

[110] R. Dugan and W. Kersting, "Induction machine test case for the 34-bus test feeder-description," in *2006 IEEE Power Engineering Society General Meeting*. IEEE, 2006, pp. 4–pp.

[111] S. Sae, "Electric vehicle and plug in hybrid electric vehicle conductive charge coupler," 2010.

[112] A. K. Verma, B. Singh, and D. Shahani, "Grid to vehicle and vehicle to grid energy transfer using single-phase bidirectional ac-dc converter and bidirectional dc-dc converter," in *2011 International Conference on Energy, Automation and Signal*. IEEE, 2011, pp. 1–5.

[113] N. Mohan and T. M. Undeland, *Power electronics: converters, applications, and design*. John wiley & sons, 2007.

[114] M. Ceraolo, "New dynamical models of lead-acid batteries," *IEEE transactions on Power Systems*, vol. 15, no. 4, pp. 1184–1190, 2000.

[115] W. D. Stevenson *et al.*, *Elements of power system analysis*. Mcgraw-hill New York, 1982, vol. 4.

[116] K. Butler, J. Momoh, and D. Sobajic, "Field studies using a neural-net-based approach for fault diagnosis in distribution networks," *IEE Proceedings-Generation, Transmission and Distribution*, vol. 144, no. 5, pp. 429–436, 1997.

[117] I. Daubechies, *Ten lectures on wavelets*. Siam, 1992, vol. 61.

[118] D. C. Robertson, O. I. Camps, J. S. Mayer, and W. B. Gish, "Wavelets and electromagnetic power system transients," *IEEE Transactions on Power Delivery*, vol. 11, no. 2, pp. 1050–1058, 1996.

[119] S. Shaaban and T. Hiyama, "Transmission line faults classification using wavelet transform," in *the 14th International Middle East Power Systems Conference (MEPCON'10), Cairo University, Egypt*, 2010.

[120] H. Zheng-You, C. Xiaoqing, and L. Guoming, "Wavelet entropy measure definition and its application for transmission line fault detection and identification;(part i: Definition and methodology)," in *2006 International Conference on Power System Technology*. IEEE, 2006, pp. 1–6.

[121] S. Mallat and W. L. Hwang, "Singularity detection and processing with wavelets," *IEEE transactions on information theory*, vol. 38, no. 2, pp. 617–643, 1992.

[122] L. Peretto, R. Sasdelli, and R. Tinarelli, "On uncertainty in wavelet-based signal analysis," *IEEE transactions on instrumentation and measurement*, vol. 54, no. 4, pp. 1593–1599, 2005.

[123] V. Malathi, N. Marimuthu, S. Baskar, and K. Ramar, "Application of extreme learning machine for series compensated transmission line protection," *Engineering Applications of Artificial Intelligence*, vol. 24, no. 5, pp. 880–887, 2011.

[124] I. Gu *et al.*, "Bridging the gap between signal and power: Assessing power system quality using signal processing techniques," *IEEE Signal Process. Mag.*, vol. 26, no. 4, pp. 12–31, 2009.

[125] N. Zhang and M. Kezunovic, "Transmission line boundary protection using wavelet transform and neural network," *IEEE Transactions on Power Delivery*, vol. 22, no. 2, pp. 859–869, 2007.

[126] R. H. Salim, K. R. C. De Oliveira, and A. S. Bretas, "Fault detection in primary distribution systems using wavelets," in *International Conference on Power Systems Transient*, 2007.

[127] B. Panigrahi and V. R. Pandi, "Optimal feature selection for classification of power quality disturbances using wavelet packet-based fuzzy k-nearest neighbour algorithm," *IET generation, transmission & distribution*, vol. 3, no. 3, pp. 296–306, 2009.

[128] X. Dong, W. Kong, and T. Cui, "Fault classification and faulted-phase selection based on the initial current traveling wave," *IEEE transactions on power delivery*, vol. 24, no. 2, pp. 552–559, 2008.

[129] E. Clarke, *Circuit analysis of AC power systems.* Wiley, 1943, vol. 1.

[130] L. Coffeen, J. McBride, and D. Cantrelle, "Initial development of ehv bus transient voltage measurement: an addition to on-line transformer fra," in *Proceedings of the 2008 EPRI Substation Equipment Diagnostics Conference XV*, 2008.

[131] X. Dong, S. Wang, and S. Shi, "Research on characteristics of voltage fault traveling waves of transmission line," in *2010 Modern Electric Power Systems.* IEEE, 2010, pp. 1–5.

[132] J. H. Wilkinson and C. Reinsch, *Handbook for Automatic Computation: Volume II: Linear Algebra.* Springer Science & Business Media, 2012, vol. 186.

[133] F. H. Magnago and A. Abur, "Fault location using wavelets," *IEEE Transactions on Power Delivery*, vol. 13, no. 4, pp. 1475–1480, 1998.

[134] A. Borghetti, M. Bosetti, M. Di Silvestro, C. A. Nucci, and M. Paolone, "Continuous-wavelet transform for fault location in distribution power networks: Definition of mother wavelets inferred from fault originated transients," *IEEE Transactions on Power Systems*, vol. 23, no. 2, pp. 380–388, 2008.

[135] X. Chen, X. Yin, X. Yin, J. Tang, and M. Wen, "A novel traveling wave based fault location scheme for power distribution grids with distributed generations," in *2015 IEEE Power & Energy Society General Meeting.* IEEE, 2015, pp. 1–5.

Biography

Ranjeet Kumar received the B.Tech degree from Uttarakhand Technical University and M.Tech degree from NIT Patna. He is currently pursuing the Ph.D. degree in Department of Electrical Engineering, Malaviya National Institute of Technology Jaipur, India. His research interest includes Power System Protection, Fault Identification and Location, Electrical Vehicles and Renewable Energy integration to Distribution System.